

SOME ASPECTS OF LOAD DURATION  
BEHAVIOUR IN WOOD

by

KENNETH BRUCE CLARK

B.A.Sc. (1972)

The University of British Columbia

A THESIS SUBMITTED IN PARTIAL FULFILMENT OF  
THE REQUIREMENTS FOR THE DEGREE OF  
MASTER OF APPLIED SCIENCE

in the Department

of

CIVIL ENGINEERING

We accept this thesis as conforming  
to the required standard

The University of British Columbia

April, 1975

In presenting this thesis in partial fulfilment of the requirements for an advanced degree at the University of British Columbia, I agree that the Library shall make it freely available for reference and study. I further agree that permission for extensive copying of this thesis for scholarly purposes may be granted by the Head of my Department or by his representatives. It is understood that copying or publication of this thesis for financial gain shall not be allowed without my written permission.

K. B. Clark

Department of Civil Engineering  
The University of British Columbia  
Vancouver 8, Canada

April 1975

## ABSTRACT

Present design stresses for structural timber include a reduction factor to account for the duration of loading. Recent studies have shown however that this factor does not apply to commercial grade timber containing knots and other irregularities of grain. It has also been shown that the apparent Young's modulus perpendicular to grain in clear material decreases greatly with longer durations of loading. It was therefore hypothesized that in commercial grade wood, stress concentrations are made less severe in long term loadings because of stress redistribution made possible by straining perpendicular to grain.

This thesis found experimentally that the amount of tensile straining perpendicular to grain around a knot in timber beams subjected to bending increased substantially with long duration loadings. In conjunction with this, a computer simulation of the material around a knot showed that a decreasing apparent Young's modulus perpendicular to grain reduces the stresses perpendicular to grain.

## TABLE OF CONTENTS

|   | Page |
|---|------|
| ABSTRACT . . . . .  | ii   |
| TABLE OF CONTENTS . . . . .                                   | iii  |
| LIST OF TABLES . . . . .                                      | vi   |
| LIST OF FIGURES . . . . .                                     | vii  |
| ACKNOWLEDGEMENTS . . . . .                                    | ix   |
| CHAPTER   |      |
| 1. INTRODUCTION . . . . .                                     | 1    |
| 1.1 Background . . . . .                                      | 1    |
| 1.2 Recent Investigations . . . . .                           | 2    |
| 1.3 Purpose and Scope . . . . .                               | 8    |
| 2. EXPERIMENTAL OBSERVATIONS . . . . .                        | 12   |
| 2.1 Introduction . . . . .                                    | 12   |
| 2.2 Selection of Method . . . . .                             | 12   |
| 2.3 Specimen Preparation . . . . .                            | 15   |
| 2.4 Loadings . . . . .  | 16   |
| 2.5 Instrumentation . . . . .                                 | 19   |
| 2.6 Test Set-Up . . . . .                                     | 20   |
| 2.7 Analysis . . . . .  | 20   |
| 2.8 Results . . . . .   | 31   |
| 2.9 Failure Modes . . . . .                                   | 37   |
| 2.10 Summary . . . . .  | 40   |
| 3. INFLUENCE OF STIFFNESS PERPENDICULAR TO<br>GRAIN . . . . . | 41   |
| 3.1 Introduction . . . . .                                    | 41   |

| CHAPTER  | Page |
|--|------|
| 3.2 The Finite Element . . . . .   | 42   |
| 3.3 The Problem . . . . .  | 43   |
| 3.4 Results of the Parametric Study . .  | 50   |
| 3.5 The $E_x/E_y$ Ratio . . . . .  | 54   |
| 3.6 Shear Modulus Effect. . . . .  | 60   |
| 3.7 Summary . . . . .  | 60   |
| 4. CIRCULAR HOLE IN A FINITE PLATE HAVING<br>GRAIN TYPE ORTHOTROPY                               |      |
| 4.1 Introduction . . . . .   | 64   |
| 4.2 The Problem . . . . .  | 65   |
| 4.3 Preliminary Tests . . . . .  | 65   |
| 4.4 Tension Zone Sizes and Positions. .  | 68   |
| 4.5 Stress Distribution on Axes of<br>Symmetry. . . . .  | 78   |
| 4.6 Summary . . . . .  | 89   |
| 5. CONCLUSIONS. . . . .  | 91   |
| REFERENCES . . . . .   | 93   |
| APPENDICES . . . . .   | 94   |
| A. THE FINITE ELEMENT . . . . .  | 94   |
| A.1 The Potential Energy Theorem. . . .  | 94   |
| A.2 Derivation of the Six Node Plane<br>Linearly Varying Strain Orthotropic<br>Triangle. . . . . | 96   |
| A.3 Derivation of Strains and Stresses.  | 109  |
| B. BEHAVIOUR AND TESTING OF THE FINITE<br>ELEMENT. . . . .                                       | 111  |

| CHAPTER                          | Page |
|----------------------------------|------|
| B.1 Convergence. . . . .         | 111  |
| B.2 Testing. . . . .             | 112  |
| C. THE COMPUTER PROGRAM. . . . . | 118  |

TABLES

| Table                                   | Page |
|---|------|
| I    Testing Schedule . . . . .         | 32   |
| II   Tension Zone Areas . . . . .       | 35   |
| III  Parametric Analysis Data . . . . . | 46   |
| IV   Input Data: Hole in Plate. . . . . | 70   |

## FIGURES

| Figure   | Page |
|--|------|
| 1.1 Madison Test . . . . .                             | 3    |
| 1.2 Duration of Maximum Load . . . . .                 | 5    |
| 1.3 Failure Loads: Clear . . . . .                     | 6    |
| 1.4 Failure Loads: No. 2 Construction . . . . .        | 7    |
| 1.5 Tension Perp.-Failure Stress: Commercial . . . . . | 9    |
| 1.6 Tension Perp.-Elastic Modulus: Clear . . . . .     | 10   |
| 2.1 Specimen Preparation . . . . .                     | 17   |
| 2.2 Specimen Control Point Layout . . . . .            | 18   |
| 2.3 Reference Frame . . . . .                          | 21   |
| 2.4 Test Set-Up . . . . .                              | 22   |
| 2.5 Validator Machine . . . . .                        | 24   |
| 2.6 Photograph Coordinates . . . . .                   | 25   |
| 2.7 Specimen P . . . . .                               | 26   |
| 2.8 Specimen 2 . . . . .                               | 27   |
| 2.9 Specimen 3 . . . . .                               | 28   |
| 2.10 Rapid Failure Mode . . . . .                      | 38   |
| 2.11 Slow Failure Mode . . . . .                       | 39   |
| 3.1 Typical Grain Pattern . . . . .                    | 48   |
| 3.2 35 Element Model . . . . .                         | 49   |
| 3.3 Bending . . . . .                                  | 51   |
| 3.4 Bending X Strains . . . . .                        | 52   |
| 3.5 Bending Y Strains . . . . .                        | 53   |
| 3.6 Tension Loading X Strains . . . . .                | 57   |
| 3.7 Tension Loading Y Strains . . . . .                | 58   |

|      |  |     |
|------|--|-----|
| 3.8  | Bending 'Slow' Test Shear Modulus Effect . . .   | 61  |
| 3.9  | Tension Shear Modulus Effect . . . . .           | 62  |
| 4.1  | 188 Element Model . . . . .                      | 66  |
| 4.2  | Edge Stresses: X Direction . . . . .             | 67  |
| 4.3  | Edge Stresses: Y Direction . . . . .             | 69  |
| 4.4  | Stress Distribution X Direction Isotropic .      | 72  |
| 4.5  | Stress Distribution X Direction $E_x/E_y = 20$ . | 73  |
| 4.6  | Stress Distribution X Direction $E_x/E_y = 40$ . | 74  |
| 4.7  | Stress Distribution Y Direction Isotropic .      | 75  |
| 4.8  | Stress Distribution Y Direction $E_x/E_y = 20$ . | 76  |
| 4.9  | Stress Distribution Y Direction $E_x/E_y = 40$ . | 77  |
| 4.10 | Strain Distribution X Direction Isotropic .      | 79  |
| 4.11 | Strain Distribution X Direction $E_x/E_y = 20$ . | 80  |
| 4.12 | Strain Distribution X Direction $E_x/E_y = 40$ . | 81  |
| 4.13 | Strain Distribution Y Direction Isotropic .      | 82  |
| 4.14 | Strain Distribution Y Direction $E_x/E_y = 20$ . | 83  |
| 4.15 | Strain Distribution Y Direction $E_x/E_y = 40$ . | 84  |
| 4.16 | Stresses in the X Direction Side DE . . . .      | 85  |
| 4.17 | Stresses in the Y Direction Side DE . . . .      | 87  |
| 4.18 | Stresses in the X Direction Side BC . . . .      | 88  |
| 4.19 | Stresses in the Y Direction Side BC . . . .      | 90  |
| A.1  | Element Configuration . . . . .                  | 97  |
| B.1  | Uniformly Loaded Membrane . . . . .              | 113 |
| B.2  | 32 Element Cantilever . . . . .                  | 114 |
| B.3  | Edge Stresses X Direction Isotropic . . . .      | 116 |
| B.4  | Edge Stresses Y Direction Isotropic . . . .      | 117 |

## ACKNOWLEDGEMENTS

I wish to thank my supervisors, Professor B. Madsen and Dr. M.D. Olson, for their advice and support throughout the preparation of this thesis. In addition, I would like in particular to thank Mr. Ron Ungless, the U.B.C. Civil Engineering Department program librarian, for advice and logistic assistance far beyond the duties of his office.

Two scholarships provided by the National Research Council of Canada enabled me to undertake these studies.

April 1975

Vancouver, British Columbia

## CHAPTER 1

### INTRODUCTION

#### 1.1 Background

Timber is employed as the main structural material in many houses, apartments, shopping centres and industrial buildings in British Columbia, and its production is a vital part of the province's economy. Until recently, allowable design stresses had been derived by extrapolation from laboratory data, and little effort had been made to understand the microscopic behavior of construction grade timber under load. Examination of this behavior may make possible more accurate and rational utilization of information derived from experimental studies of small wood specimens. Because allowable stresses for structural timber include reductions to account for long term loadings, the mechanisms that produce this effect deserve detailed study. The first major work on this subject was carried out at the Forest Products Laboratory in Madison Wisconsin and was reported in 1951.<sup>1</sup> One hundred and twenty-six one inch by one inch matched clear specimens

of Douglas Fir were tested in bending. One of each pair was loaded to failure in a static test taking about five minutes. The matched specimen was then given a constant bending moment to produce a stress equal to from 60 to 95 per cent of the failure stress of its partner.

Based on these results, some of which were obtained from 6 per cent and some from 12 per cent moisture content specimens, and some from heat treated specimens, Fig. 1.1 was obtained.<sup>1</sup> It predicts that the long term strength of specimens (fifty years of applied load) is over 40 per cent lower than the short term strength (from a five minute test). This reduction, derived from bending tests on small clear specimens has been empirically applied to the bending, shear and tension perpendicular to grain strengths of full size timber containing knots, checks and adverse slopes of grain.

### 1.2 Recent Investigations

Investigations from 1970 to the present of the load duration effects on commercial grade wood have been carried out at the University of British Columbia, and have shown disagreement with the Madison Wisconsin results. In Madsen's (U.B.C.) experiments,<sup>2,3,4,5</sup> several rates of stepwise ramp loading were used to study the strengths of clear and commercial grade full size lumber. One hundred and eighty-nine clear 2x6's and two hundred and eighty-five number two grade 2x6's were tested to failure in bending at six

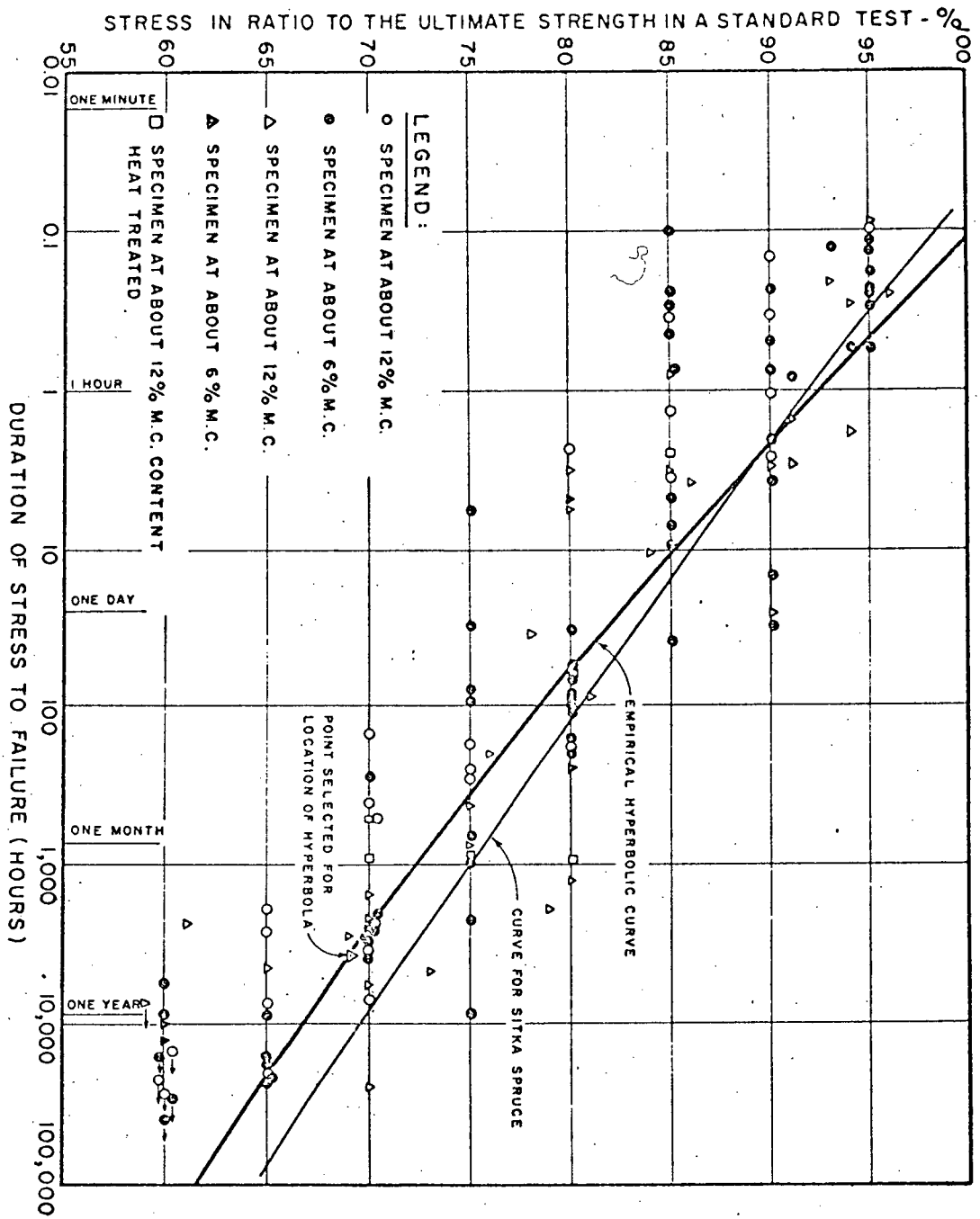
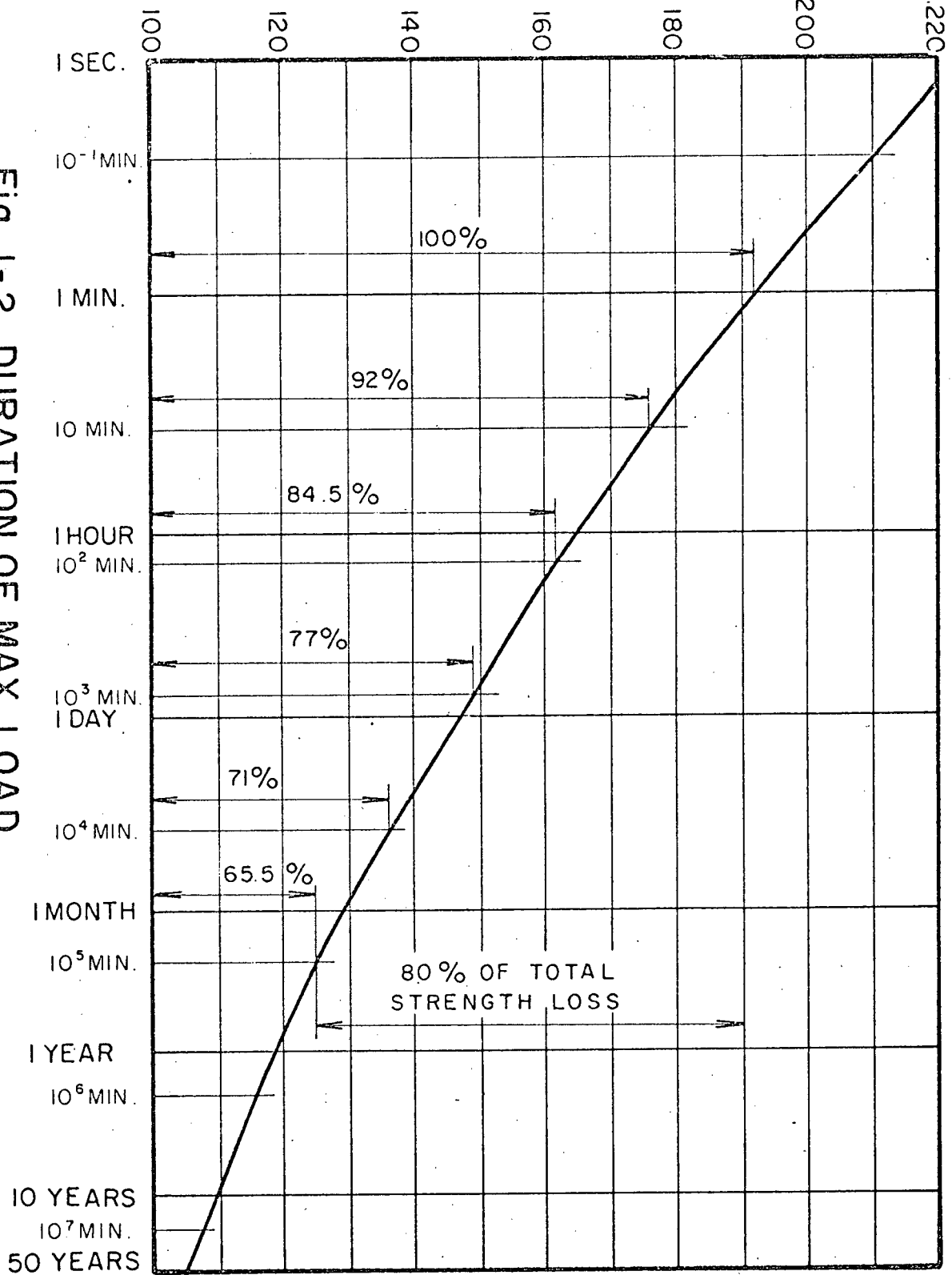


Fig. 1-1 MADISON TEST.

rates of loading such that failure occurred about 1, 10, 100, 1000, 10000 and 100000 minutes after initial load application. The number two grade specimens contained knots and other grain irregularities. Fig. 1.2, adapted from the Madison Wisconsin report, shows that approximately 80 per cent of the total strength reduction would occur within the longest of these time spans. From Fig. 1.3 and Fig. 1.4 it is apparent that while the load duration strength reduction effects predicted by Fig. 1.2 might represent the behaviour of clear material, they cannot be blindly applied to materials containing irregularities of grain. This is particularly true in the neighbourhood of the 5th percentile of strength, from which design stresses are derived. This should have been obvious since commercial material, containing knots and adverse slopes of grain, has different modes of failure than clear material. The latter often develops wrinkles in the compression zone as a prelude to final failure, while the former usually fails near one of the irregularities because of stress concentrations in the tension zone.<sup>2,3</sup> Analagous results were obtained for dry lumber subjected to shear.<sup>4</sup> Dry lumber subjected to pure tension perpendicular to grain however exhibited considerable reductions in strength and apparent stiffness with time.<sup>5</sup> From a one minute test to a two month test, the average reduction in failure stress on the gross section for number two grade lumber was 33 per cent, of the same order as

RATIO OF WORKING STRESS TO RECOMMENDED  
STRESS FOR LONG-TIME LOADING - %

Fig. 1-2 DURATION OF MAX. LOAD.



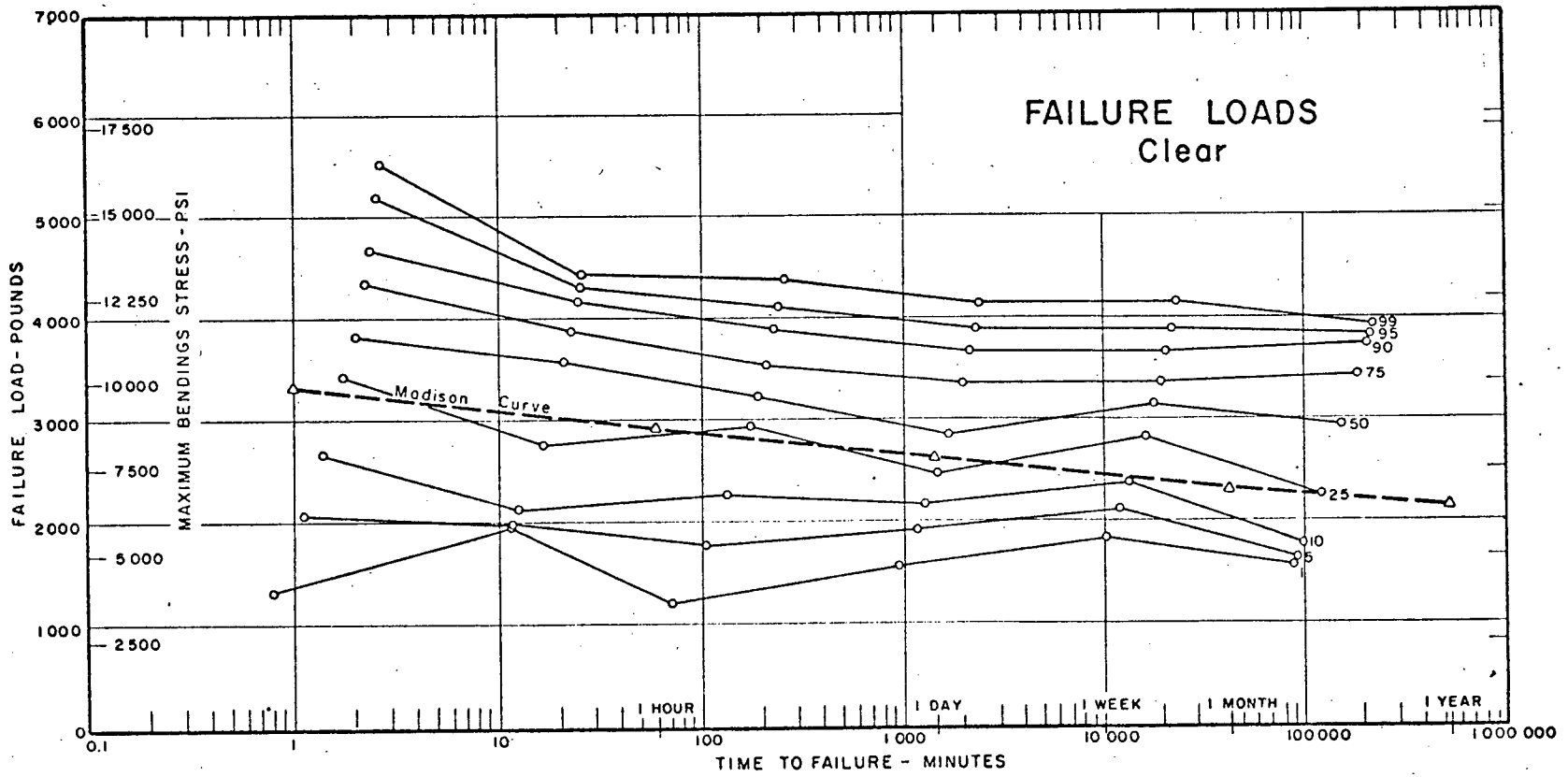


Figure 1-3

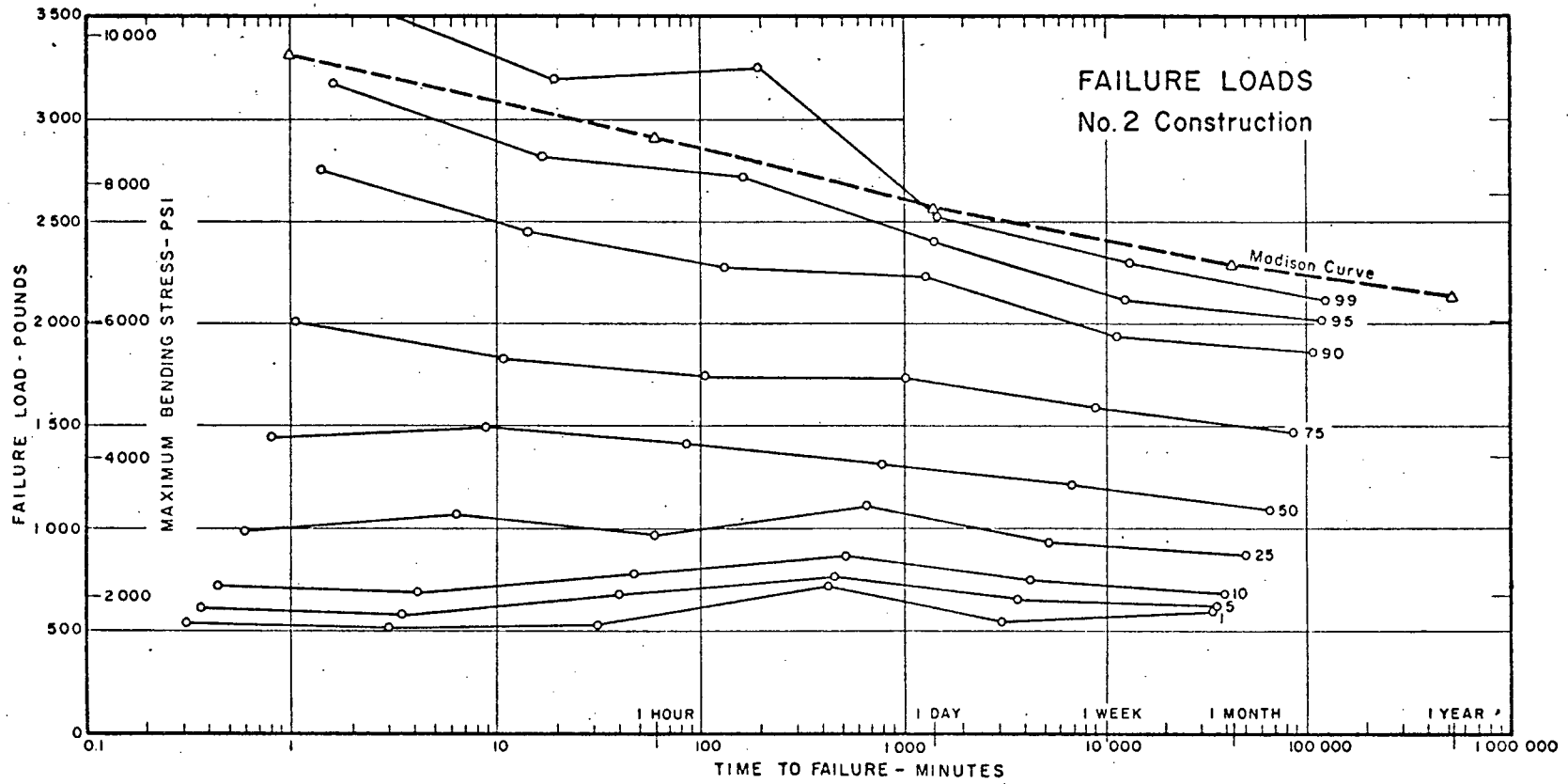
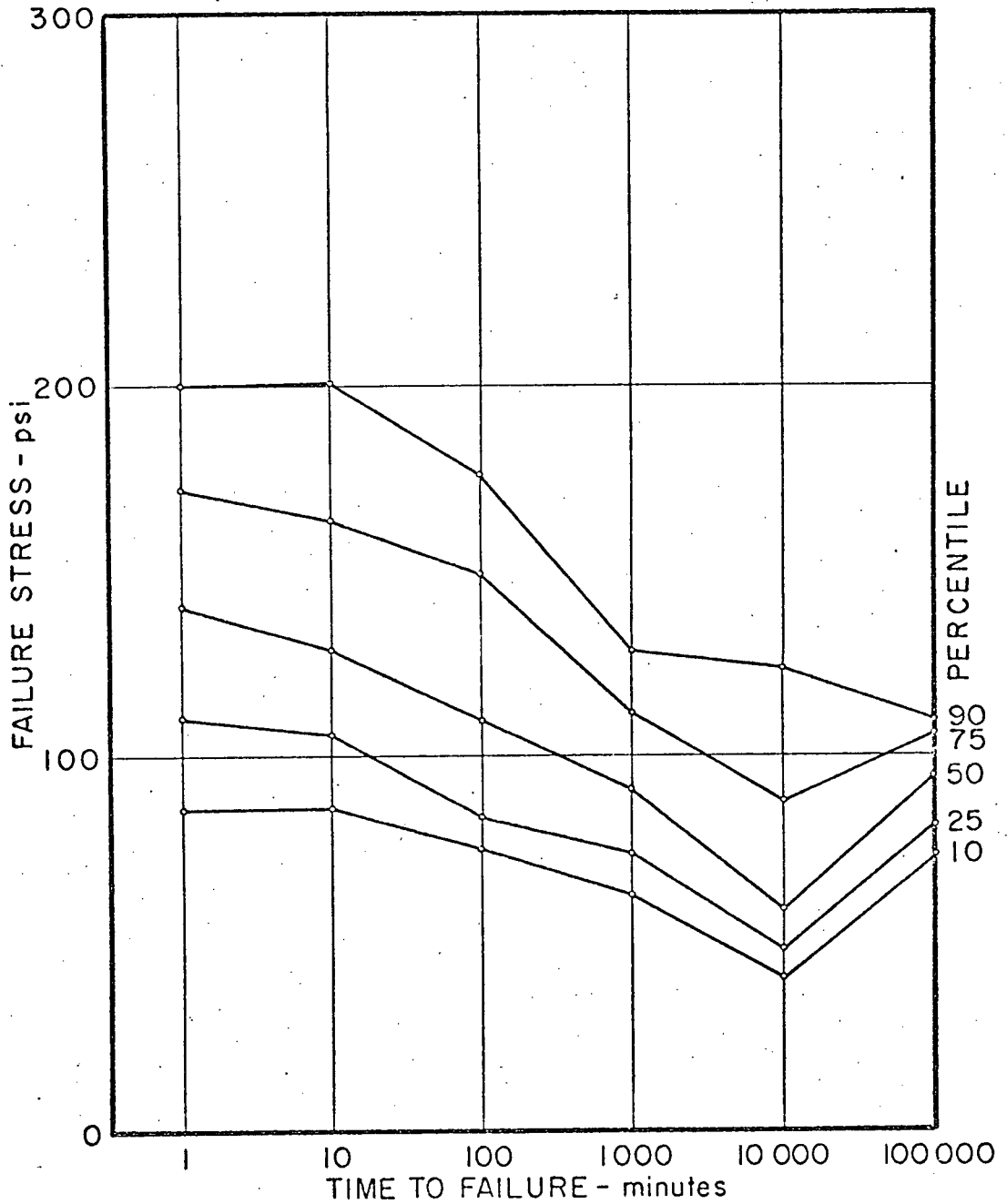


Figure 1-4

the 35 per cent reduction predicted by the Madison test results of Fig. 1.2. The time dependent stiffness was however an average of approximately eight times smaller for a 100,000 minute test than for a 1 minute test. Stiffnesses were not considered in the Madison work. The strength phenomenon was shown by Fig. 1.5 for commercial material, and the time dependent stiffness reduction by Fig. 1.6 for clear material. In this paper, time dependent stiffness will refer to total strains (elastic and creep) while under load.

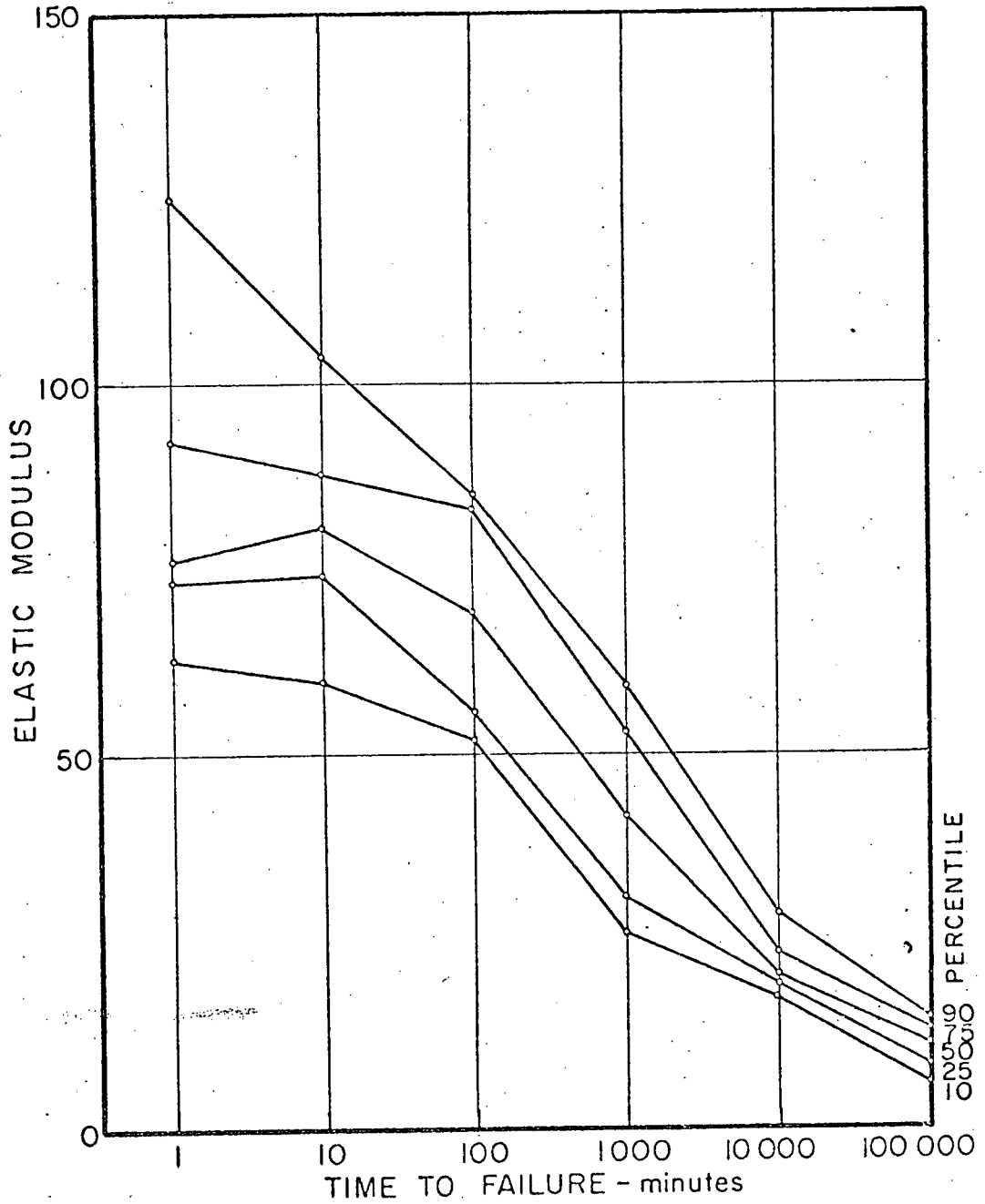
### 1.3 Purpose and Scope

From these results, the hypothesis was drawn that the effects of stress concentrators like knots decrease with time because of redistributions of stress in material adjacent to irregularities of grain. This effect would increase the failure strength of commercial material to at least partially compensate for the strength reductions with time found in clear lumber by the Madison tests. It was further hypothesized that the very large reductions of the time dependent stiffness perpendicular to grain could, in a long term loading, permit extensive tensile straining perpendicular to grain and lead to some kind of flow in the material surrounding stress concentrators. Stresses perpendicular to grain to cause this straining would be set up by the more marked curvature of grain in commercial than in clear material.



TENSION PERP. - FAILURE STRESS  
COMMERCIAL

FIG. I-5



TENSION PERP. - ELASTIC MODULUS  
CLEAR

FIG. I-6

The purpose of the present investigation was then twofold. The first purpose was to experimentally determine whether or not the amount of tensile straining perpendicular to grain in wood containing irregularities increases significantly with the duration of load. The second purpose was to discover through a computer simulation whether or not a time-dependent stiffness perpendicular to grain could produce a significant effect that did not exist in clear material.

## CHAPTER 2

### EXPERIMENTAL OBSERVATIONS

#### 2.1 Introduction

The load duration behaviour of wood containing stress raisers has been observed to be different from that of straight grained material. A necessary part of the proving of the hypothesis involves an experimental investigation of the strains under load in irregular material. Strains parallel and perpendicular to the longitudinal axis (approximately parallel and perpendicular to the assumed grain pattern) of a beam having a single edge knot in the middle of an otherwise clear segment were studied. The measured strains included creep, if occurring, as inelastic mechanisms contribute to redistribution of stress.

#### 2.2 Selection of Method

Although any method of testing would at best show only the behaviour of the surface plane of material, at the least an indication of the total strain distribution inside the board could be obtained. One constraint on the testing procedure was that the character of the wood surface

should not be altered by attaching any material more stiff than the specimen itself. Anything coupled to the surface must be guaranteed to deform exactly as the material beneath it. As well, the grain pattern should be visible so that the point of failure initiation could be seen and so that strains could be related during analysis to the board configuration. Because the behaviour was not predictable, it was also desirable to have the capability of measuring strains at several stress levels. Finally, the strains had to be amenable to recording while the test was in progress without disturbing the specimen.

Strains could have been measured directly using strain gauges or brittle coatings. Displacements could have been measured by using moire grids. There were however objections and logistic difficulties to these methods. Because the number of strain gauges required would have obliterated the face of the specimen, and the gluing process could have changed the surface character, this method was discarded. Brittle coatings had several drawbacks. They crack only once at a prescribed strain, and further cracking occurs elsewhere only as this same strain is reached. A complete strain distribution cannot therefore be obtained at any time; the entire approach is iterative and the behaviour at any position after a crack has formed is unknown. As well, coating specifications indicated that viscous flow would occur during a slow

test to such an extent that straining due to creep would not be visible. The cracking process is irreversible; shock loadings resulting from settlement of the apparatus or tearing of a few fibres near the knot would cause permanent cracking although the board might rebound elastically. Finally, the coating is opaque and the cracks resulting from even extreme loadings were found not to be readily visible.

Using moire grids, contours of displacement can be obtained directly and strains can be calculated. Some problems were that it would have been logistically very difficult to maintain a reference grid and that rigid body rotations resulting from the unsymmetric curvature of a beam would appear as displacement fringes and would have to be subtracted from the results. In one attempt for this study, a lithographer duplicated two hundred line per inch screens onto transparent stripping film. Ideally the grid would have separated from the film after gluing so that only a matrix of lines would have remained on the board. Two problems arose however. First, the film did not strip cleanly, and second, the special stripping film cement caused the wood to expand in ridges. Undercoatings were used to prevent the glue moisture from penetrating the wood, but all waterproof varnishes cracked on loading thereby altering the character of the specimen face.

The method finally used was the most direct.

A two-dimensional grid of .013 inch diameter shallow holes spaced one-half inch centre to centre was punched into the surface of a board, and the distances between holes were measured before and after loading. During straining of course the holes were deformed, but if the deformation was assumed to be symmetric (a reasonable assumption over .013 inch) then the centre of the hole was a suitable point for measurement. A greater problem was that since the diameters were much larger than the displacements occurring between them, shear strains calculated from distances on the board face lacked significance although the normal strains were meaningful. Advantages of this method were that rigid body motions could be ignored, displacements at each stress level could be easily recorded on film, and the measurement process did not affect the sample once the holes had been punched. An experimental study of clear grained material was not undertaken because only the surface material was visible, and while the presence of a knot can be guaranteed through the thickness of a board, the absence of grain irregularities cannot.

### 2.3 Specimen Preparation

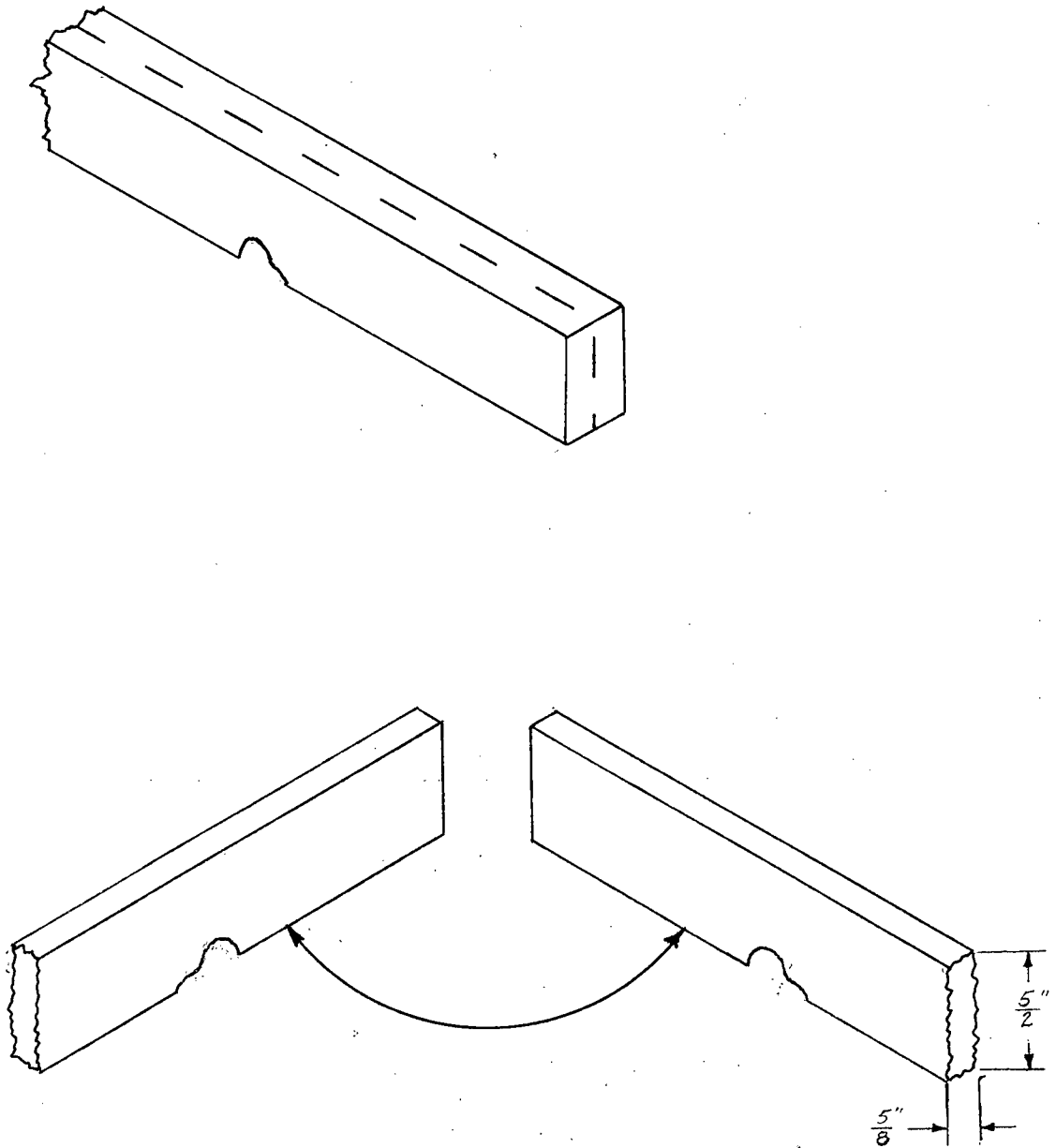
To minimize the number of unknowns in relating this work to that of Madsen, the aspect ratio of the specimens was made similar to that of a 2x6.<sup>3,4</sup> Pairs of specimens as nearly identical as possible were examined, one at a fast and one at a slow loading rate. Specimens

.625 inch by 2.500 inches having an aspect ratio of .250 (as compared to .273 for a 2x6), made by splitting 2x6's as in Fig. 2.1, were used. They were 84 inches long with a single approximately semicircular edge knot of .5 to 1.5 inch radius in the middle. The knot had to extend through the board with minimal change in diameter from one side to the other and have its longitudinal axis orthogonal to the faces of the specimen. To simplify the later modelling of the discontinuity on the computer, the knots chosen were as simple as possible with apparently smooth flowing grain around them.

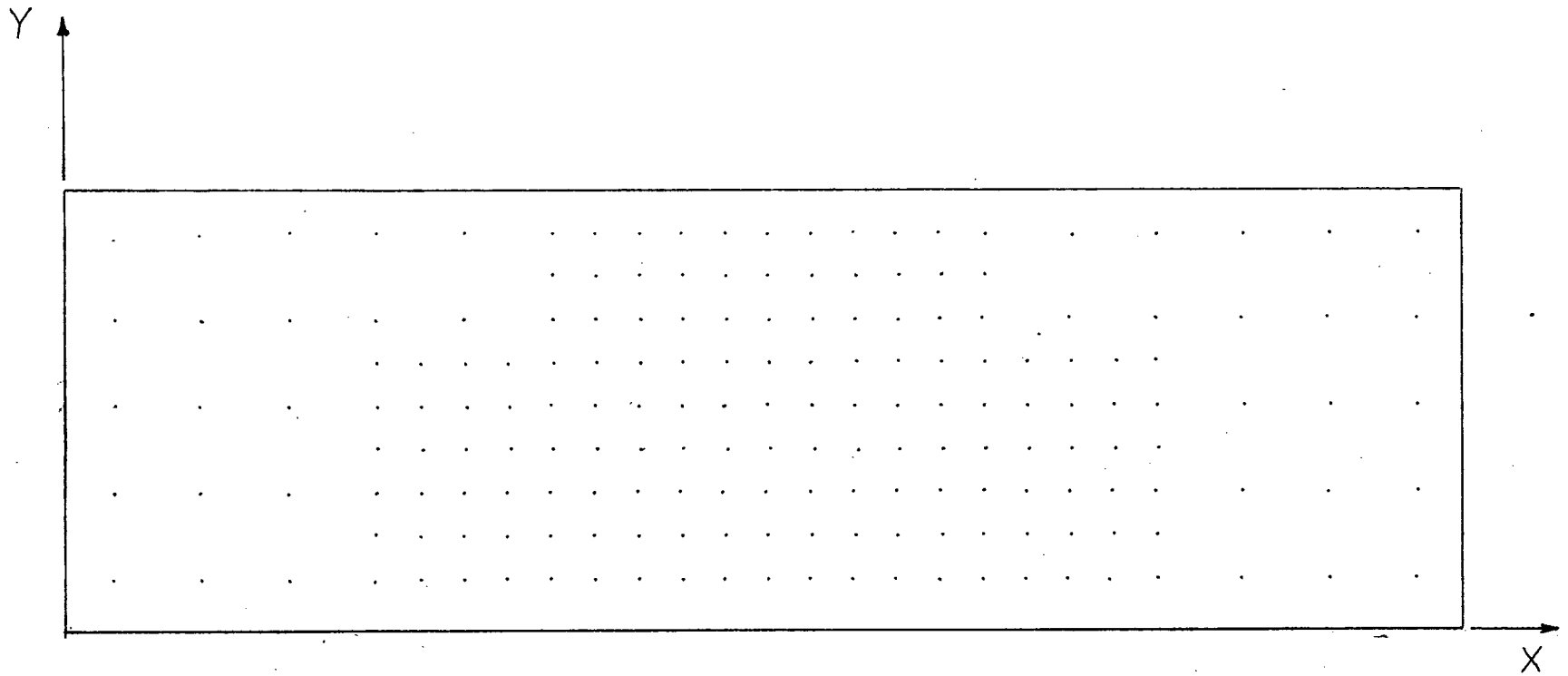
The 2x6's were cut lengthwise to produce a section approximately 2.75 inches by 1.50 inches so as to create a half knot near the middle of one edge. This board was then jointed before being run lengthwise through a saw to become two sections 84 inches by 2.75 inches by .625 inch, which were mechanically planed to the final size. An eight inch long section in which the knot was centred was then finely sanded. A brass grid containing one hundred and eighty-five holes was clamped over this section and the .013 inch diameter holes were punched into the specimen using a special tool designed to ensure that penetration was perpendicular to the face of the board and of approximately .020 inch depth. The pattern of holes is illustrated in Fig. 2.2.

#### 2.4 Loadings

To be consistent with previous work and because



Specimen Preparation.  
Fig. 2 -1



Specimen Control Point Layout .  
Fig.2-2

it was the simplest type of arrangements, the specimens were tested in uniform bending.<sup>2,3</sup> Failure stresses at the extreme fibres of approximately 4000 psi were expected and at least five increments to failure were desirable if intermediate stress levels were to be examined. Stress increments of about 5000 psi on the gross section were therefore used. Rates of loading were selected so that failure could be expected in either approximately eight minutes or eight days. These rates, if uniform would have been equivalent to 480 psi/minute and 480 psi/day (or .33 psi/minute), producing a ratio of loadings of 1440 to 1. This ratio of loadings will be called the rate factor throughout this study. A preliminary set of specimens was tested to failure in order to see the type of results that would occur. When they were analyzed it became apparent that further tests would be required in order to establish significant results. The analysis however required monopolization of laboratory equipment. A total of three sets of specimens was loaded to failure.

## 2.5 Instrumentation

A reference frame, consisting of a thin aluminum border onto whose perimeter were glued steel rules marked in hundredths of an inch, rested on top of the specimen on a rocker and a roller so that the bending

was not restrained and the test region was surrounded as in Fig. 2.3. The specimens were photographed onto black and white film before and after every load increment by an Hasselblad E.L.M. single lens reflex camera with a 50 millimetre wide angle lens onto 2.25 inch square negatives. The camera was set on a tripod with three dimensional control so that its platform could be maintained horizontal while it was lowered to match the vertical deflexions of the specimens. This kept the negative face of the camera parallel to the face of the board.

## 2.6 Test Set-Up

The specimen, reference frame and loading pan were set up as in Fig. 2.4. The specimen board was supported on metal semicircles at each end and was restrained from lateral motion by plywood forks attached to a fixed support mechanism. The forks were spaced at sixteen inches centre to centre and were sufficiently deep to prevent instability type failures of the specimen. Loads were applied by twenty-five pound lead ingots laid on the loading pan shown in Fig. 2.4 so that a uniform bending moment resulted over the thirty-two inch long section in which the knot was centred.

## 2.7 Analysis

The 2.25 inch square negatives of the test region were enlarged so that the specimen in the photograph was approximately twice life-size. The enlargements were



Fig. 2-3 REFERENCE FRAME

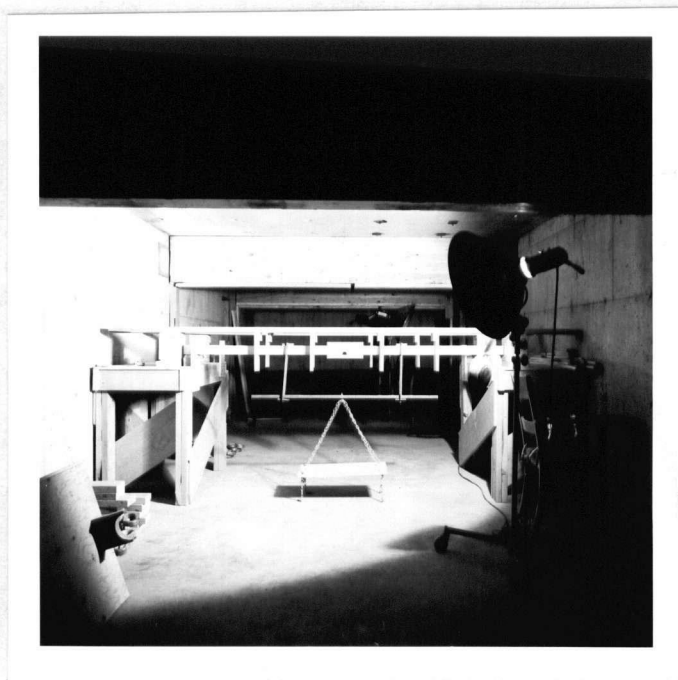


Fig. 2-4 TEST SET-UP

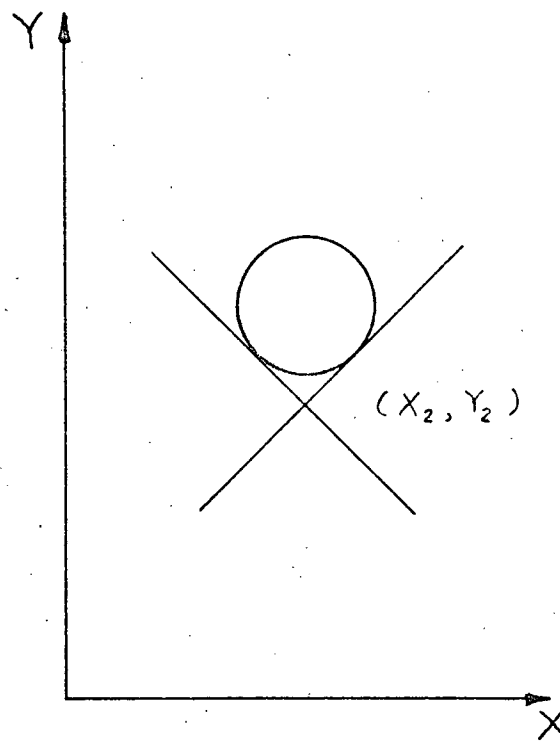
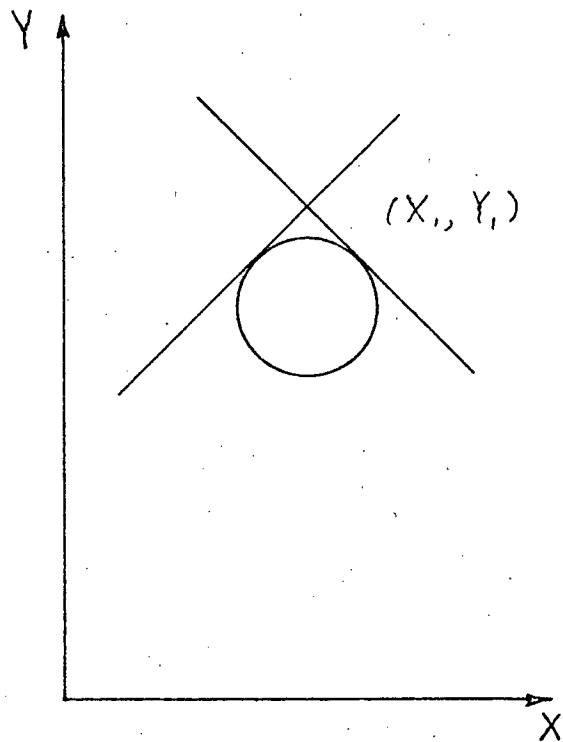
then placed on a Browne and Sharpe Validator measuring machine equipped with a microscope (Fig. 2.5) so that the X- and Y- coordinates of the centre of each hole could be measured with an accuracy of .0002 inch and a precision of .0001 inch. The hole centre was located by an averaging of two readings as in Fig. 2.6.

Because of the small displacements occurring between any hole and those adjacent, only the preliminary photo and the final photo before visible cracking were useful for numerical analysis. The different stress levels this procedure produced for each pair of photographs was justified because the knots varied in size and the stresses calculated from the gross section only approximated the true stresses near the knot. The stress levels used are shown in Figs. 2.7, 2.8 and 2.9. Calibration was performed on the Validator machine by comparing the distances on the reference frame scales with the true distances. A computer program was written which, given the photographic coordinate data, calculated strains in both the X and Y directions by dividing the calibrated displacements by the true distances between the centres of holes. The average strain from the end of each row or column to each point was also calculated but was not found to be a useful parameter.

Because of film over-exposure, the preliminary tests did not produce results as complete as those produced by later tests. The former did however show in



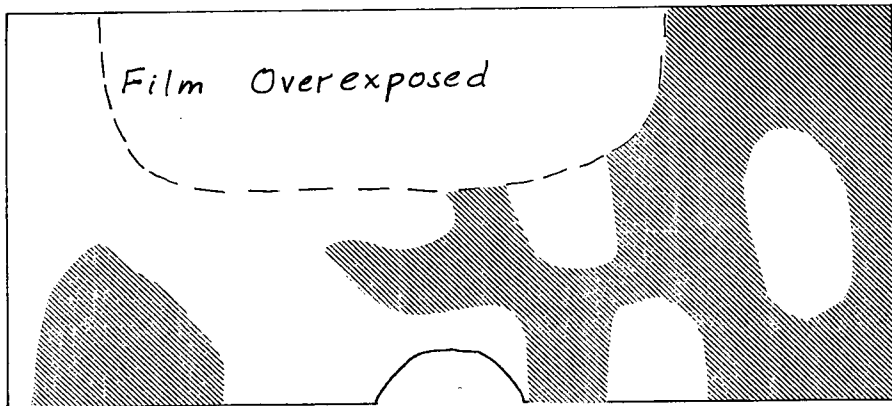
Fig. 2-5 VALIDATOR MACHINE



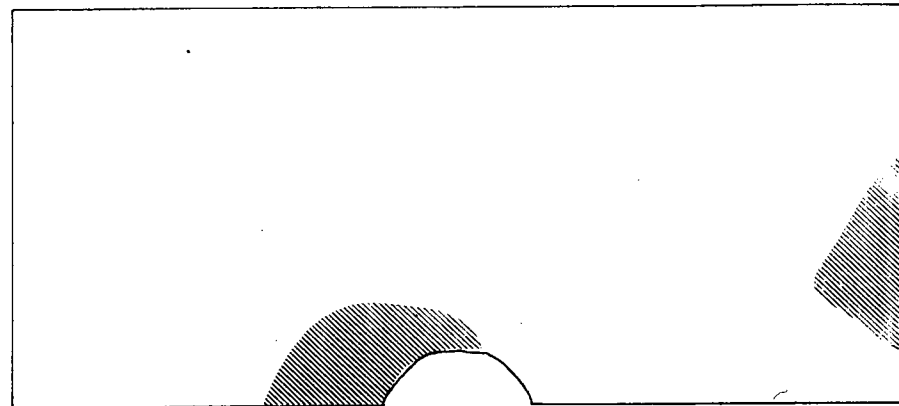
$$X = (X_1 + X_2) / 2$$

$$Y = (Y_1 + Y_2) / 2$$

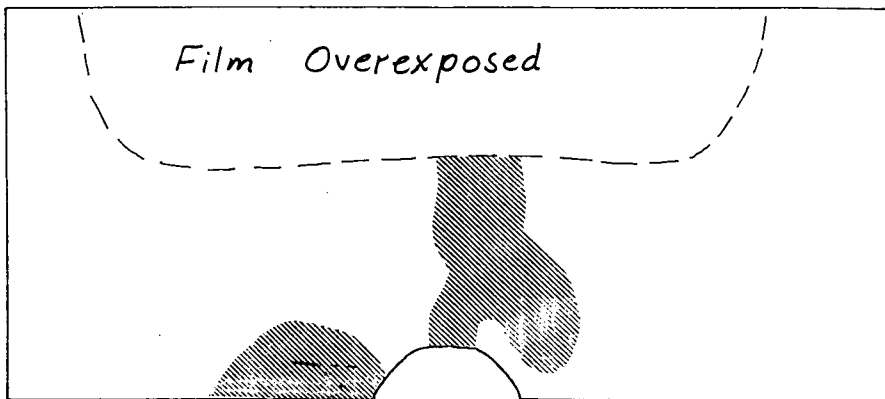
Fig. 2-6 PHOTOGRAPH COORDINATES



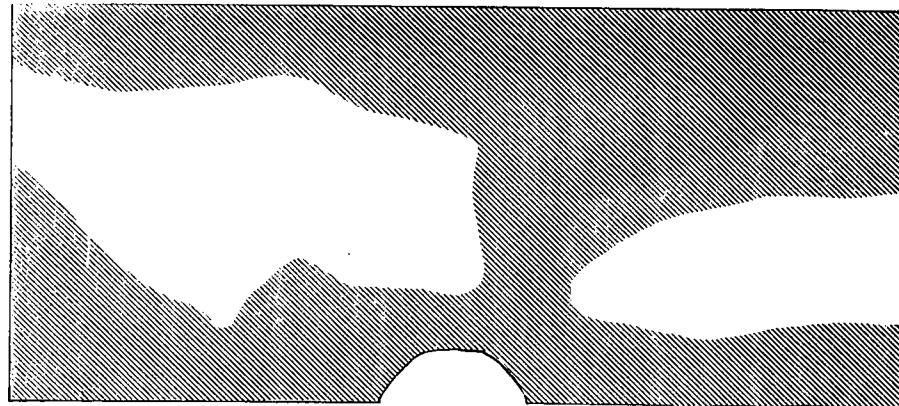
X STRAINS - FAST TEST  
4800 PSI



X STRAINS - SLOW TEST  
1920 PSI

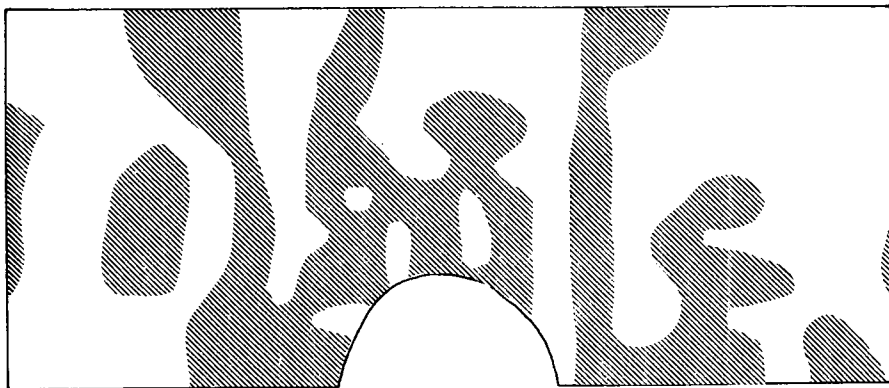


Y STRAINS - FAST TEST  
4800 PSI

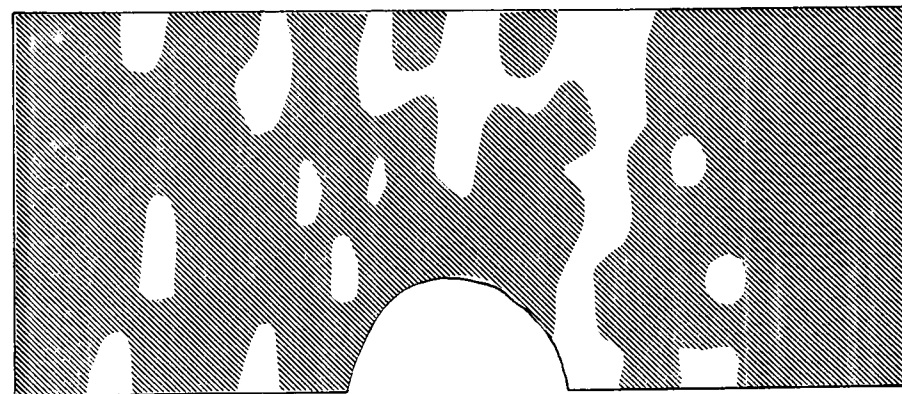


Y STRAINS - SLOW TEST  
1920 PSI

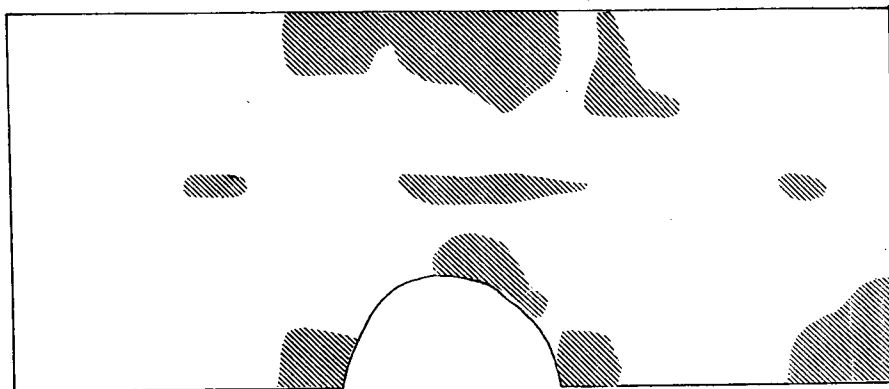
SPECIMEN P TENSION SHOWN SHADED  
Fig. 2-7



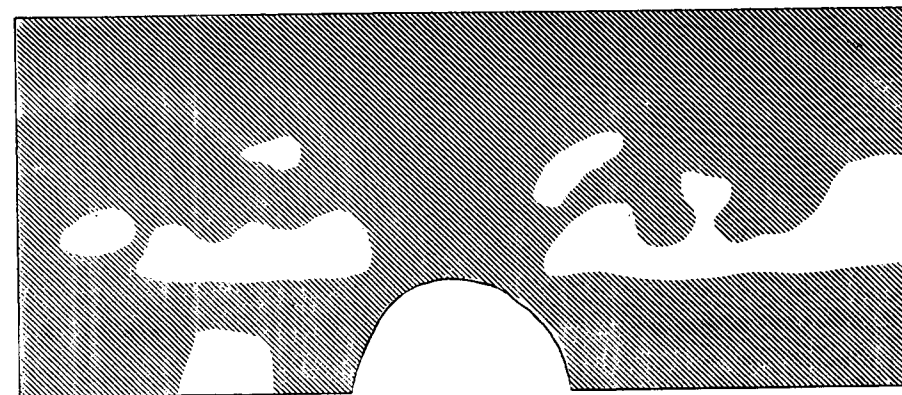
X STRAINS - FAST TEST  
2880 PSI



X STRAINS - SLOW TEST  
2880 PSI

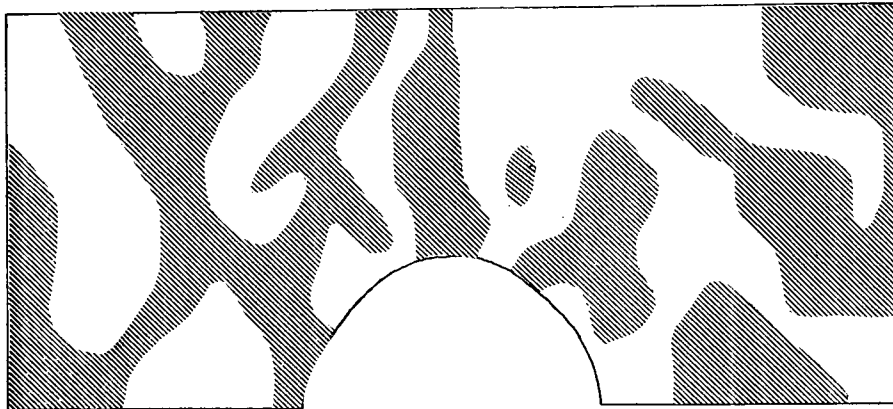


Y STRAINS - FAST TEST  
2880 PSI

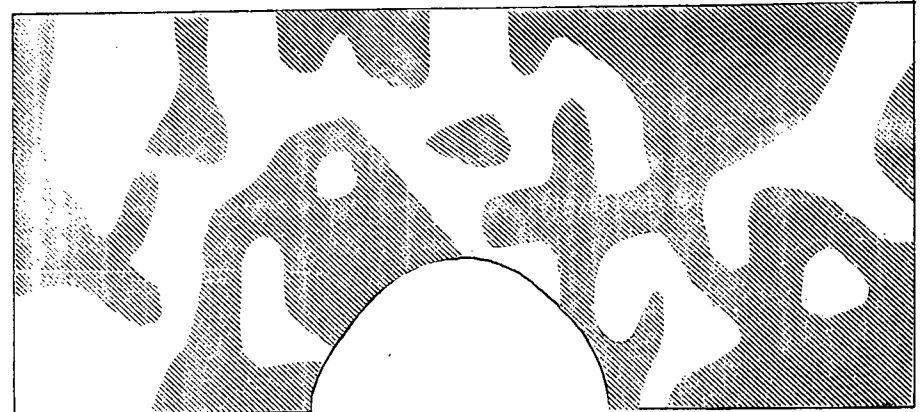


Y STRAINS - SLOW TEST  
2880 PSI

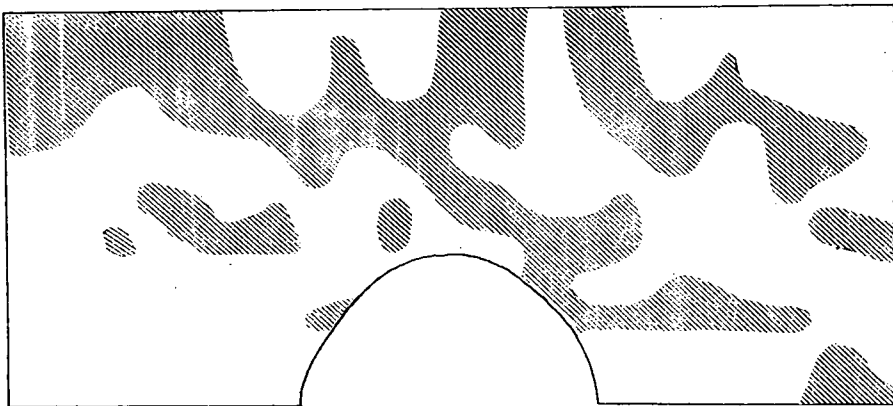
SPECIMEN 2 TENSION SHOWN SHADED  
Fig. 2 - 8



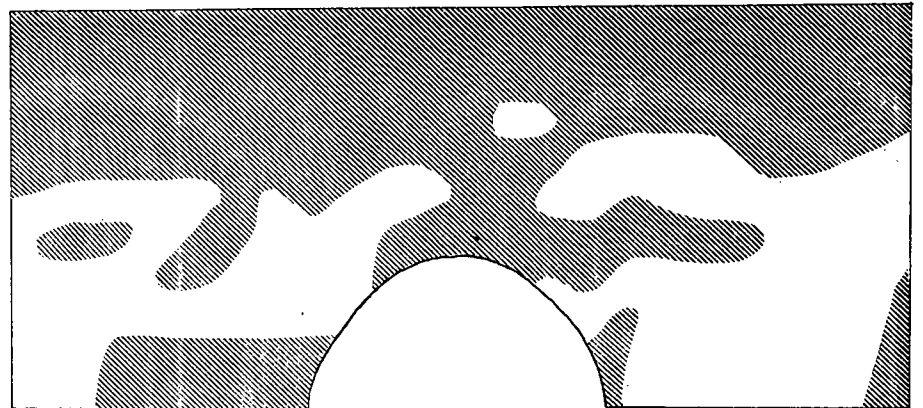
X STRAINS - FAST TEST  
1920 PSI



X STRAINS - SLOW TEST  
1920 PSI



Y STRAINS - FAST TEST  
1920 PSI



Y STRAINS - SLOW TEST  
1920 PSI

SPECIMEN 3 TENSION SHOWN SHADED  
Fig. 2 - 9

Fig. 2.7 that the hypothesis of an expanding tension region perpendicular to grain adjacent to a knot might have validity. The preliminary tests were useful as well in demonstrating how the experimental results could best be organized for reduction on the computer. The remaining four tests were performed and analyzed according to the method explained above.

The strains in the X and Y directions were plotted independently for each test, and the fast test results were compared with those for the slow tests. Attempts were initially made to plot contours of strain magnitude, but following an error analysis it was found that the strain magnitude at discrete points had less significance than the sizes of the regions in tension and compression, which were consistent through the error study. Because of errors inherent in the method, the calculated strains represented a set of numbers which was useful and consistent although individual strain magnitudes might not be strictly accurate. Strains between two points were plotted at the midpoint of the straight line joining them, and linear interpolation was used in separating the tension from the compression regions. Some discretion was used in smoothing the curves. Figs. 2.7, 2.8 and 2.9 represent identical faces of the specimens for both the fast and the slow test of each set. It can be noted from Fig. 2.1 that if the photographs had been used directly, mirror images of the strain fields would be shown. This correction was

made internally by the computer program.

Before discussing the results, some of the uncertainties in the analysis should be mentioned. The dots on the photographs had poorly defined edges so that they could not be trapped as precisely as in Fig. 2.6. After finishing the measurements on each photograph however, several points were remeasured and the positions of their centres were found to be in agreement to within .001 to .003 inches of the original readings. Any incremental error as readings were taken from one side of the photograph to the other was minimal since a given point was compared only with those immediately adjacent to it, and the positions of all points were independently related to the reference frame scale. Another possible error arose from the measurement of displacements in the X direction along straight lines rather than along curved lines parallel to an assumed neutral axis. This problem was examined and the differences between the method used and a more accurate one were found to be negligible in even the most severe cases.

The camera was set up only twenty inches horizontally from the specimen so that wide variations in calibration were observed over the area of the photograph and the linear interpolations used in calibrations may not have been strictly accurate. As well, the photographic enlargement process was carried out by a commercial establishment which, although doing everything possible to

maintain accuracy, could not guarantee the precision. All of these uncertainties were minor but could have had some effect on individual strain magnitudes. Any changes measured between the fast and slow tests were significant however since all of these considerations were consistent for all tests.

## 2.8 Results

A summary of the specimen failure stresses and of the stresses on the gross section at which the strains were measured from the photographs is presented in Table 2.1. The photographs measured were those showing the board having only the weight of the loading frame applied and those at the maximum load before visible cracking. The latter were chosen because the largest possible displacements were desirable in order to give the greatest significance of results. Measuring visibly cracked material involved discontinuous displacements and would have precluded comparison with simple computer simulations as well as with structural material before failure. In design, the important stress level in a material is that which can be accepted prior to failure.

Specimen P had different loading rates, a different loading rate factor (as defined above), and a much smaller knot than did the specimens of series 2 and 3. The P series results indicated that the logistics of adjusting the camera required a slower fast test, and that a larger knot

## TESTING SCHEDULE

| Specimen | Loading Rate                             | Failure Stress on Gross Section<br>psi | Stress Increment on Gross Section Analyzed<br>psi |
|----------|--|--|---|
| P-1      | $\frac{480 \text{ psi}}{15 \text{ sec}}$ | 4800                                   | 4800  |
| P-2      | $\frac{480 \text{ psi}}{24 \text{ hrs}}$ | 2880                                   | 1920  |
| 2-1      | $\frac{480 \text{ psi}}{\text{min}}$     | 3360                                   | 2880  |
| 2-2      | $\frac{480 \text{ psi}}{24 \text{ hrs}}$ | 2880                                   | 2880  |
| 3-1      | $\frac{480 \text{ psi}}{\text{min}}$     | 2880                                   | 1920  |
| 3-2      | $\frac{480 \text{ psi}}{24 \text{ hrs}}$ | 3360                                   | 1920  |

Table 2.1

was required if significant displacements were to be easily measured.

The strains in the X direction (i.e. perpendicular to grain immediately to the left and right of the knot and approximately parallel to grain elsewhere) ranged from approximately  $-.0150$  to  $+.0200$ . The average X- strains in all regions were of similar magnitude although pockets of high tensile and compressive strains appeared near the knots. The main difference in X- strain magnitudes from fast to slow tests was a strong tendency toward increased tension (or reduced compression) in the latter. The size of this strain change varied from zero to about  $+.0020$  although most of the regions enjoyed relatively small alterations of the order of  $+.0050$ . The area around the knot did not show any more of a difference in strain magnitudes in the X direction than did the rest of the board when the fast and slow series were compared.

The strain magnitudes in the Y direction (i.e. in general perpendicular to grain above the knot and some distance to the sides of it, and approaching parallel to grain immediately beside the knot) were of the order of  $-.0150$  to  $+.0150$  in fast tests,  $-.0200$  to  $+.0200$  in one slow test (specimen 2) and  $-.0100$  to  $+.0070$  in the other slow test (specimen 3). The difference in strain magnitudes was about three times greater for specimens 2 than for specimens 3, indicating perhaps that the creep effect perpendicular to grain was greatly accented by a higher

stress level. As well, in specimen 2 shown in Fig. 2.8, all of the differences were towards tensile strains while specimen 3, shown in Fig. 2.9, had some of its strains approach compression for the slow test as compared to the fast one. The general tendency for specimen 3 was however toward increased tension in the Y direction. For both series 2 and 3 the strains in the Y direction in the middle third of the test region, where the knot was located, were 75 per cent higher than were those farther away. This indicated that the presence of a knot greatly accents the straining perpendicular to grain. All series showed a marked increase for slow tests over fast tests in the magnitudes of the tensile strains and in the size of the tensile region in the Y direction.

The areas of the tensile regions in both the X and Y directions in the test area were measured using a planimeter on Figs. 2.7, 2.8 and 2.9. The results are presented in Table 2.2. The rate factor is the ratio of the loading rate in the fast case to that of the slow case. Tests P were not included in the averages because of the different loading rates, the smaller knot and the smaller number of points available for the calculation of strains.

Although the tensile strain area in the X direction experienced substantial magnification, it appeared that the majority of relaxation took place in the Y direction. Relaxation is defined here as a tendency

## TENSION ZONE AREAS

| Specimen | Rate Factor | Fast Test Per cent Tension | Slow Test Per cent Tension | Magnification $\frac{\% \text{ Slow Tension}}{\% \text{ Fast Tension}}$ |
|----------|-------------|----------------------------|----------------------------|---|
| P        | 5760        | 54                         | 8                          | .15   |
| 2        | 1440        | 39                         | 82                         | 2.10  |
| 3        | 1440        | 57                         | 65                         | 1.14  |

Average magnification of 2 and 3= 1.62

Table 2.2A X Direction

| Specimen | Rate Factor | Fast Test Per cent Tension | Slow Test Per cent Tension | Magnification $\frac{\% \text{ Slow Tension}}{\% \text{ Fast Tension}}$ |
|----------|-------------|----------------------------|----------------------------|---|
| P        | 5760        | 14                         | 66                         | 4.71  |
| 2        | 1440        | 23                         | 86                         | 3.74  |
| 3        | 1440        | 34                         | 62                         | 1.82  |

Average magnification of 2 and 3= 2.78

Table 2.2B Y Direction

toward inelastic straining under constant load. It does not imply that local stresses are constant. Examining Figs. 2.7, 2.8 and 2.9 for strains in the X direction, an increase in the size of the tensile strain zone adjacent to the knot can be seen for the slow tests. To the sides of each knot this strain in the X direction has a substantial component perpendicular to grain.

The tensile strain field areas in the Y direction were substantially larger for all specimens in the slow tests than in the fast tests as can be seen in Table 2.2. Further, the fields became more uniform in tension on the knot periphery. That is, the tensile zone tended to surround the knot rather than just abut onto it in places. The majority of the tension perpendicular to grain zone increase occurred above the knot and along the edges of the board. By combining the tension fields in the X direction beside the knot and in the Y direction above it a tremendous growth in the size of the region in tension perpendicular to grain can be seen for the slow tests over the fast tests. It was unfortunate that because of the small displacements observed it was impossible to examine intermediate stress levels to determine the stresses at which the majority of the straining perpendicular to grain took place.

The strain diagrams seem to show that the laws of equilibrium in bending have been violated. It was not clear exactly what caused this effect but it was seen in

all cases. Most likely, the strain pattern through the wood varies somewhat from that visible on the surface so that overall a typical bending strain distribution is present. This does not affect the significance of the measured increases in strain perpendicular to the surface grain.

## 2.9 Failure Modes

The rapidly loaded specimen of series P failed away from the knot, but the five others broke adjacent to it. Initiated usually by perpendicular to grain cracking at the adverse grain slope adjacent to the knot, failure occurred in one of two ways. The first, which happened in fast tests, involved a rapid fracturing of material so that the board was broken explosively as in Fig. 2.10. The second, occurring in the slow tests, was preceded by a large amount of tensile straining perpendicular to grain above the knot. This caused a crack or cracks to open up above the knot, and this crack gradually spread along the grain with further applications of load until either a shear type failure occurred or the cracked grain reached the edge of the board. There was visible cracking for some time before final failure. An example of this second mode is shown in Fig. 2.11. These two types of failure reinforce the suspicion that since different modes of failure are likely to occur for different rates of loading, the effect of a knot or other dis-

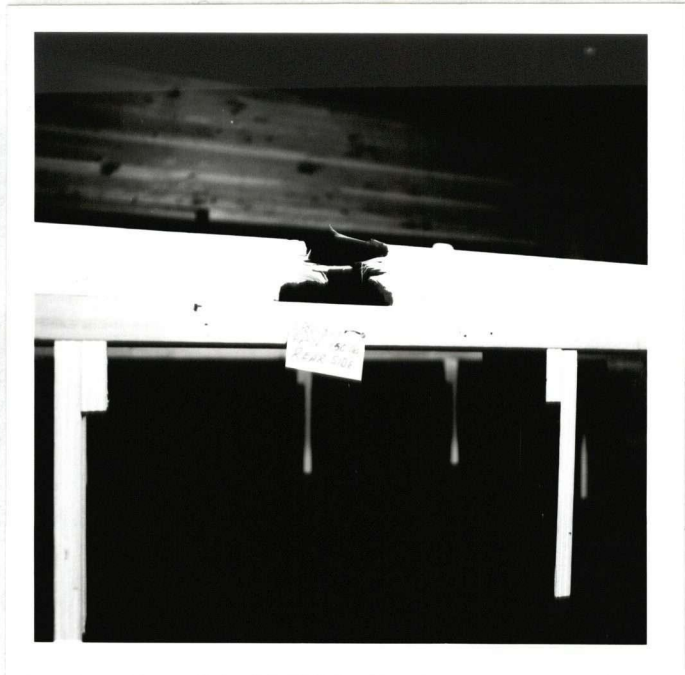
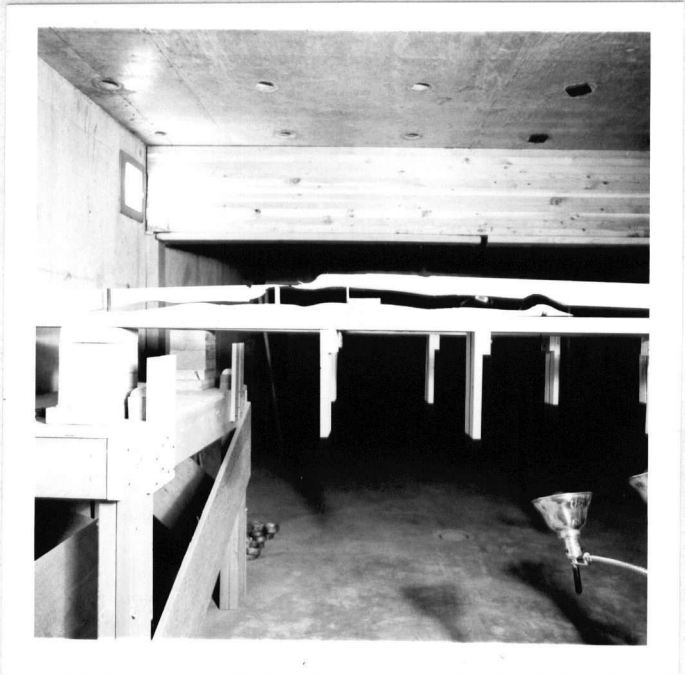


Fig. 2-10 RAPID FAILURE MODE



CRACKS PROPPED OPEN BY SPACERS

Fig. 2-11 SLOW FAILURE MODE

continuity on the strength will also vary with the rate of loading.

### 2.10 Summary

The first part of the two part problem defined in section 1.3 has now been investigated within the scope of this present research. The tensile straining perpendicular to grain is significantly greater for slow loadings than for fast loadings in both magnitude and the size of the area which is affected. The majority of relaxation occurred perpendicular to grain above the knot, indicating that the presence of a grain irregularity increases the amount of straining and therefore the capability for stress redistribution. That some smoothing of stress raising irregularities occurs with long duration loadings is indicated by the greater uniformity of the shape of the tensile strain zones than with fast loading. The evidence of this smoothing effect is further reinforced by the 'softer' or more gradual type of failure experienced by slowly loaded specimens.

## CHAPTER 3

### INFLUENCE OF STIFFNESS PERPENDICULAR TO GRAIN

#### 3.1 Introduction

The work of the previous chapter showed that considerably more tensile straining perpendicular to grain occurred in slow tests than in rapid tests. The next stage in investigating the hypothesis of section 1.3 was to investigate whether or not a time dependent stiffness perpendicular to grain, such as found in pure specimens, would produce strain fields similar to those found experimentally around a knot.

The procedure chosen for the investigation of the effect of stiffness perpendicular to grain was the finite element method. Plane stress behaviour in bodies of irregular shape can be thus programmed for solution on a computer. In this way as well, grain structure can be modelled and then assembled to form the final structure of the material.

### 3.2 The Finite Element

The basic finite element theory is well known<sup>6</sup> so that only a brief description need be presented here. Consider a body subjected to stresses and displacements along parts of its boundary, and then consider dividing this domain into a number of subdomains with nodes along their edges. By deducing how each subdomain or element behaves in terms of displacements and forces at these nodes, and then combining all of these elements by matching degrees of freedom and summing corresponding forces at the nodes a solution can be obtained. This produces the standard stiffness problem and can be solved by traditional methods.

In order to model the in-plane behaviour of a beam, plane stress finite elements were used. The constraints on the particular element for this problem were that stiffnesses must be amenable to alteration parallel and perpendicular to the grain of the wood and not just to global axes, strings of elements must be able to change direction to model the curvature of the grain, the elements must be able to represent tension, compression and shear stresses, and there must be sufficient accuracy to ensure that the changing of a single elastic modulus will produce significant and consistent results. Constant strain triangles were initially used but were found to be grossly inaccurate when tested on a cantilever beam. A linear stress orthotropic six node triangle with

different elastic modulae parallel and perpendicular to one edge was therefore selected. The derivation of this element was carried out and the elements were tested in a few simple cases. Details are presented in Appendices A and B, and a copy of the computer program is enclosed as Appendix C.

### 3.3 The Problem

To obtain satisfactory results and to model the grain curvature as accurately as possible, it was desirable to examine a fine mesh of finite elements. Because of the expense involved however, a parametric analysis was performed on a fairly coarse mesh in order to select the optimal modulae for input to a larger problem, to investigate how some of the elastic parameters affect the strain distribution around a knot, and to obtain some preliminary results for comparison with the experimentally obtained strain distributions.

It was beyond the scope and the purpose of this investigation to try to refine a finite element that would accurately reflect the behaviour of wood. One stage modelling only was used. Simplifications like assuming the same elastic modulae for wood in tension and compression and ignoring the effects of local fibre tearing were made. The sole purpose here was to examine the effect of one set of orthotropic stress-strain modulae on the overall strain pattern of the model described below.

Madsen's recent work has shown that the time dependent stiffness (combined elastic and inelastic straining) decreases with the rate of loading. Tests on material containing knots, adverse grain slope, and other discontinuities showed little variation in either the modulus parallel to grain or the bending strength, with the duration of load application for those boards in a sample which fail at the lower per centiles of strength.<sup>2,3</sup> The time dependent stiffness perpendicular to grain did however exhibit a very marked decrease as the duration of loading was lengthened. To repeat the original hypothesis then, large magnitude tensile straining perpendicular to grain might provide a mechanism for stress redistribution around discontinuities so as to minimize their effect on the strength of the material.

Decreasing the elastic stiffness perpendicular to grain in the finite elements was used to model the effects of long duration loadings on the stresses and strains around a simulated knot. Since in the parametric analysis of an elastic body all changes are relative and linear, it was found useful to arbitrarily fix the apparent modulus parallel to grain at  $1.8 \times 10^6$  psi and the Poisson's ratio for straining perpendicular to grain resulting from application of load parallel to grain at .30. The former is believed to decrease by only 10 to 20 per cent during the time periods examined here, and reliable information could not be found about the latter.

Table 3.1 shows the input data used for the main part of the investigation. The subscripts x and y on  $E_x$  and  $E_y$  refer to the element x and y axes, not to the global X and Y axes. A series of test calculations was run in which the ratio of Poisson's ratios  $\nu_{yx}/\nu_{xy}$  was varied and in which the shear modulus was increased by a factor of 10. In the 'slow-G reduced' test calculations, the shear modulus was reduced by 30 per cent to approximately model to findings of a previous study.

It was recognized that by altering the apparent Young's modulae without changing the Poisson's ratios, the laws of conservation of energy and in particular the reciprocal theorem were violated. This problem was ignored for two reasons. First, in the real material it was unclear how much each Poisson's ratio would change and second, the reduced apparent Young's modulus perpendicular to grain was in the real case likely caused by creep, an inelastic effect, so that conservation of energy did not apply. As well, a series of tests showed alterations in the Poisson's ratio to have had negligible effect on results in the program.

Using a high power microscope, the grain around five knots (that is, twenty quarters of knots) was traced. Using these tracings, the distance in radii from the knot centre to the beginning of grain curvature, and the angle of grain at specific normalized coordinate locations were measured for each case. After averaging

## PARAMETRIC ANALYSIS DATA

| Case Name  | $E_x$<br>psi      | $E_y$<br>psi      | $\nu_{xy}$ | $\nu_{yx}$ | G<br>psi           | $E_x/E_y$ |
|------------|-------------------|-------------------|------------|------------|--------------------|-----------|
| Isotropic  | $1.8 \times 10^6$ | $1.8 \times 10^6$ | .30        | .30        | $6.90 \times 10^5$ | 1         |
| Fast       | $1.8 \times 10^6$ | $.9 \times 10^5$  | .05        | .30        | $1.15 \times 10^5$ | 20        |
| Median     | $1.8 \times 10^6$ | $.3 \times 10^5$  | .05        | .30        | $1.15 \times 10^5$ | 60        |
| Slow       | $1.8 \times 10^6$ | $.1 \times 10^5$  | .05        | .30        | $1.15 \times 10^5$ | 180       |
| Slow G red | $1.8 \times 10^6$ | $.1 \times 10^5$  | .05        | .30        | $.85 \times 10^5$  | 180       |

$E_x$  = Young's modulus parallel to grain

$E_y$  = Young's modulus perpendicular to grain

$\nu_{xy}$  = Poisson's ratio for straining parallel to grain caused by stress applied perpendicular to grain

$\nu_{yx}$  = Poisson's ratio for straining perpendicular to grain caused by stress applied parallel to grain

Table 3.1

these parameters, the single quarter knot which most closely resembled the average was used for modelling. Unfortunately the grain density could not be directly measured. When lines were made continuous to follow the known directions of grain at every point however, a grain density resulted. Finally, an element mesh was drawn into the diagram and the result was a problem consisting of thirty-five elements and eighty-eight nodes. The resulting model is shown in Fig. 3.1. This was small enough to be solved in the core of the computer and was sufficiently inexpensive to run that it was suitable for a parametric study. Fig. 3.2 shows this mesh. The finite elements were placed into the modelled grain by forcing a certain edge of each element (the 1-2 edge in Appendix A) to be oriented parallel to the grain boundary. The elastic modulae of each element were oriented parallel and perpendicular to this edge. The edges parallel to grain have double lines in Fig. 3.2.

The loadings were of arbitrary magnitude and were applied in both bending and pure tension. The examination in bending was for comparison with experimental results and that in tension was to show a little more clearly the effects of parametric manipulations since the applied stress/strain gradient would be absent. Since the problem was programmed as linear elastic, a pure compression loading would have produced exactly the same results as for pure tension but with the signs reversed.

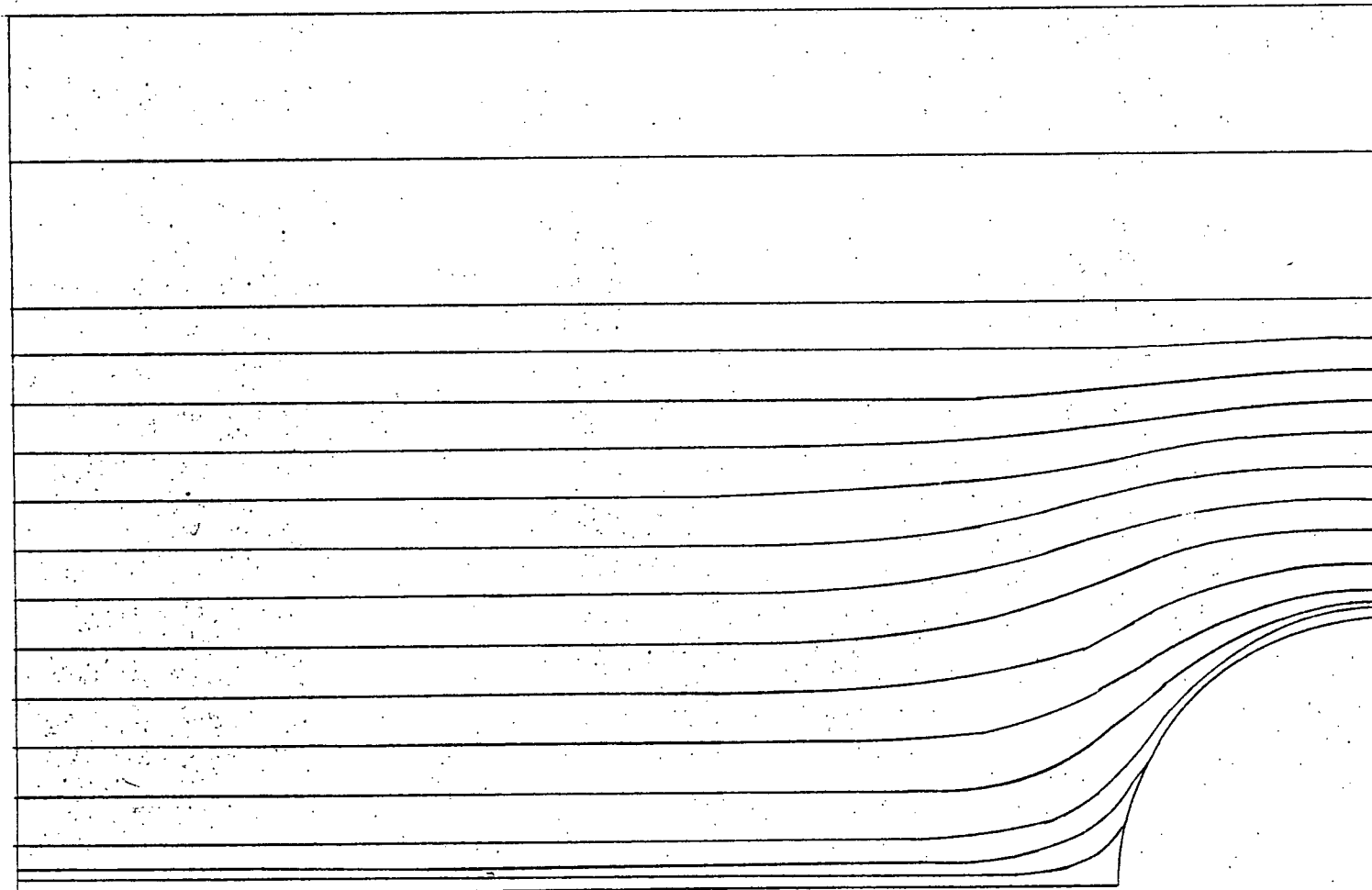


Fig. 3-1 TYPICAL GRAIN PATTERN

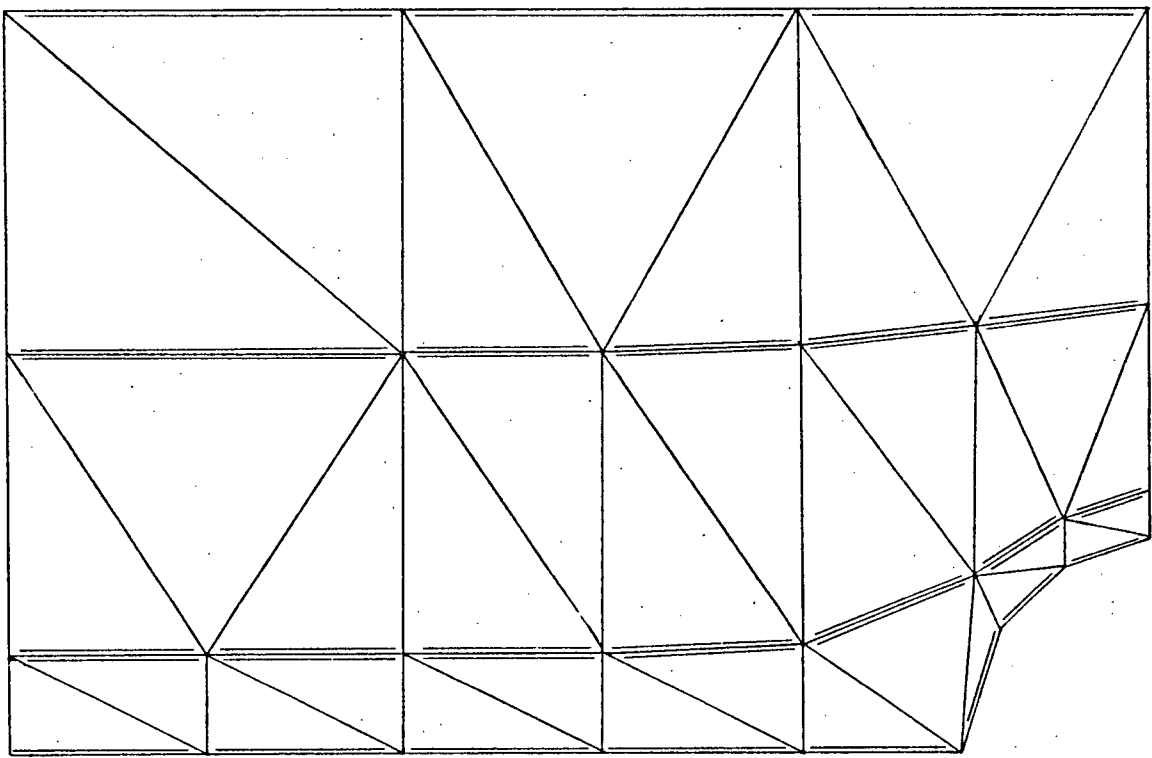


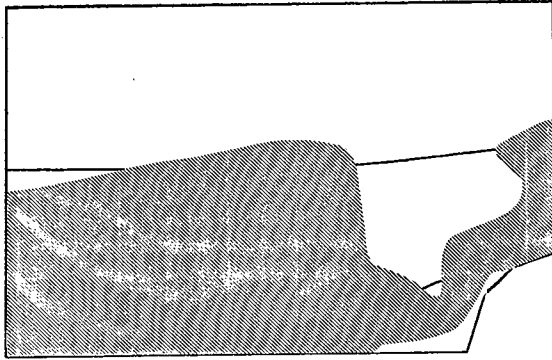
Fig. 3-2 35 ELEMENT MODEL

Symmetry was employed by forcing the nodes above the right hand edge of the knot to have zero horizontal displacement. Vertical support was supplied by restraining one of the nodes at the left hand side of the mesh. The boundary conditions did not provide any restraint along the bottom edge of the model.

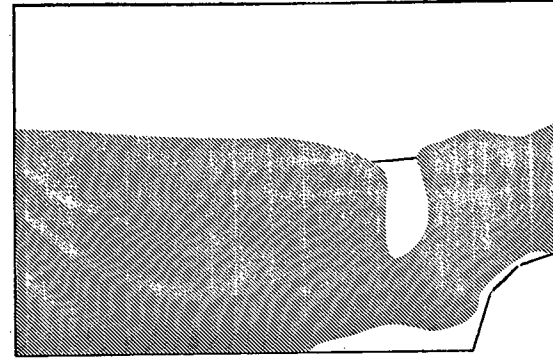
### 3.4 Results of the Parametric Study

The calculated results obtained directly were strains in the global X and Y directions at each node. By rotating all strains into these axes an average strain was obtained that could be presented in the same form as the experimental results. Using the strains in the global coordinate directions, plots showing the tension and compression regions of the model were drawn. These were important in showing those regions in which tension perpendicular to grain was produced and in which therefore large scale stress redistribution would be encouraged. The relative magnitudes of the strains were also examined.

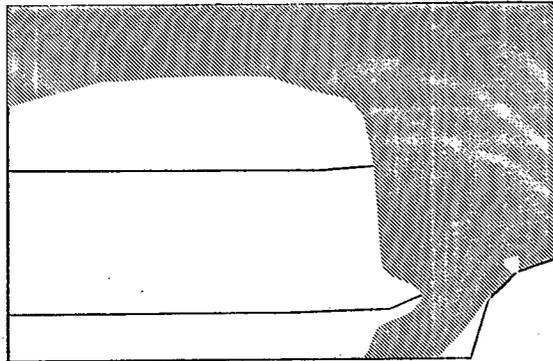
Figures 3.3, 3.4 and 3.5 show the positions and sizes of the tension and compression regions for bending moment loading. Fig. 3.3 was produced for comparison with Figs. 2.7, 2.8 and 2.9. It may be observed that the tensile strain fields in the global Y direction grew laterally as the ratio of  $E_x/E_y$  was increased. Similarly, the strains in the global X direction tended to become more tensile beside the knot as  $E_x/E_y$  increased.



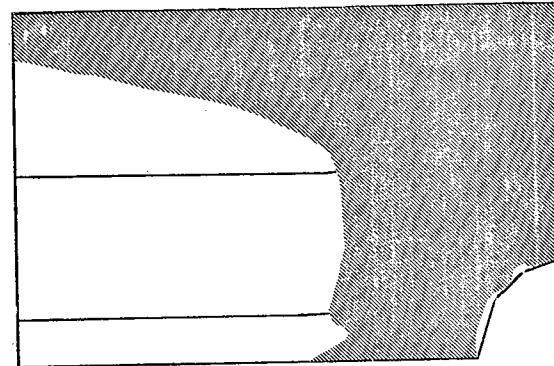
(a) 'Fast' X Strains  
 $E_y = .9 \times 10^5$



(b) 'Slow' X Strains  
 $E_y = .1 \times 10^5$



(c) 'Fast' Y Strains  
 $E_y = .9 \times 10^5$



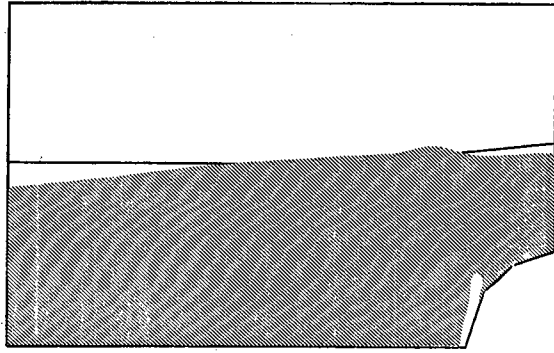
(d) 'Slow' Y Strains  
 $E_y = .1 \times 10^5$

|                         |
|-------------------------|
| (a),(b),(c),(d)         |
| $E_x = 1.8 \times 10^6$ |
| $\nu_{xy} = .05$        |
| $\nu_{yx} = .30$        |
| $G = 1.15 \times 10^6$  |

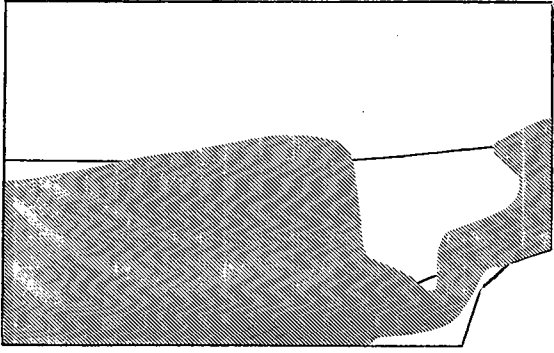
TENSION SHOWN SHADED

BENDING

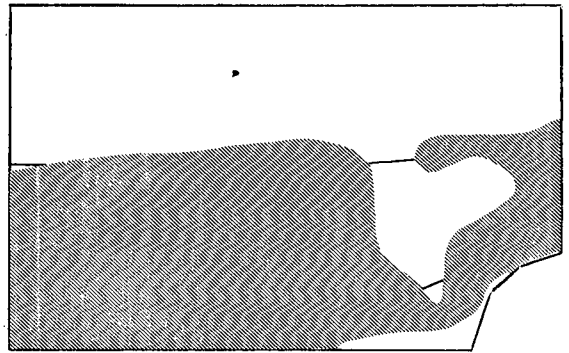
Fig. 3-3



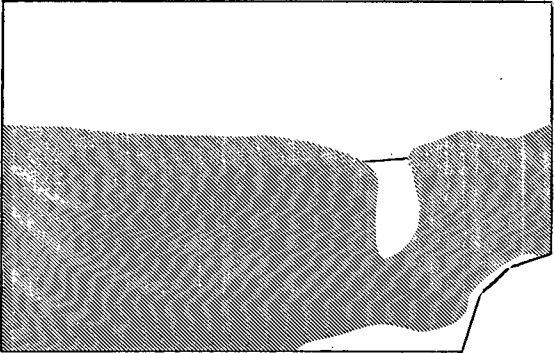
(a) Isotropic



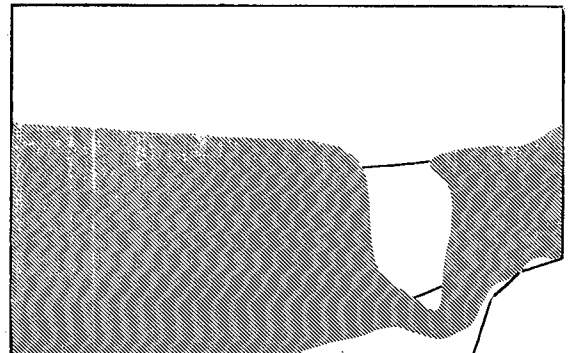
(b) 'Fast'  $E_y = .9 \times 10^5$



(c) 'Medium'  $E_y = .3 \times 10^5$



(d) 'Slow'  $E_y = .1 \times 10^5$

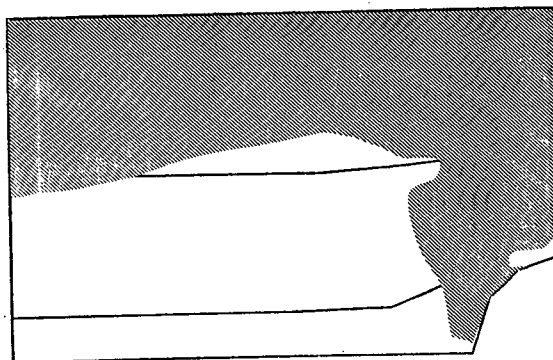


(e) 'Slow - G Reduced'  $E_y = .1 \times 10^5$

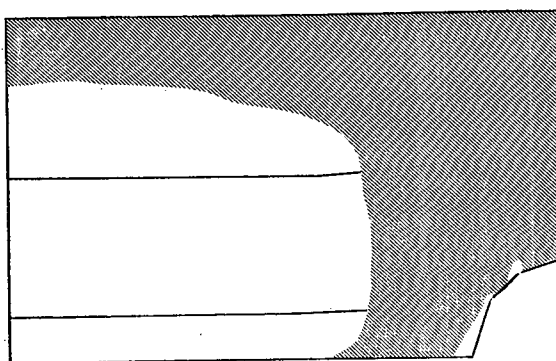
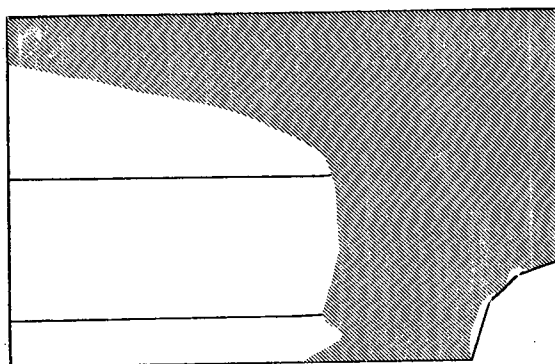
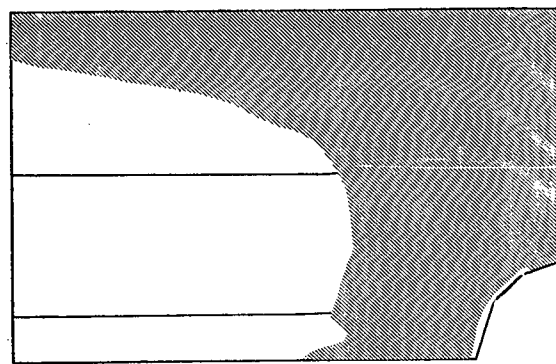
| (a)                     | (b),(c),(d)        | (e)               |
|-------------------------|--------------------|-------------------|
| $E_x = 1.8 \times 10^6$ | $1.8 \times 10^6$  | $1.8 \times 10^6$ |
| $E_y = 1.8 \times 10^6$ |                    |                   |
| $\nu_{xy} = .30$        | .05                | .05               |
| $\nu_{yx} = .30$        | .30                | .30               |
| $G = 6.9 \times 10^5$   | $1.15 \times 10^5$ | $.85 \times 10^5$ |

TENSION SHOWN SHADED  
BENDING X STRAINS

Fig. 3-4



(a) Isotropic

(b) 'Fast'  $E_y = .9 \times 10^5$ (c) 'Medium'  $E_y = .3 \times 10^5$ (d) 'Slow'  $E_y = .1 \times 10^5$ (e) 'Slow - G Reduced'  $E_y = .1 \times 10^5$ 

| (a)                     | (b),(c),(d)        | (e)               |
|-------------------------|--------------------|-------------------|
| $E_x = 1.8 \times 10^6$ | $1.8 \times 10^6$  | $1.8 \times 10^6$ |
| $E_y = 1.8 \times 10^6$ |                    |                   |
| $\nu_{xy} = .30$        | .05                | .05               |
| $\nu_{yx} = .30$        | .30                | .30               |
| $G = 6.9 \times 10^5$   | $1.15 \times 10^5$ | $.85 \times 10^5$ |

TENSION SHOWN SHADED

BENDING Y STRAINS

Fig. 3-5

Adjacent to the knot, the strains in both the X and Y directions were tensile. These trends are the same as the experiment if one takes higher  $E_x/E_y$  ratios to represent slower test loadings. However the amount of tensile strain region growth here was not as much as in the experiments.

The disparities in the sizes of tension regions between the experiment and the finite element solution probably resulted from the crude modelling of the problem. In real material, the elastic modulae need not be identical throughout the specimen and may vary with changes in the grain density as it curves around the knot. As well, of course the modulae are not perfectly elastic in real material. Further the difference in the elastic modulae for tension and compression was not included. However the modelling did reproduce the experiment trends and therefore further work using this model seemed justified.

### 3.5 The $E_x/E_y$ Ratio

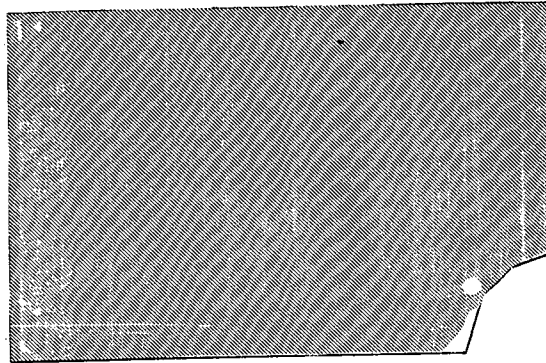
Under bending simulation, the strains in the X direction along the bottom of the board became smaller as the knot was approached, and the distance from the knot at which this decrease became significant increased with the  $E_x/E_y$  ratio. As the simulated knot was approached from the left the maximum tensile strains moved away from the base of the board toward the midheight until the knot was reached at which point the maximum strains in the X direction

occurred again at the bottom of the section (that is, directly above the knot). This effect was accentuated as  $E_x/E_y$  was increased indicating that the material immediately beside the knot was carrying less load as the stiffness perpendicular to grain was reduced, and that therefore the semicircular notch was becoming relatively more shallow and less of a stress or strain concentrator. Strains in the X direction near the knot were much larger than those away from it in the same grain in the tension region, and the strain concentration factor (comparing average strains in the bottom grain away from the knot with those in the same grain above the knot in an ad hoc manner) increased from 1.56 for the isotropic case to 2.88 for  $E_x/E_y = 20$  to 4.95 for  $E_x/E_y = 180$ . That is, reductions in  $E_y$ , the apparent stiffness perpendicular to grain, produced much greater changes in the X- strain in the curved area near the knot than in the straight grain farther away. The strains perpendicular to grain were also much greater near the knot than away from it, but strain concentration factors as calculated for the X direction could not be obtained here because at some ratios of  $E_x/E_y$  many of the nodal strains in the affected region were in compression. Figs. 3.4 and 3.5 show as well that the tensile strain fields both parallel and perpendicular to grain increased in size as the  $E_x/E_y$  ratio was increased.

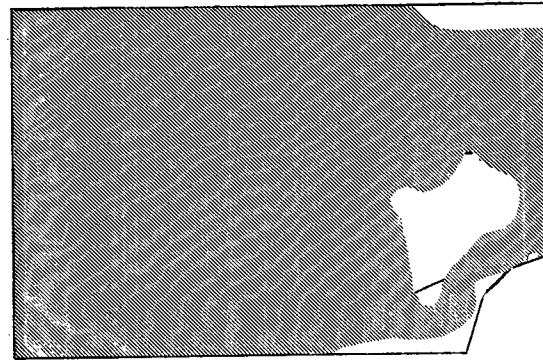
With pure tension loading there was of course

no neutral axis. Figs. 3.6 and 3.7 show the tension regions loaded for this case. The uniform tensile strains in the X direction at the left hand edge of the model became concentrated toward the centre of the beam as the knot was approached. As in bending however, the maxima occurred immediately above the knot. With  $E_x/E_y = 20$  a compression zone existed to the left and slightly above the knot. Both the size of this compression zone and the magnitude of its strains decreased as the degree of orthotropy was increased. At the same time, the bottom edge of the board became less highly strained in the X direction. The strain concentration factors as defined above were for this case 2.77 for isotropic, 4.13 for  $E_x/E_y = 20$  and 7.18 for  $E_x/E_y = 180$  so that again increasing orthotropy had greater effect on strains near the knot than on those away from it. The strains in the Y direction were, as expected, in uniform compression away from the knot. As the knot was approached from the left, this compression became localized toward the centre of the board until near the knot the entire section went into tension. Maximum strain magnitudes were found directly above the knot and, as for bending, the sizes of the tension fields in both the X and Y directions increased with  $E_x/E_y$ .

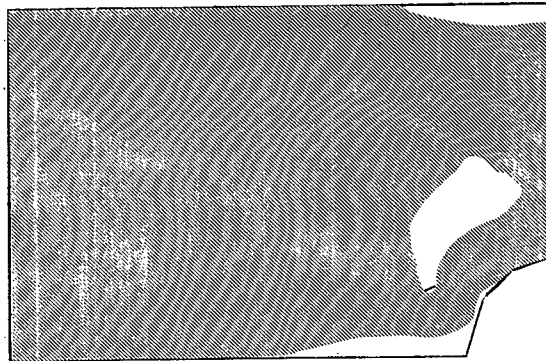
The directions of principal stress and strain were produced by the computer program, but the coarseness of the mesh and the small number of points at which the stresses and strains were calculated made it impossible



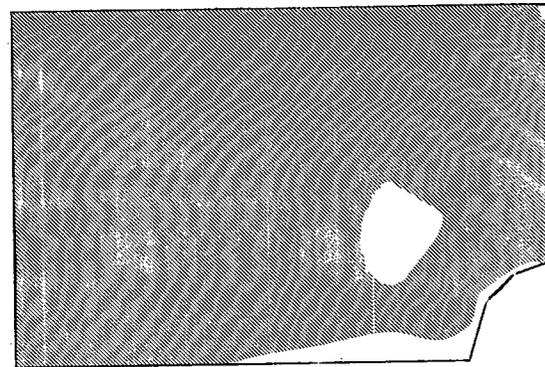
(a) Isotropic



(b) 'Fast'  $E_y = 9 \times 10^5$



(c) 'Medium'  $E_y = 3 \times 10^5$

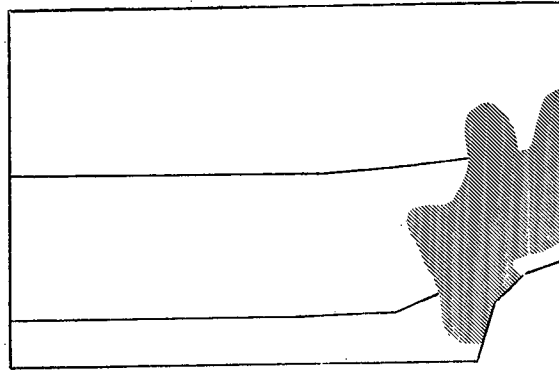


(d) 'Slow'  $E_y = .1 \times 10^5$

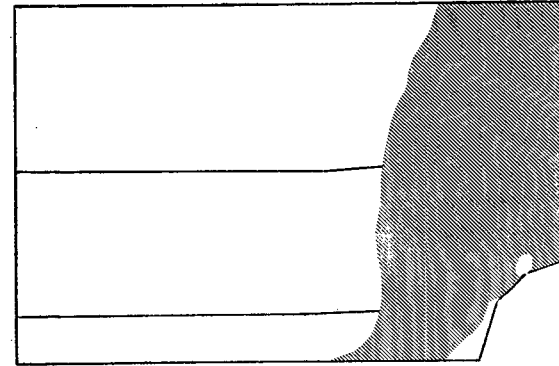
| (a)                     | (b),(c),(d)        |
|-------------------------|--------------------|
| $E_x = 1.8 \times 10^6$ | $1.8 \times 10^6$  |
| $E_y = 1.8 \times 10^6$ |                    |
| $\nu_{xy} = .30$        | .05                |
| $\nu_{yx} = .30$        | .30                |
| $G = 6.9 \times 10^5$   | $1.15 \times 10^5$ |

TENSION SHOWN SHADED  
TENSION LOADING X STRAINS

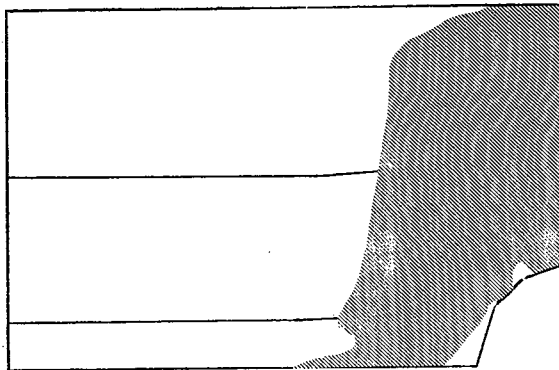
Fig. 3 - 6



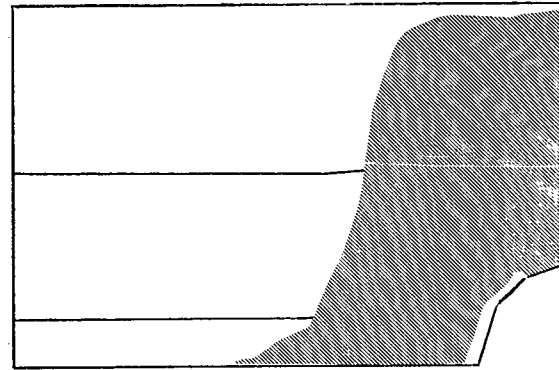
(a) Isotropic



(b) 'Fast'  $E_y = 9 \times 10^5$



(c) 'Medium'  $E_y = 3 \times 10^5$



(d) 'Slow'  $E_y = 1 \times 10^5$

| (a)                     | (b),(c),(d)        |
|-------------------------|--------------------|
| $E_x = 1.8 \times 10^6$ | $1.8 \times 10^6$  |
| $E_y = 1.8 \times 10^6$ |                    |
| $\nu_{xy} = .30$        | .05                |
| $\nu_{yx} = .30$        | .30                |
| $G = 6.9 \times 10^5$   | $1.15 \times 10^5$ |

TENSION SHOWN SHADED  
TENSION LOADING Y STRAINS

Fig. 3 - 7

with this problem to produce a coherent plot of the results. This was done however for a larger problem which will be discussed in the next chapter. Under purely tensile modelling, the principal strains were parallel to grain throughout the mesh except for a region to the left of the knot where they seemed to tend towards being perpendicular to grain. This tendency and the size of the region increased with increasing levels of orthotropy. The same was true for the bending moment model except that because of the applied strain gradient the effects were a little more difficult to see directly. The amount of tension strain perpendicular to grain increased substantially as the apparent Young's modulus ratio was increased.

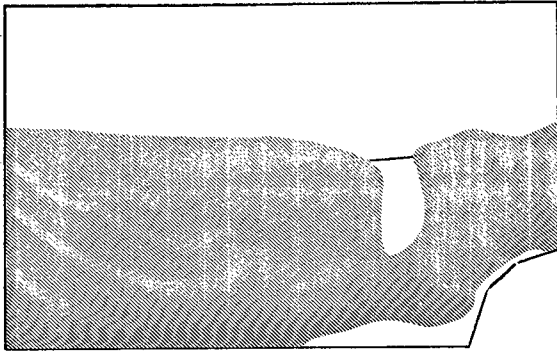
The principal stress directions in pure tension were parallel to grain throughout except near the knot and along the bottom of the beam as the knot was approached. The increase in orthotropy tended to take stress away from the bottom of the beam and redistribute it so that the principal lines of tension flowed smoothly around the knot and apparently made the section approach that of a beam with a gradually decreasing cross-section instead of that of a beam of constant cross-section having a semi-circular notch. This same behaviour was visible in the moment loading case as well.

### 3.6 Shear Modulus Effect

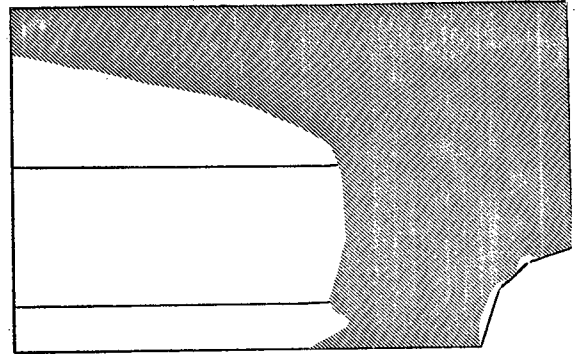
Arbitrarily increasing the shear modulus  $G$  by a factor of 10 also produced virtually the same result as with  $G$  left unchanged. It was found in general that the stiffer the model was in shear, the larger was the tensile strain field in the global  $X$  direction. Since the region of compressive strains in the  $X$  direction more closely approached the knot (in the region where  $X$ - strains approach being perpendicular to grain) when  $G$  was small, a more marked reduction in load with time might be expected for materials weak in shear. Fig. 3.8 shows these effects and indicates as well the danger involved in drawing conclusions from such a peripheral effect. Finally, a larger shear modulus produced a more uniform distribution of strains, and slightly smaller strains in the  $Y$  direction. Fig. 3.9 for tensile loading shows that the tension fields in the  $Y$  direction expand for 'slow' tests with the shear modulus magnified by 10, in the same manner as with the original shear modulus.

### 3.7 Summary

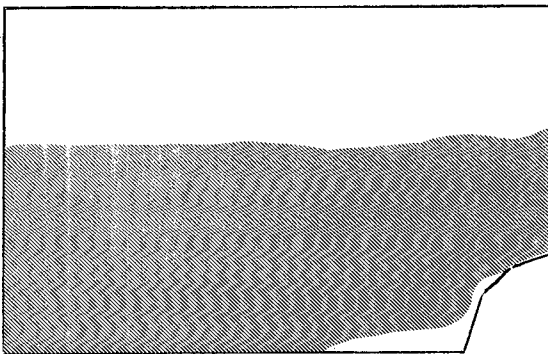
From the preceding work a few conclusions were drawn. First, as the orthotropy of the model was increased, the material on the tension edge of a bending problem adjacent to the knot became relatively stressless and became thereby a less important part of the load carrying mechanism. Second, as this was happening, the tensile



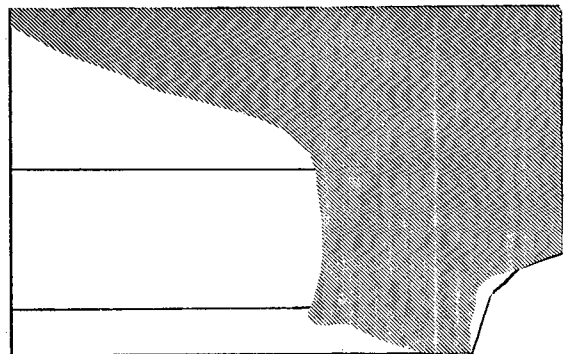
(a) X Strains



(b) Y Strains



(c) X Strains

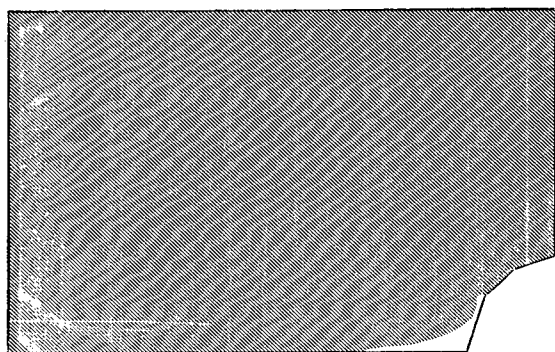


(d) Y Strains

| (a),(b)                 | (c),(d)            |
|-------------------------|--------------------|
| $E_x = 1.8 \times 10^6$ | $1.8 \times 10^6$  |
| $E_y = .1 \times 10^5$  | $.1 \times 10^5$   |
| $\nu_{xy} = .05$        | .05                |
| $\nu_{yx} = .30$        | .30                |
| $G = 1.15 \times 10^5$  | $1.15 \times 10^6$ |

TENSION SHOWN SHADED  
 BENDING 'SLOW' TEST SHEAR MODULUS EFFECT

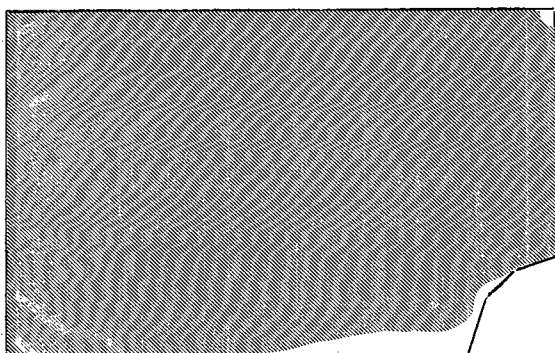
Fig. 3-8



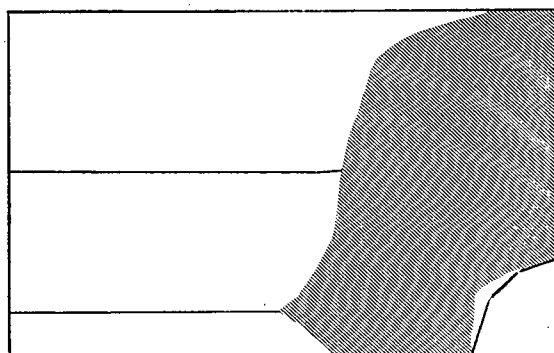
(a) 'Fast' X Strains



(b) 'Fast' Y Strains



(c) 'Slow' X Strains



(d) 'Slow' Y Strains

| (a),(b)                 | (c),(d)            |
|-------------------------|--------------------|
| $E_x = 1.8 \times 10^6$ | $1.8 \times 10^6$  |
| $E_y = .9 \times 10^5$  | $.1 \times 10^5$   |
| $\nu_{xy} = .05$        | .05                |
| $\nu_{yx} = .30$        | .30                |
| $G = 1.15 \times 10^6$  | $1.15 \times 10^6$ |

TENSION SHOWN SHADED

TENSION SHEAR MODULUS EFFECT

Fig. 3-9

strains in the Y direction (roughly perpendicular to grain) were increasing in this region and could have been a factor in allowing stress redistribution. Therefore third, the effect of the knot as a stress raiser was being decreased. This bears out the results of previous studies which have shown construction grade material not to experience significant decreases in strength with time.<sup>2,3</sup> A rapidly loaded beam fails at a knot as if it had been notched, whereas slowly loaded beams have been found to fail in shear or at some adverse slope of grain away from a knot. These different failure mechanisms imply that material with defects cannot be considered to be the same as clear material into which a notch has been cut. Slope of grain apparently magnifies the tensile strain perpendicular to grain and contributes to a smoothing of discontinuities. The results indicated that the semicircular notch in the model tended to behave as a broader defect, avoiding the very high stress concentrations which occur at sharp corners.

## CHAPTER 4

### CIRCULAR HOLE IN A FINITE PLATE HAVING GRAIN TYPE ORTHOTROPY

#### 4.1 Introduction

In Chapter 3, a finite element investigation was made of the effects of orthotropy on the stresses and strains around a semicircular notch on one edge of a beam. The model was subjected to uniform tensile stresses in one case and to a linearly varying stress gradient in another. These simulations were related to experimental work with an edge knot. In real material however, the knot or other discontinuity may occur away from an edge. As an approach to a more general case, a circular hole in a finite plate was modelled. Curving grain surrounded the hole so that the problem was different from that of a hole in a material having orthotropy relative to global X and Y axes. The elements were triangular and had their elastic modulae parallel and perpendicular to one edge. This edge (the 1-2 edge of Fig. A.1) was oriented along the local grain line. The model of this investigation was more detailed than

the 35 element simulation of Fig. 3.2.

#### 4.2 The Problem

The problem configuration was similar to that of Fig. 3.1. Fig. 4.1 shows the model used. It has 419 nodes and 188 elements. Double symmetry was employed by forcing the nodes along the bottom of the finite element mesh to have zero Y displacement and the nodes along the right hand side to have zero X displacement. A consistent uniform tensile load vector of arbitrary magnitude was applied to the left hand side of the model. The elements were those described in Section 3.2 and Appendix A.

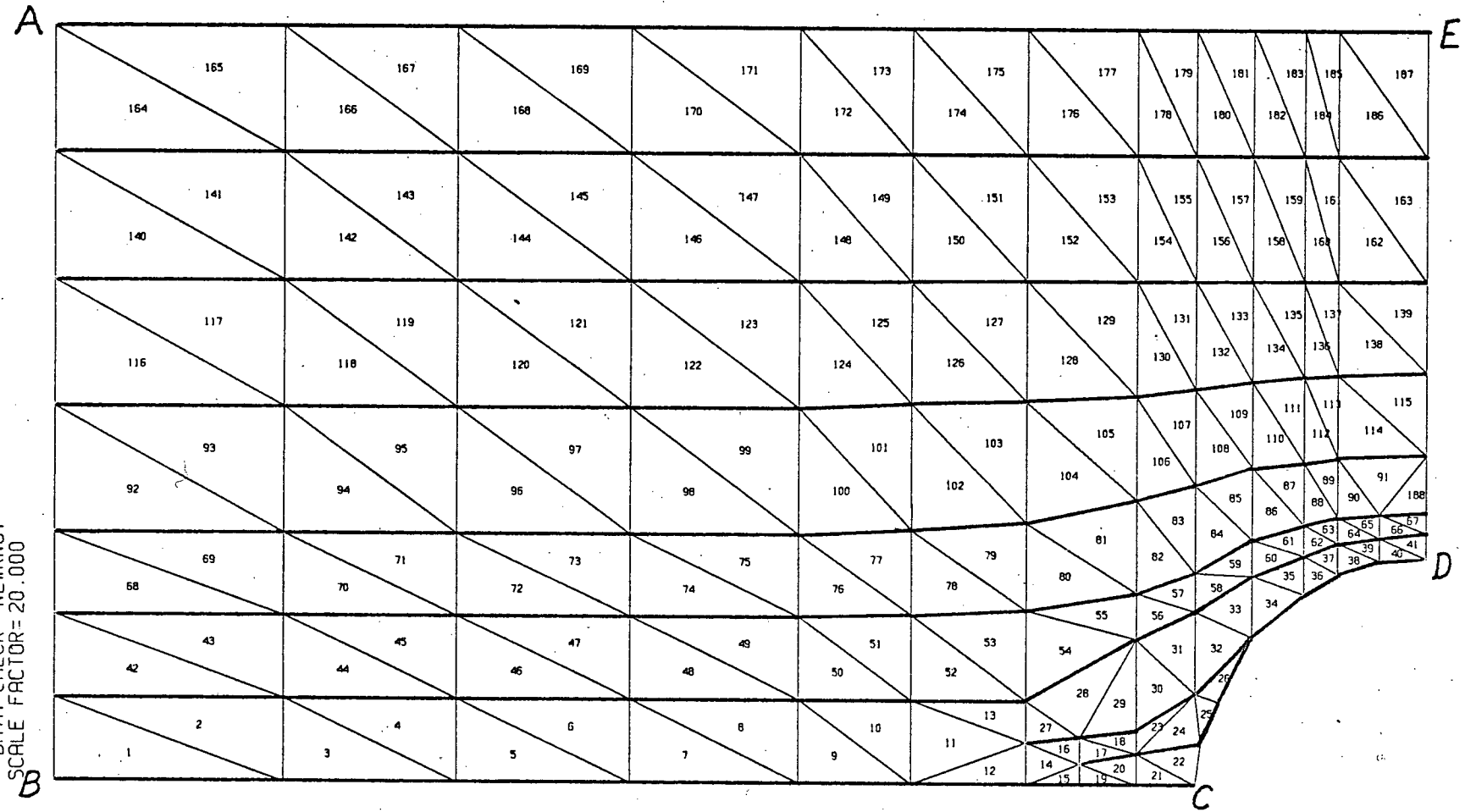
#### 4.3 Preliminary Tests

The model was first examined in the isotropic and  $E_x/E_y = 100$  cases. The results were recorded in Figs. 4.2 and 4.3 for stresses in the X and Y directions respectively. Fig. 4.2 for stresses in the X direction shows that the finite element solution for Fig. 4.1 had good agreement with the analytic solution for an infinite plate when elastic modulae are isotropic. When a large orthotropy ( $E_x/E_y = 100$  with subscripts x and y referring to element axes) was applied, the region adjacent and to the left of the hole went into compression in the X direction. This would tend to decrease the likelihood of tensile cracking as a prelude to failure. In the region above the hole, the peak stress in the X direction was greatly magnified by the application of orthotropy.

CNTR

CLAR PLOT# 00839048.

DATA CHECK--NEWKNOT  
SCALE FACTOR=20.000



HEAVY LINES MARK THE DIRECTION OF GRAIN

Fig. 4-1 188 ELEMENT MODEL

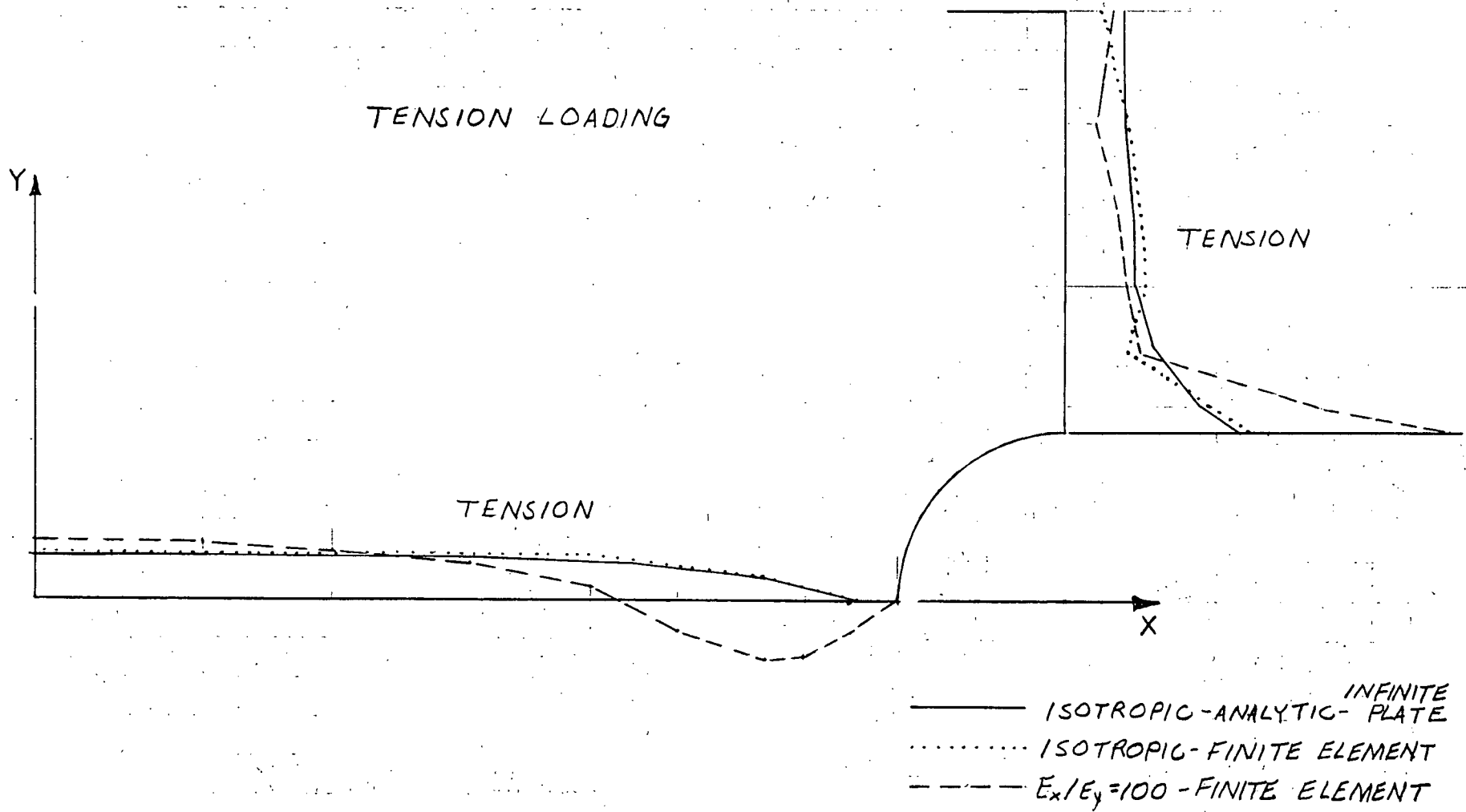


Fig. 4-2 EDGE STRESSES X DIRECTION

The location of the peak stress (immediately above the hole) was unchanged.

Fig. 4.3 for stresses in the Y direction shows substantial differences between the finite element solution of Fig. 4.1, and the analytic solution for a hole in an infinite plate. This was because the finite element model was finite in the Y direction, although it could be considered infinite in the X direction. The distribution of stress was however similar in both cases, with peak stresses occurring in the same locations. With  $E_x/E_y = 100$ , the peak stresses along both edges of the model were reduced and the stresses in the Y direction above the hole oscillated before reaching zero at the top edge of the model. The Y stress immediately above the hole was non-zero, thereby apparently violating equilibrium. For this reason, further analysis was performed at  $E_x/E_y$  ratios of 1, 20 and 40. At an orthotropic ratio of 40 it was found that the normal stress above the hole was approximately zero. At  $E_x/E_y = 20$ , the modulae in timber subjected to short duration loadings are approximately represented.

#### 4.4 Tension Zone Sizes and Positions

The elastic modulae input for the series of test calculations are given in Table 4.1. The G modulus for orthotropic cases was taken to represent the values found by Madsen. It was found in Madsen's tests that the shear modulus varies very little with the duration

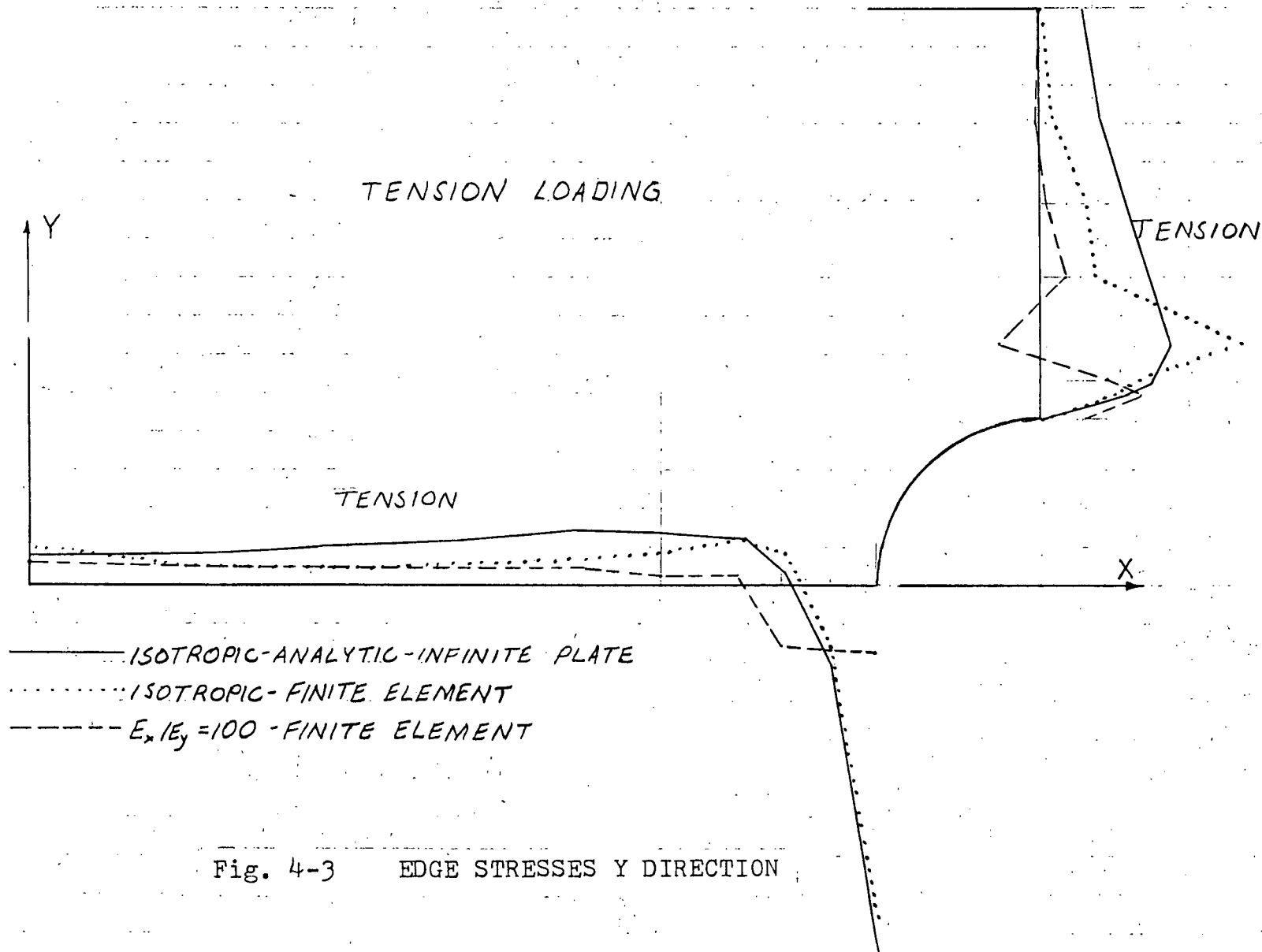


Fig. 4-3 EDGE STRESSES Y DIRECTION

| $E_x/E_y$ | $E_x$<br>psi | $E_y$<br>psi | $\nu_{xy}$ | $\nu_{yx}$ | G<br>psi |
|-----------|--------------|--------------|------------|------------|----------|
| 1         | 100          | 100          | .30        | .30        | 38       |
| 20        | 100          | 5            | .015       | .30        | 6        |
| 40        | 100          | 2.5          | .0075      | .30        | 6        |

$E_x$  = apparent Young's modulus parallel to grain

$E_y$  = apparent Young's modulus perpendicular  
to grain

$\nu_{xy}$  = Poisson's ratio for straining parallel to  
grain caused by stress applied perpendicular  
to grain

$\nu_{yx}$  = Poisson's ratio for straining perpendicular  
to grain caused by stress applied parallel  
to grain

Table 4.1 Input Data

of load.

The sizes and locations of the tensile stress zones in the X and Y directions are shown in Figs. 4.4 to 4.9 inclusive. A heavy line separates regions of tension and compression, and the tension zones are indicated. The numbers written at the element corners are relative values of stress. The arbitrary scale on which the values are measured is different for stresses in the Y direction than in the X direction. One unit of stress in the X direction is equivalent to ten units of stress in the Y direction.

Analogous to the results of Chapter 3, the stresses in the X direction as shown in Figs. 4.4, 4.5 and 4.6 indicate that the region immediately to the left of the hole became less highly stressed in tension as the degree of orthotropy was increased. This bore out the hypothesis that in general the material to the left of the hole contributes less to the load carrying capacity of the section as the degree of orthotropy is increased.

The stresses in the Y direction as presented in Figs. 4.7, 4.8 and 4.9 show that the size of the tension zones adjacent to the hole increase with increasing orthotropy. In the region above the hole the stresses in the Y direction (approximately perpendicular to grain) are significantly smaller for  $E_x/E_y = 40$  than for  $E_x/E_y = 20$ . As a crude measure of this, the average of all tensile Y strains above the hole in the former is 25, and in the latter is 30 ( the strains being relative only ). This

CNTR

CLAR PLOT# 00839048.

DATA CHECK--NEWKNOT  
SCALE FACTOR=20,000

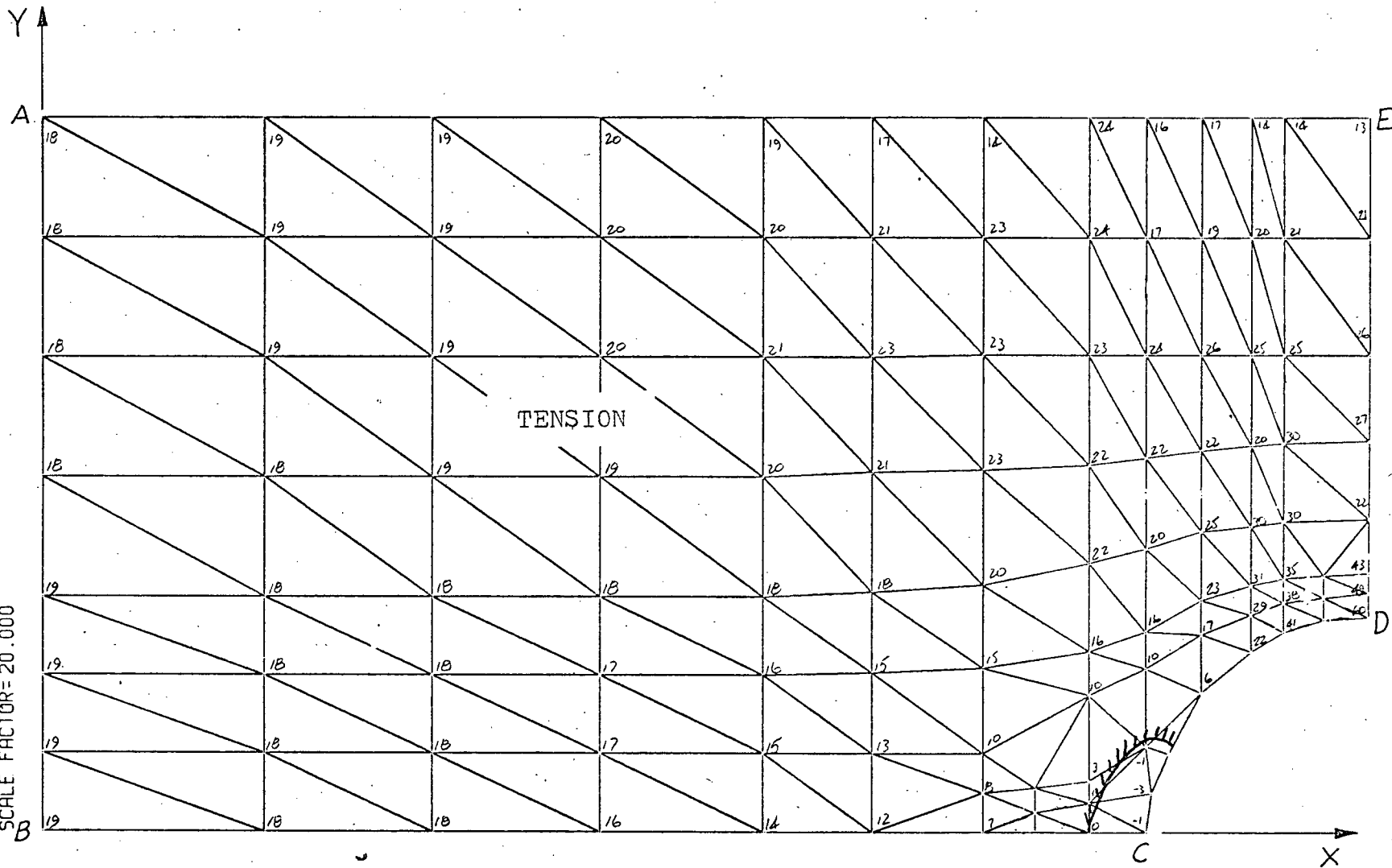


Fig. 4-4 STRESS DISTRIBUTION X DIRECTION ISOTROPIC

CNTR

CLAR PLOT# 00839048.

DATA CHECK--NEWKNOT  
SCALE FACTOR=20.000

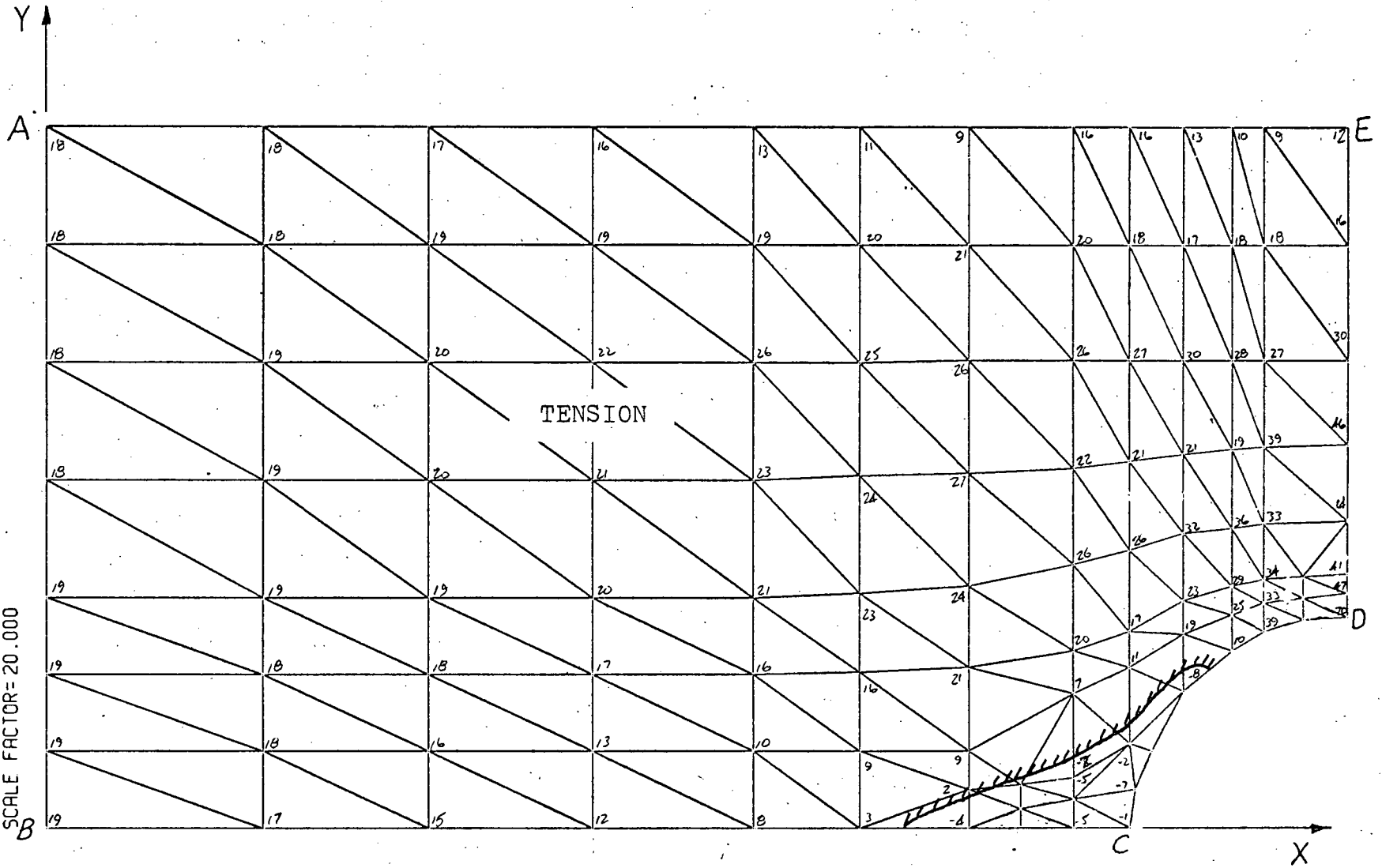


Fig. 4-5 STRESS DISTRIBUTION X DIRECTION  $E_x / E_y = 20$

CNTR

CLAR PLOT# 00839048.

DATA CHECK--NEWKNOT  
SCALE FACTOR=20.000

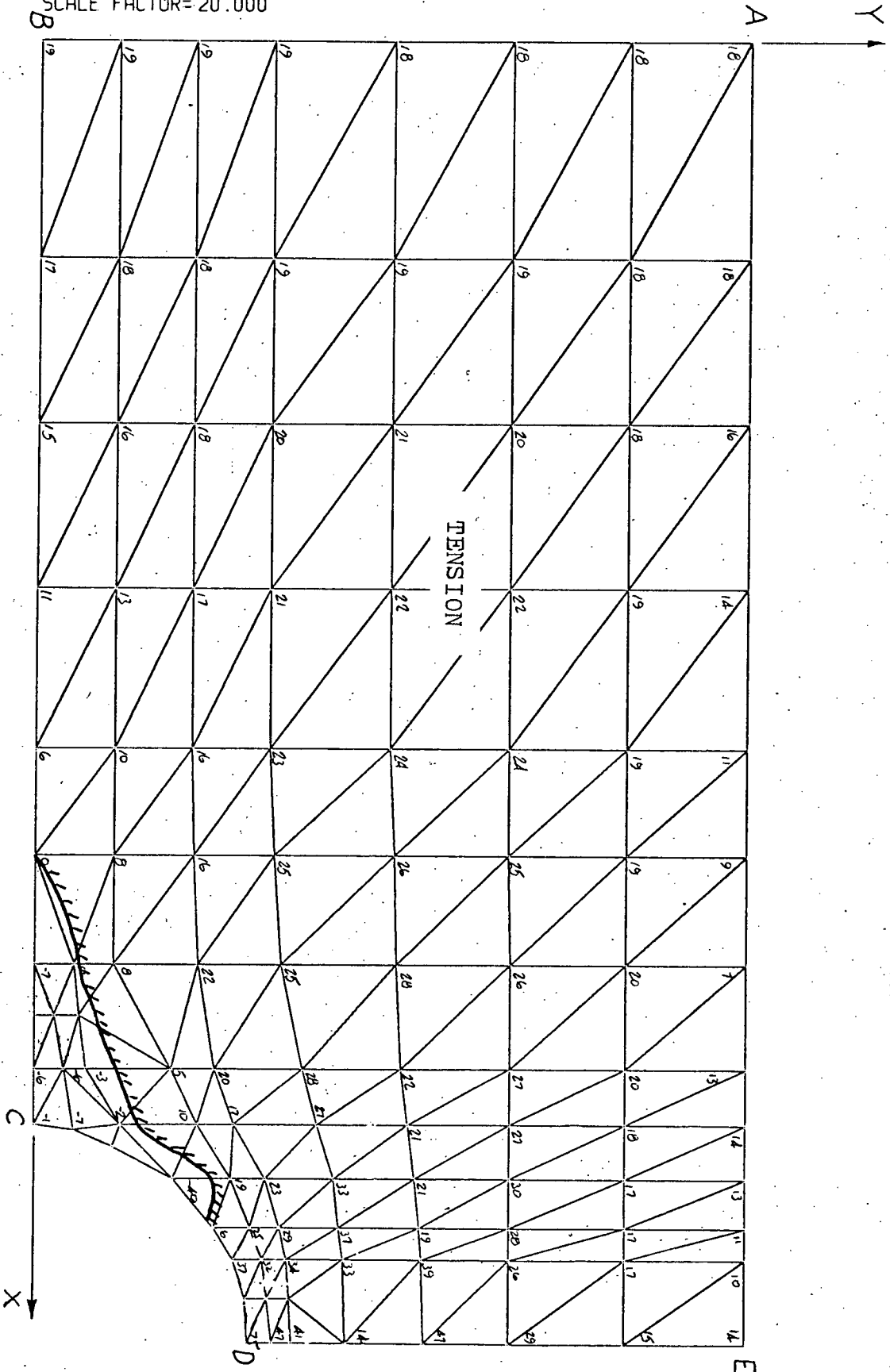


Fig. 4-6 STRESS DISTRIBUTION X DIRECTION  $E_x/E_y = 4.0$

CNTR

CLAR PLOT# 00839048.

DATA CHECK--NEWKNOT  
SCALE FACTOR= 20.000

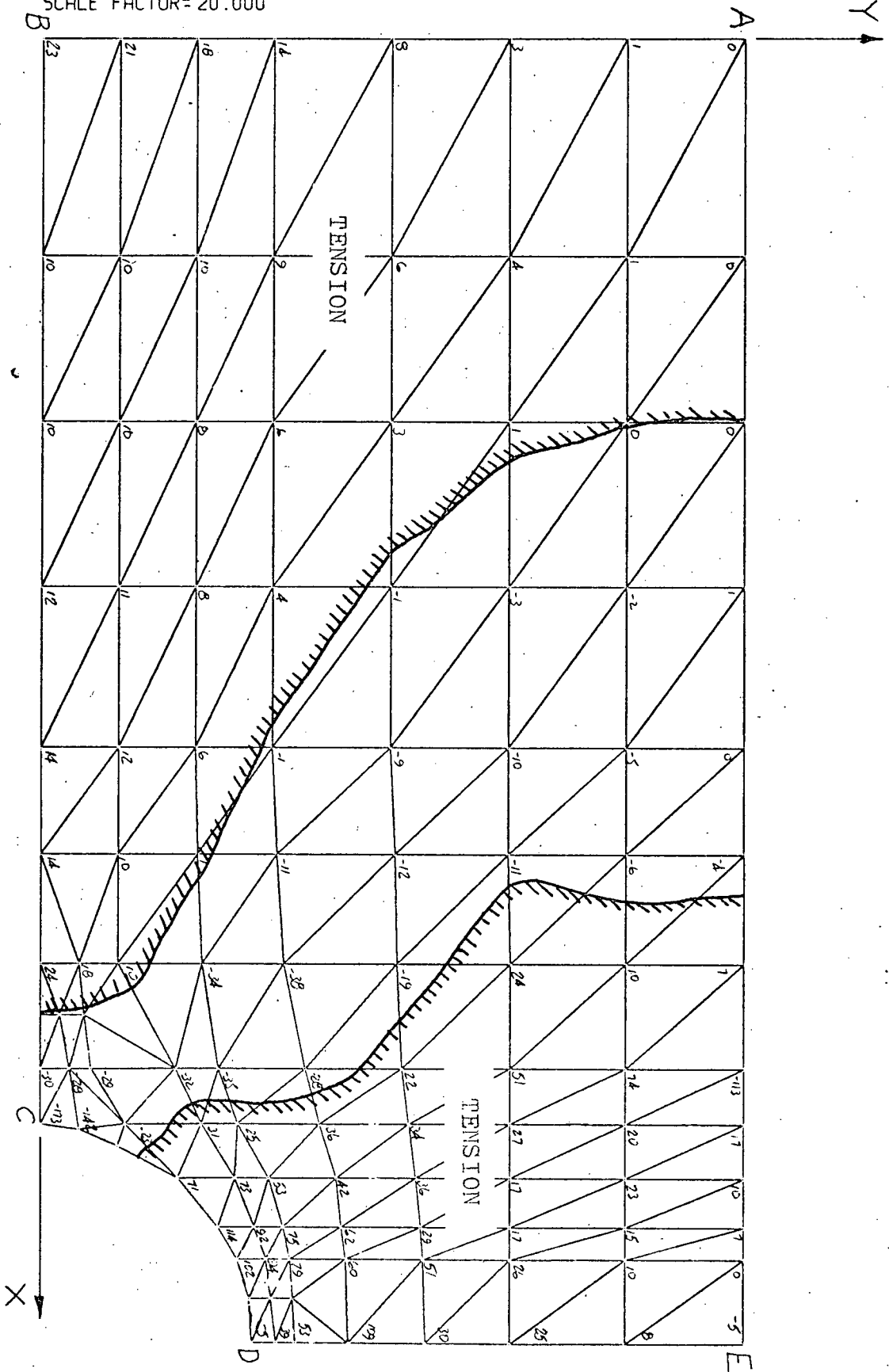


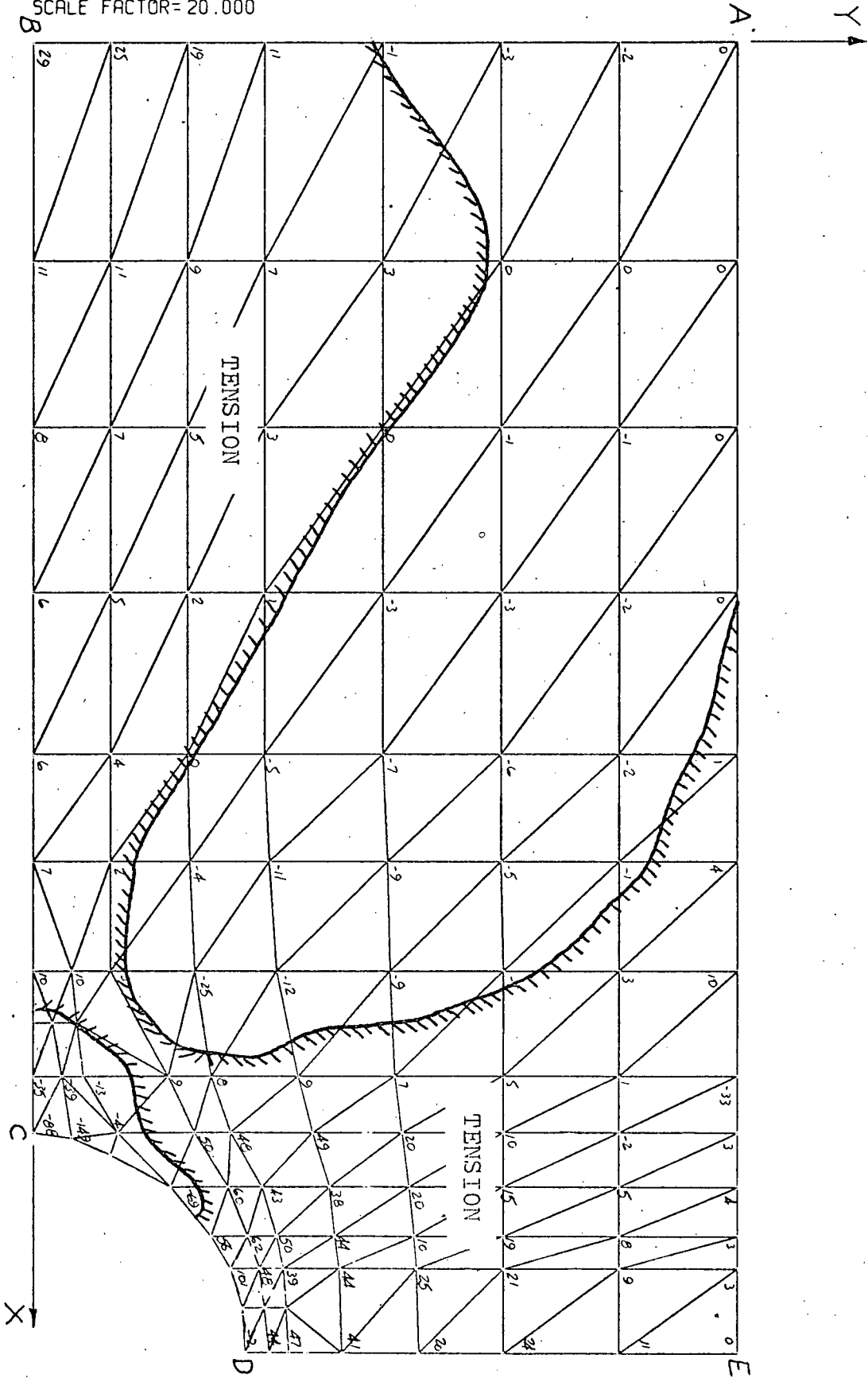
Fig. 4-7 STRESS DISTRIBUTION Y DIRECTION ISOTROPIC

CNTR

CLAR PLOT# 00839048.

DATA CHECK--NEWKNOT  
SCALE FACTOR= 20.000

Fig. 4-8 STRESS DISTRIBUTION Y DIRECTION  $E_x/E_y = 20$

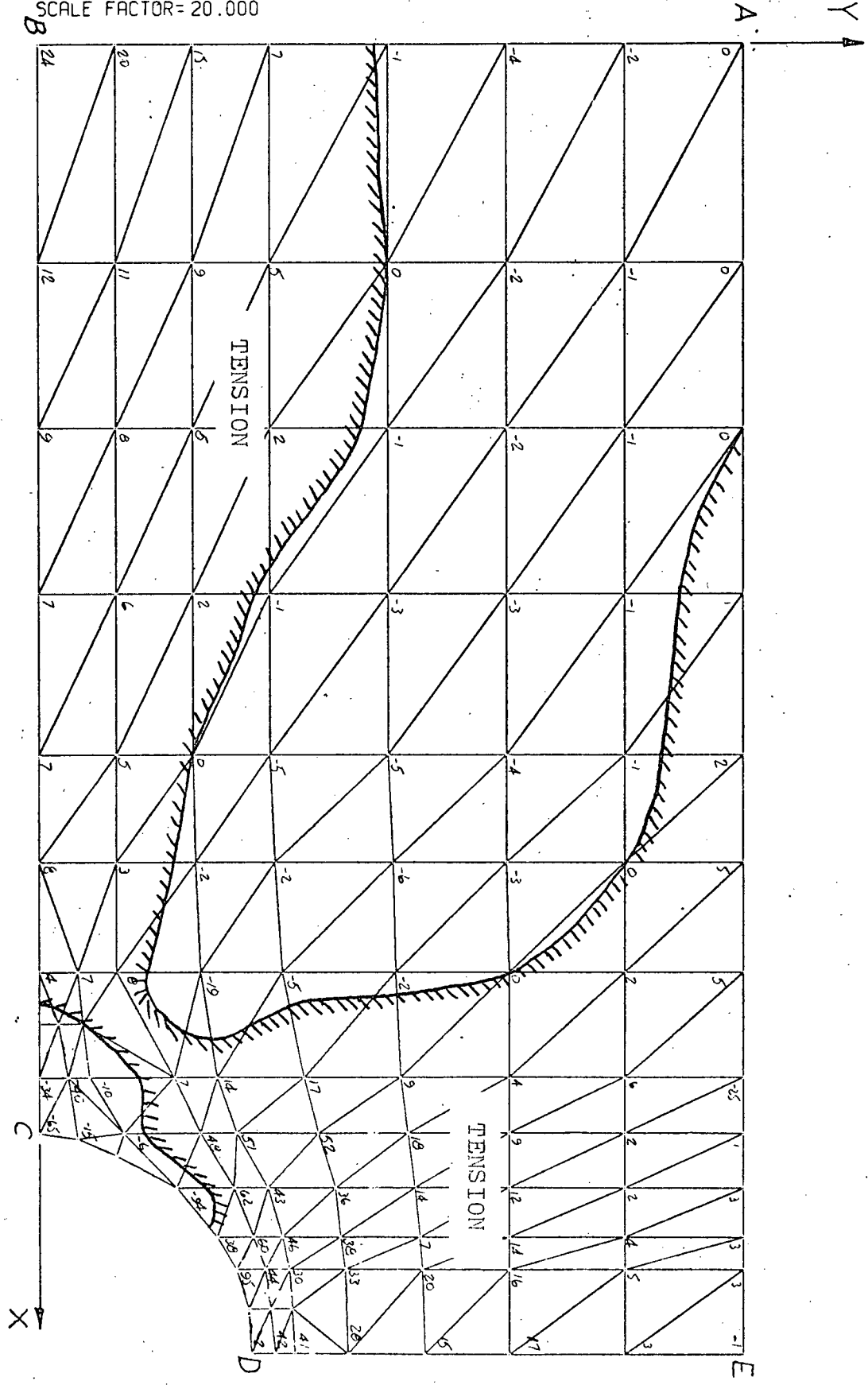


CNTR

CLAR PLOT# 00839048.

DATA CHECK--NEWKNOT  
SCALE FACTOR= 20.000

Fig. 4-9 STRESS DISTRIBUTION Y DIRECTION  $E_x / E_y = 1/10$



reduction of stress perpendicular to grain with increasing orthotropy could tend to reduce the deleterious effect of curving grain on the strength perpendicular to grain in wood.

The strains in the X direction as shown in Figs. 4.10, 4.11 and 4.12 indicate that as the degree of orthotropy was increased, the region to the left of the hole was less highly strained in tension.

Figs. 4.13, 4.14 and 4.15 for strains in the Y direction show an expanding zone of tensile strains perpendicular to grain as the degree of orthotropy was increased. As discussed in previous chapters, the additional straining perpendicular to grain could assist in the redistribution of stresses. The magnitudes of the strains perpendicular to grain increased substantially as the apparent Young's modulus perpendicular to grain was reduced.

#### 4.5 Stress Distribution on Axes of Symmetry

Graphs were produced showing the stress distributions along edges BC and CD (see Fig. 4.1) of the model of this chapter. Distributions were shown for the finite element solutions of  $E_x/E_y$  equal to 1, 20 and 40. In addition, the analytic solution for an infinite plate with a central hole was shown in Figs. 4.16 to 4.19 inclusive.

Along edge DE (above the hole) the stresses in the X direction were shown by Fig. 4.16 to have a fundamentally different distribution for orthotropic than

CNTR

CLAR PLOT# 00839048.

DATA CHECK--NEWKNOT  
SCALE FACTOR= 20.000

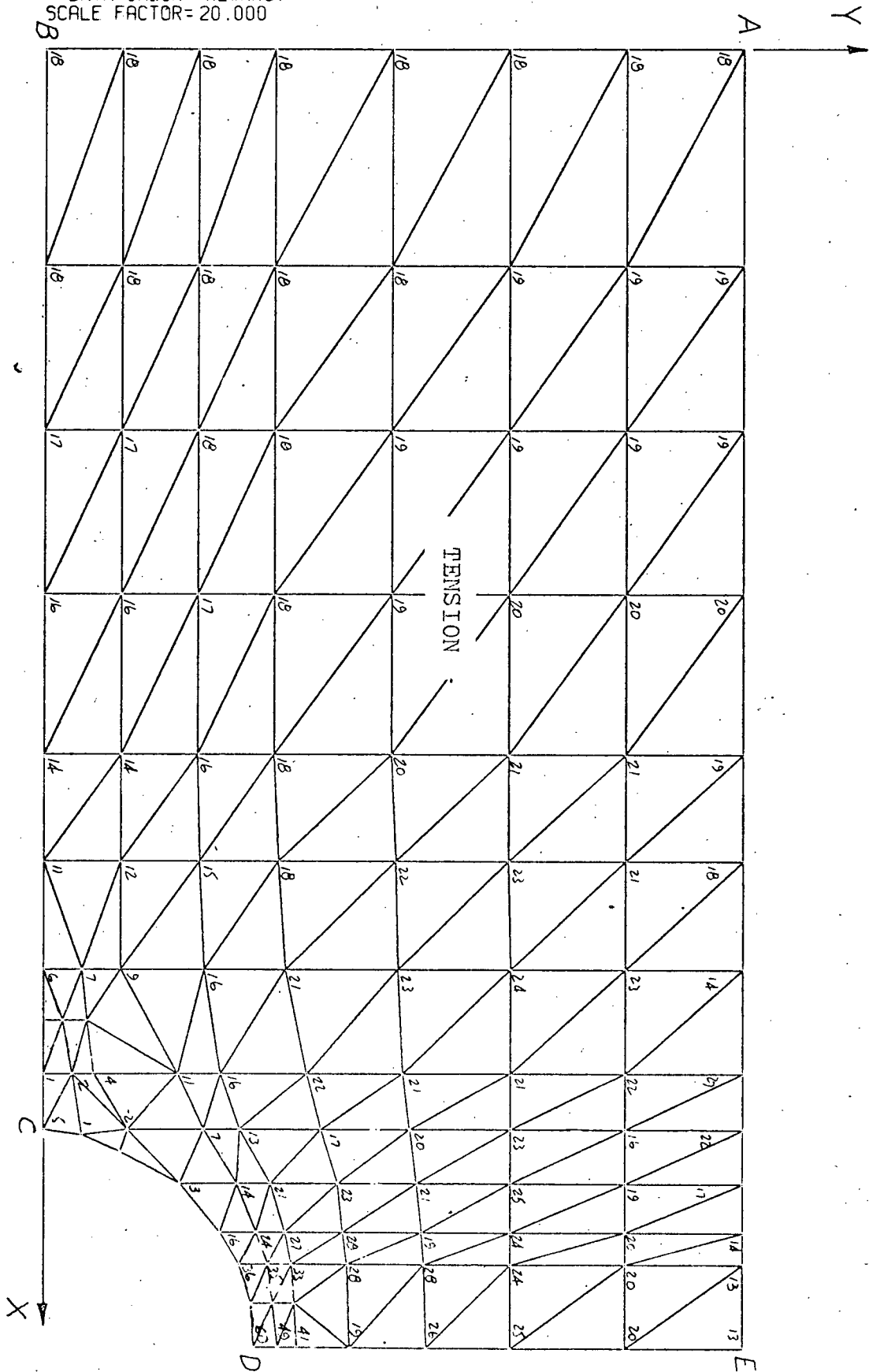


Fig. 4-10 STRAIN DISTRIBUTION X DIRECTION ISOTROPIC

CNTR

CLAR PLOT# 00839048.

DATA CHECK--NEWKNOT  
SCALE FACTOR= 20.000

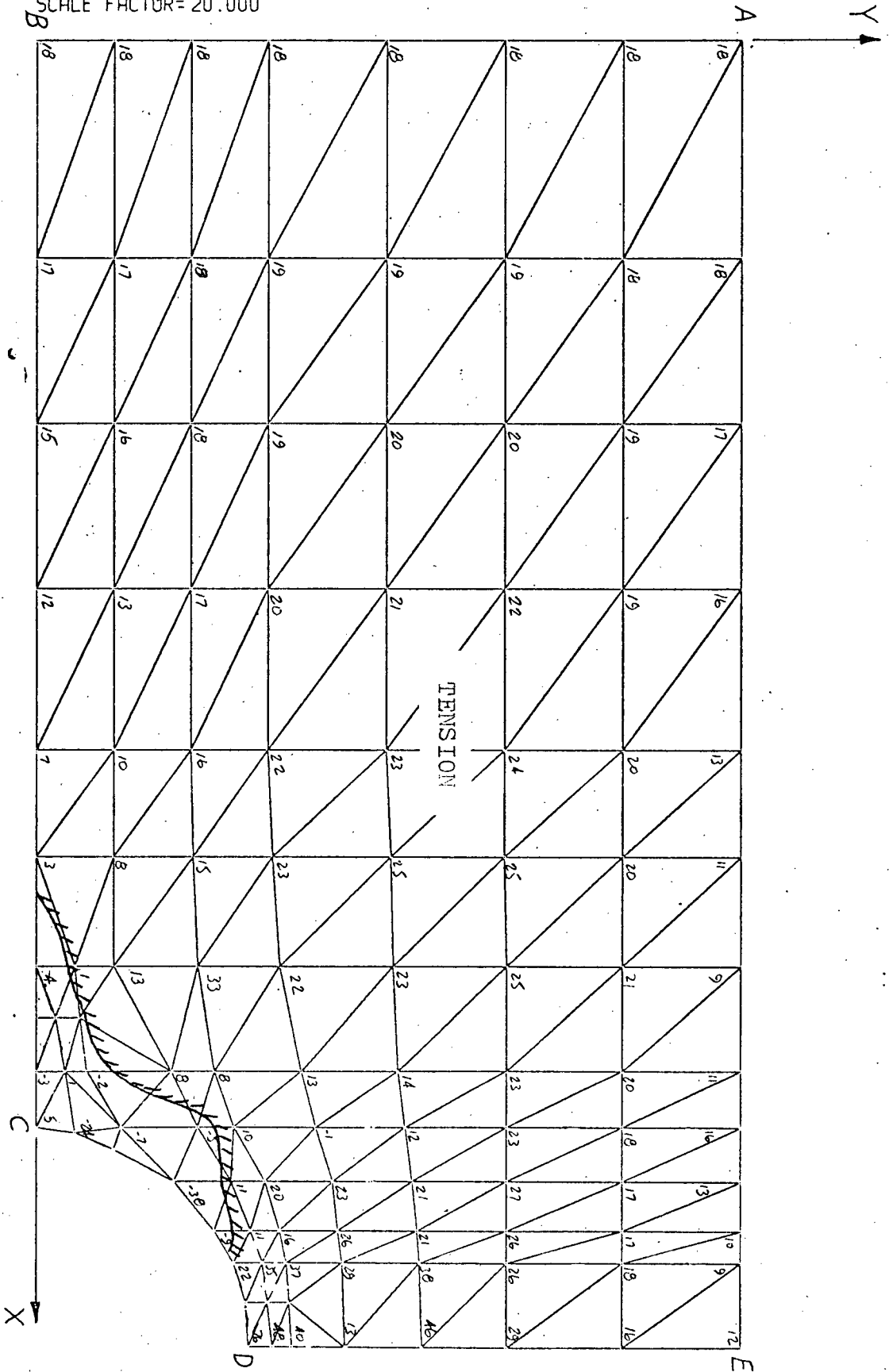


FIG. 4-11 STRAIN DISTRIBUTION X DIRECTION  $E_x / E_y = 20$

CNTR

CLAR PLOT# 00839048.

DATA CHECK--NEWKNOT  
SCALE FACTOR=20.000

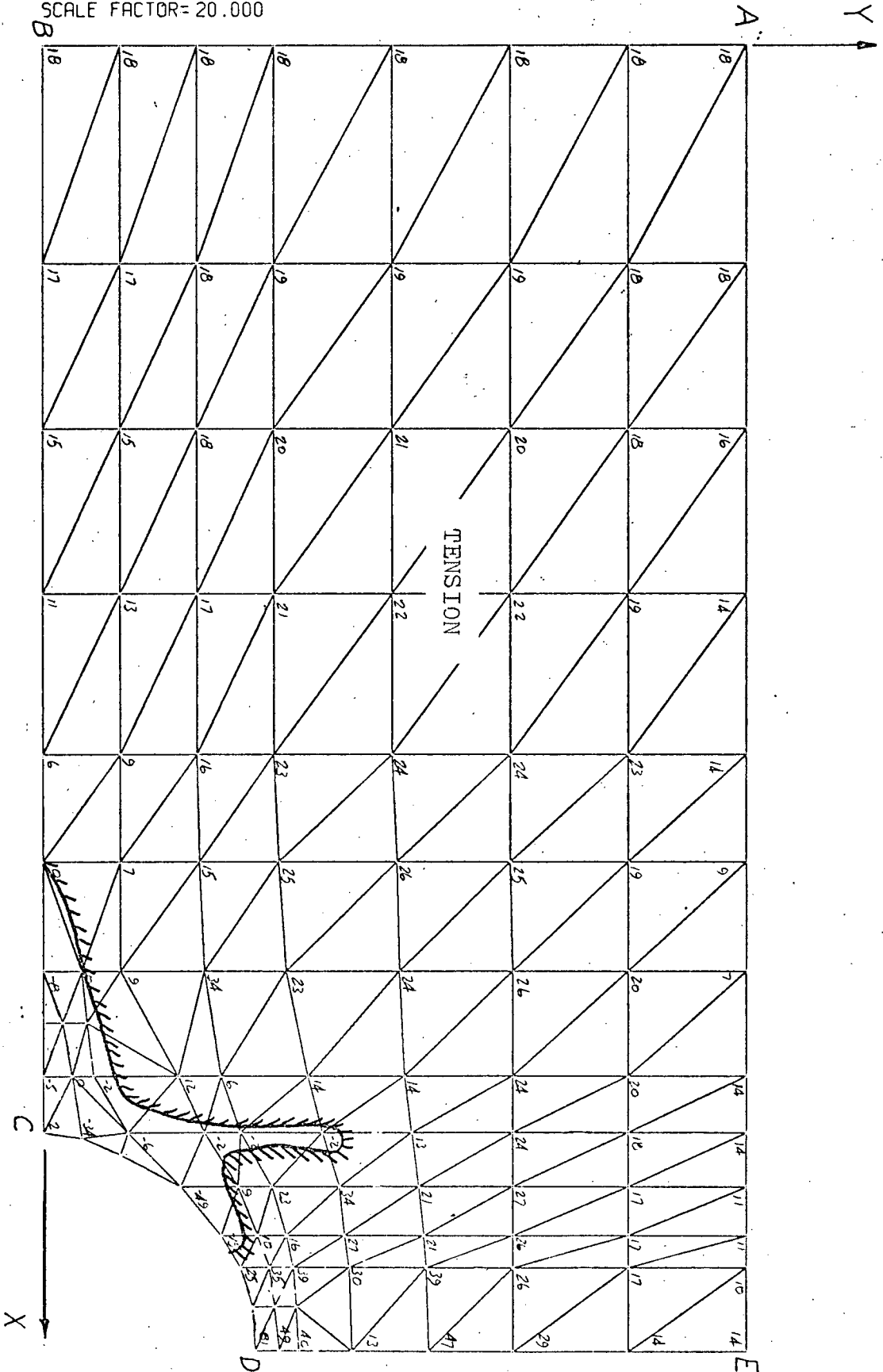


FIG. 4-12 STRAIN DISTRIBUTION X DIRECTION  $\epsilon_x / \epsilon_y = 1/10$

CNTR

CLAR PLOT# 00839048.

DATA CHECK--NEWKNOT  
SCALE FACTOR= 20.000

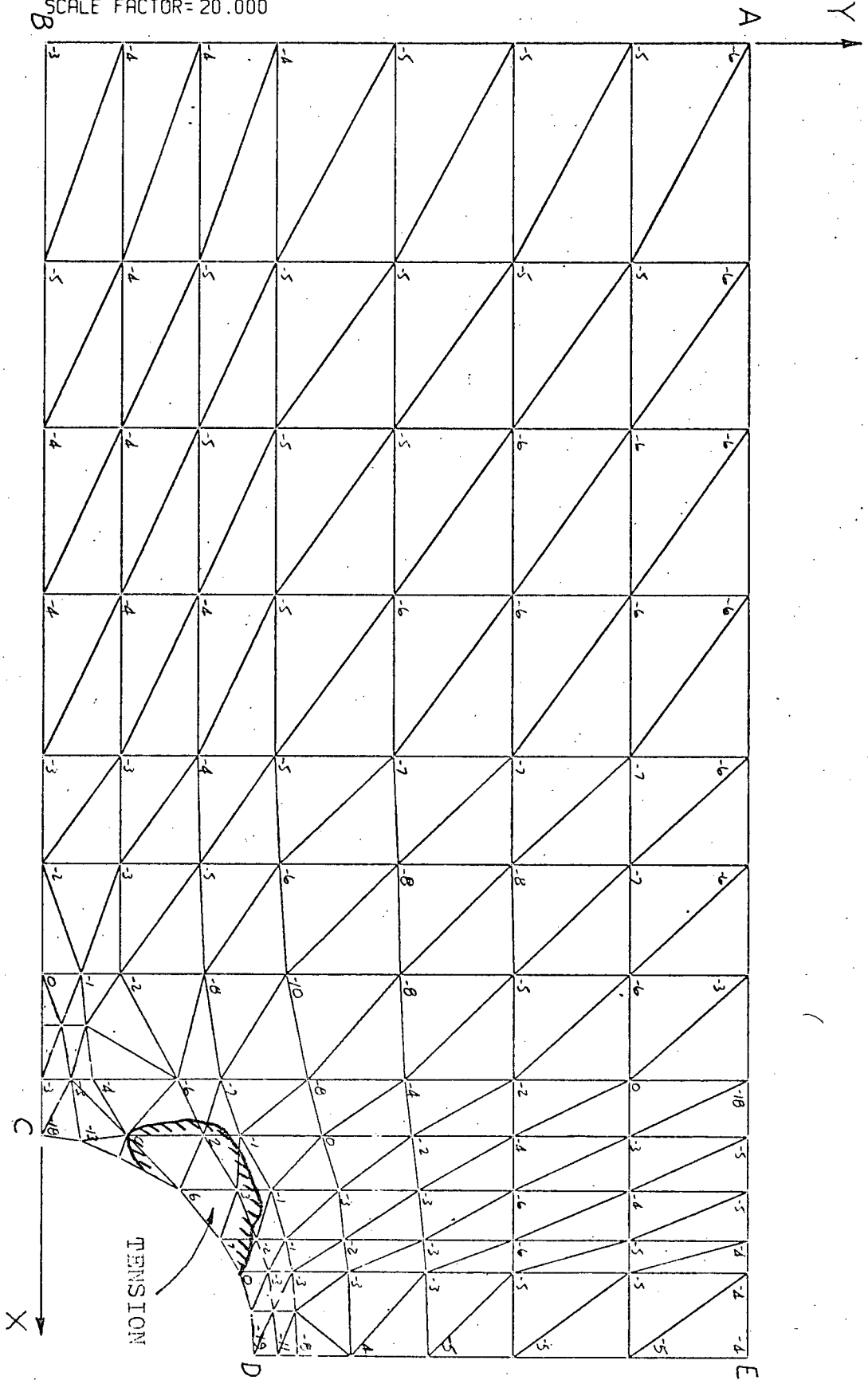


FIG. 4-13 STRAIN DISTRIBUTION Y DIRECTION ISOTROPIC

CNTR

CLAR PLOT# 00839048.

DATA CHECK--NEWKNOT  
SCALE FACTOR= 20.000

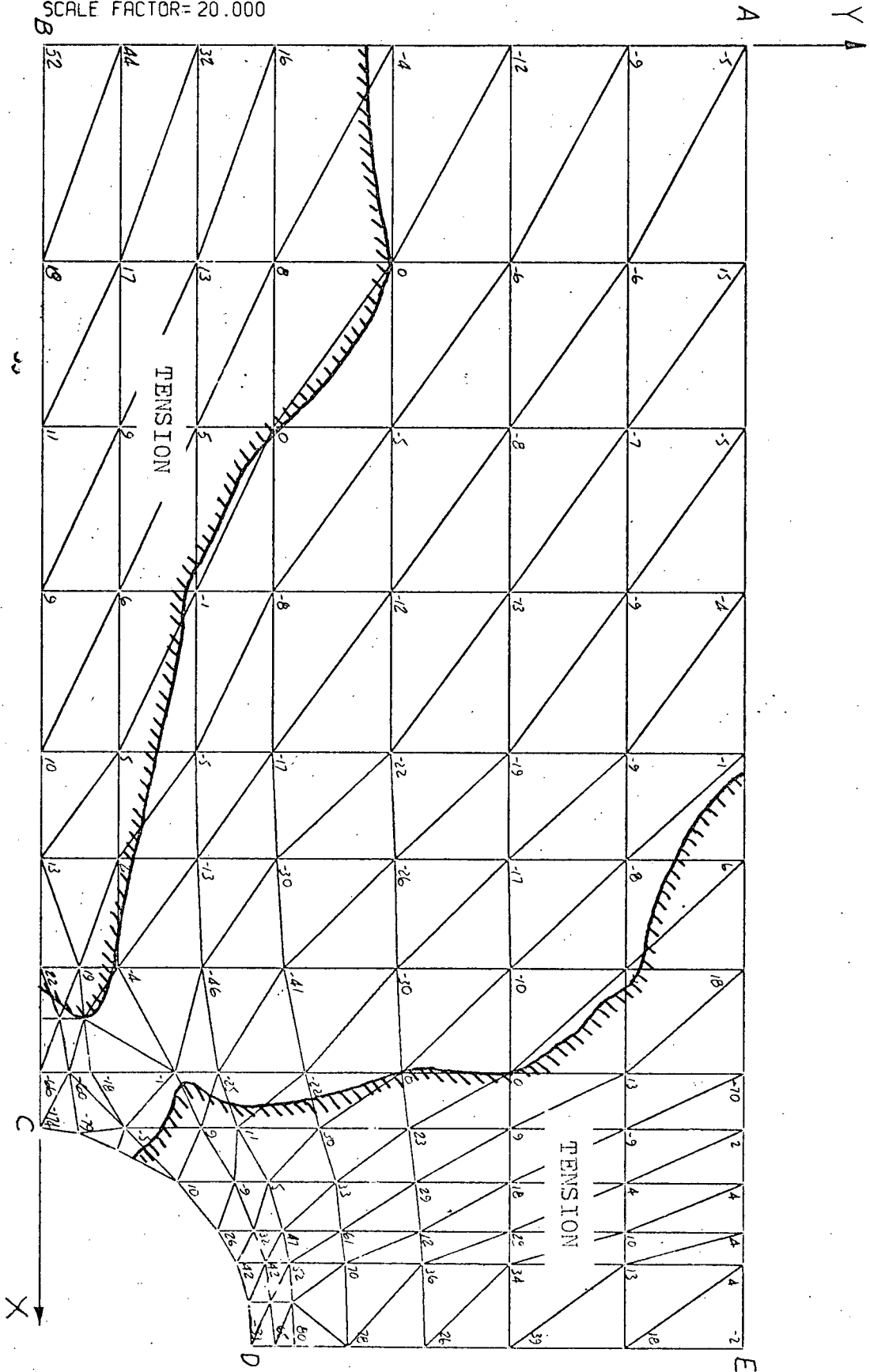


FIG. 4-14 STRAIN DISTRIBUTION Y DIRECTION  $E_x / E_y = 20$

CNTR

CLAR PLOT# 00839048.

DATA CHECK--NEWKNOT  
SCALE FACTOR= 20.000

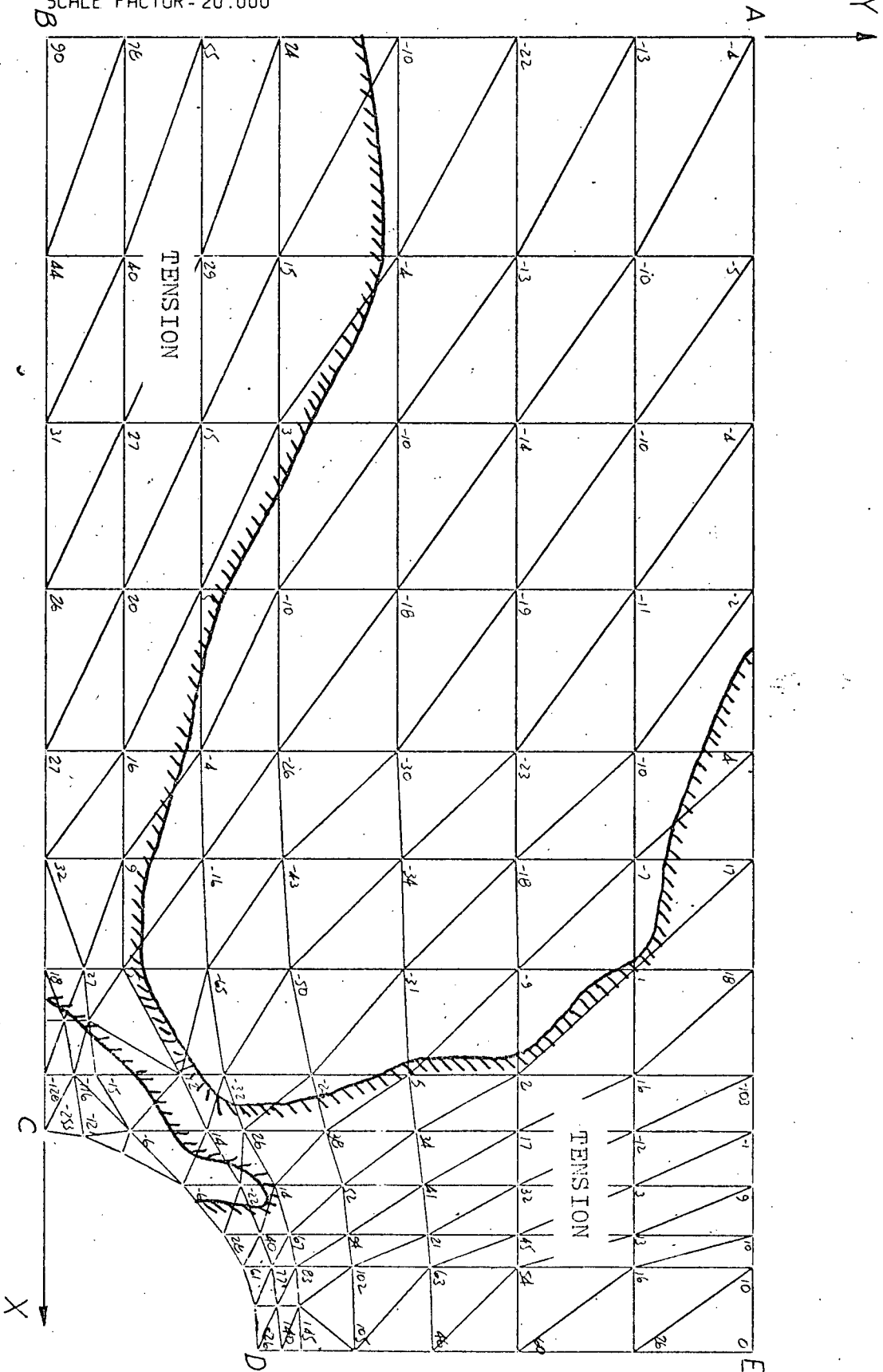


FIG. 4-15 STRAIN DISTRIBUTION Y-DIRECTION  $E_x/E_y = 1.0$

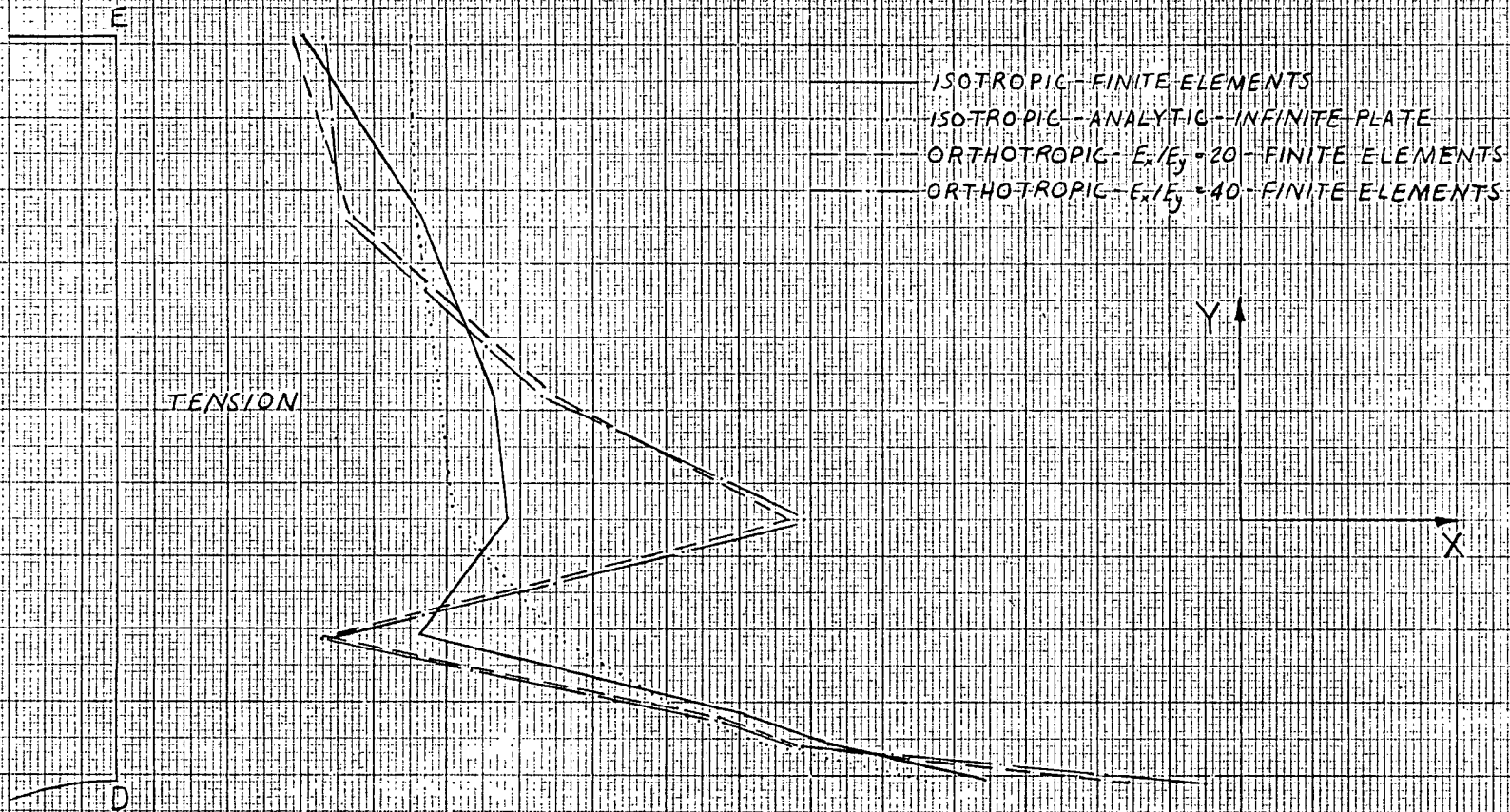


Fig. 4-16 STRESSES IN THE X DIRECTION SIDE DE

for isotropic elastic modulae. The isotropic case had a relatively smooth decrease in stress from D towards E. The orthotropic cases experienced a large oscillation in stress parallel to the Y axis. The isotropic analytic solution was provided only for reference since it was calculated for an infinite plate and did not apply directly to the model of Fig. 4.1. From  $E_x/E_y = 20$  to  $E_x/E_y = 40$ , the change in behaviour was minimal although the peak stress did increase slightly with increasing orthotropy.

In Fig. 4.17 for stresses in the Y direction on side DE, a 60 per cent decrease in peak stress perpendicular to grain was experienced from the isotropic case to  $E_x/E_y = 20$ . A further 15 per cent decrease was experienced from  $E_x/E_y = 20$  to  $E_x/E_y = 40$ . The stress distribution was similar for all cases. The reduction in stress perpendicular to grain would diminish the likelihood of the cracking perpendicular to grain that was described in Chapter 2 as being the usual mode of failure initiation for slowly loaded timber containing knots.

Along edge BC to the left of the hole, the material was shown by Fig. 4.18 to be less highly stressed in the X direction as the degree of orthotropy was increased. In the isotropic case, all of the material along the edge was in tension. In going to  $E_x/E_y = 20$  and  $E_x/E_y = 40$ , the magnitudes of tensile stresses decreased and the magnitudes of tensile stresses decreased and the magnitudes of comp-

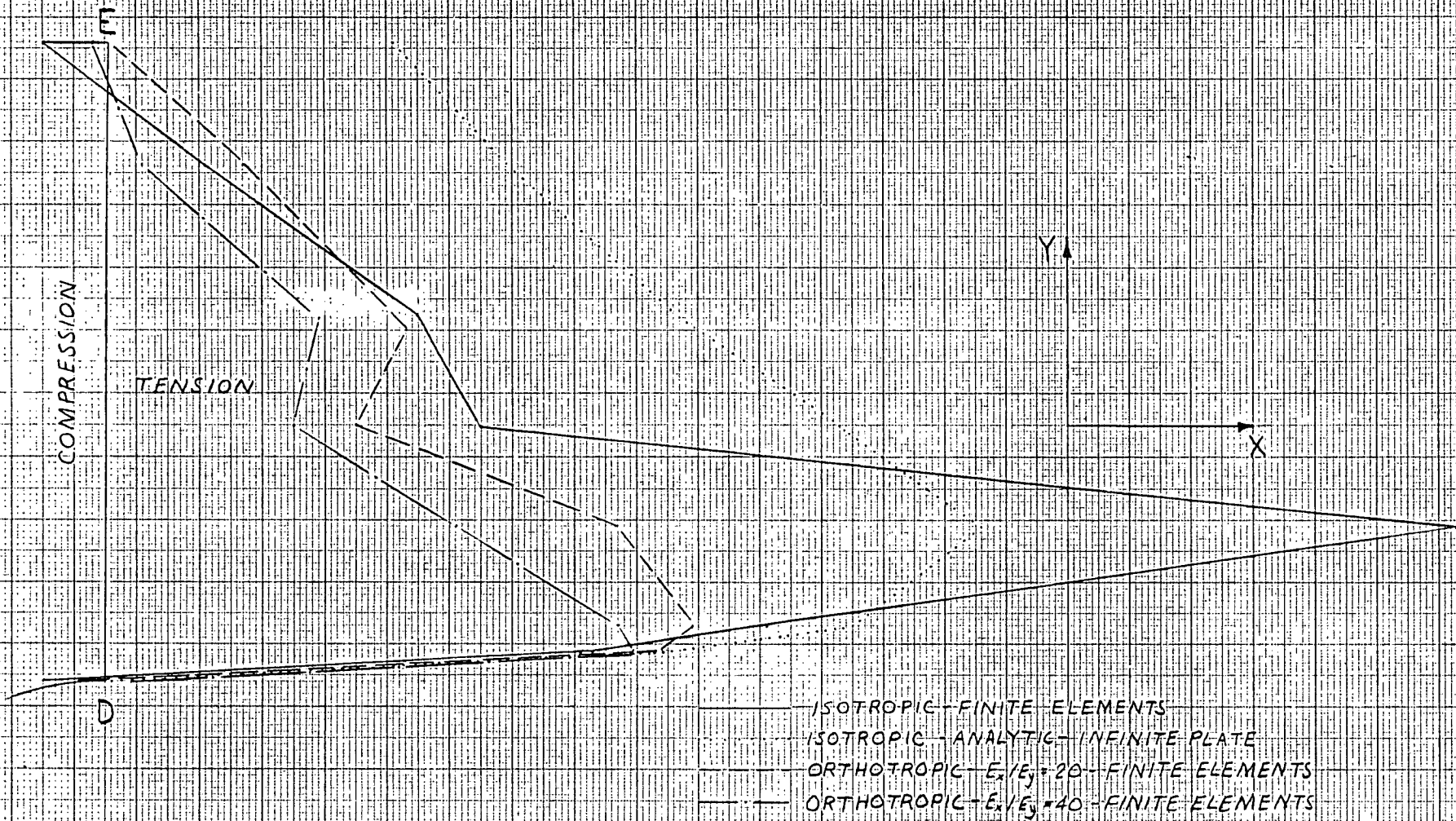


Fig. 4-17 STRESSES IN THE Y DIRECTION SIDE DE

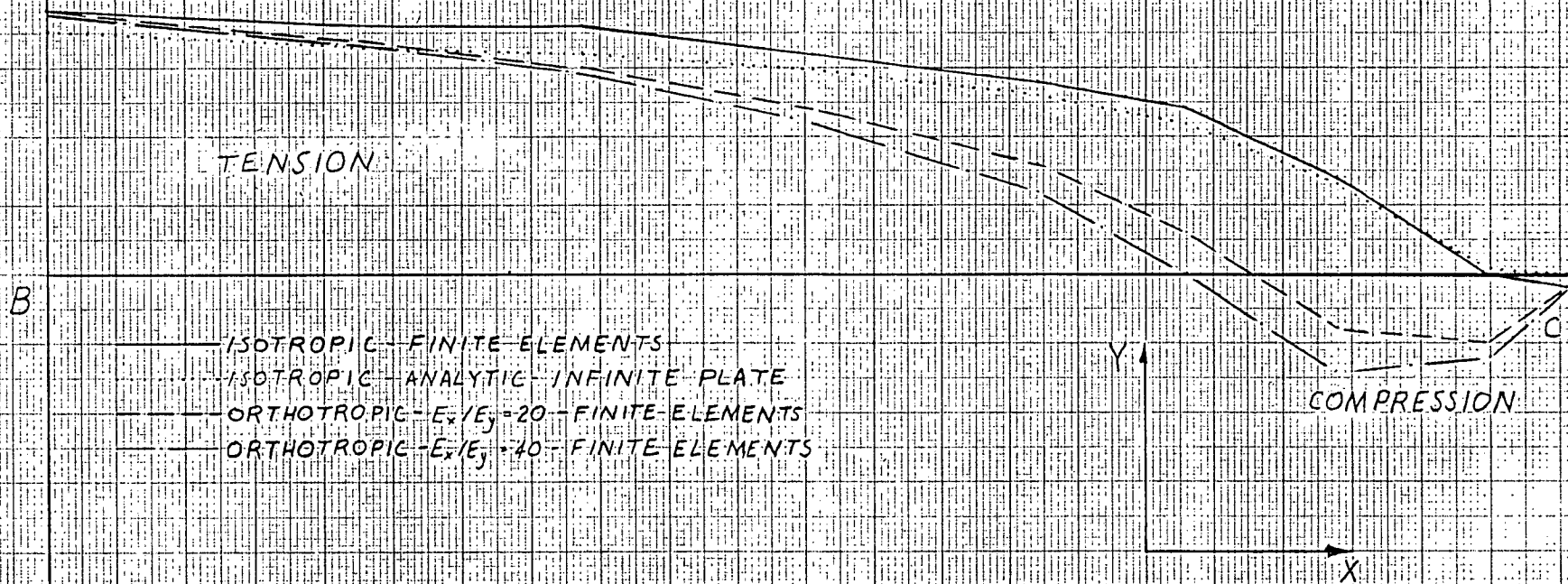


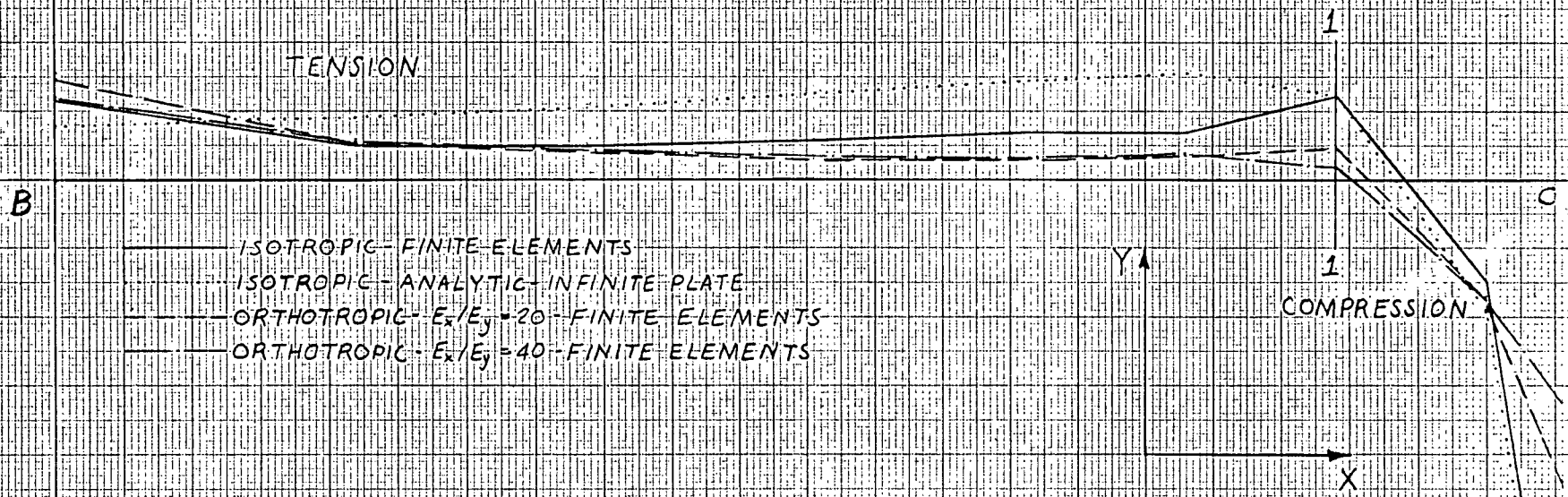
Fig. 4-18 STRESSES IN THE X DIRECTION SIDE BC

ressive stresses adjacent to the hole increased.

Fig. 4.19 for stresses in the Y direction along edge BC showed a significant decrease in peak tensile stress perpendicular to grain near the hole in going from isotropic modulae to increasing levels of orthotropy. This was particularly apparent at section 1-1. The smaller stresses perpendicular to grain would inhibit the opening of cracks adjacent to the hole.

#### 4.6 Summary

The study of this chapter produced results analagous to those of Chapter 3. The material to the left of the hole became less highly stressed in the direction of load application as orthotropy was increased. The sizes of the regions in tension perpendicular to grain increased with increasing orthotropy. The most important result of this study was however the decrease in peak stress perpendicular to grain above and to the left of the hole as the orthotropy was increased. Since the degree of orthotropy is believed to increase with the duration of a loading, the opening of cracks perpendicular to grain would be inhibited in slow loadings. The stress reduction perpendicular to grain would therefore partially compensate in slow tests for the reduction in strength found in clear material by the Madison Tests.



B

C

- ISOTROPIC-FINITE-ELEMENTS
- - - ISOTROPIC-ANALYTIC-INFINITE PLATE
- · - · ORTHOTROPIC- $E_x/E_y = 20$ -FINITE ELEMENTS
- · · ORTHOTROPIC- $E_x/E_y = 40$ -FINITE ELEMENTS

Fig. 4-19 STRESSES IN THE Y DIRECTION SIDE BC

## CONCLUSIONS

The region surrounding an edge knot in a timber beam experienced greater tensile straining perpendicular to grain with long duration loadings than with short duration loadings. Both the size of the tensile strain zone perpendicular to grain and the magnitudes of its constituent strains increased for slower tests. In addition, the strain field became more uniform.

It was found, through a computer simulation of the physical tests, that a reduction of stiffness perpendicular to the lines of grain would reproduce the trends found experimentally. The area of the tension field perpendicular to grain increased with increasing orthotropy. A detailed modelling of a hole in the centre of a plate having grain type orthotropy showed an expanding tension field and increasing tensile strain perpendicular to grain. It also showed that if the material did behave elastically, the stresses perpendicular to grain above and beside the hole would be reduced with increasing levels of orthotropy.

These results provided some basis for the findings of previous studies.<sup>2,3,4</sup> Madsen's work at U.B.C. showed specimens subjected to tensile loadings perpendicular to grain to be accompanied by very

substantial decreases in stiffness perpendicular to grain as the duration of the loadings was increased. It was shown in this thesis that the increased straining perpendicular to grain also took place in beams subjected to long term bending applications. It was shown by modelling that this straining could be caused by decreasing stiffness perpendicular to grain. Large scale straining perpendicular to grain could be a mechanism to promote stress redistribution and reduce peak stresses perpendicular to grain. This would be a reason for the different behaviours found for clear material and material containing knots or other grain irregularities when load duration is considered.

REFERENCES

1. Lyman Wood. Relation of Strength of Wood to Duration of Load. Report 1916 Forest Products Laboratory, Madison Wisconsin, Forest Service, U.S. Department of Agriculture, 1951.
2. Borg Madsen. Duration of Load Tests on Dry Lumber in Bending. Structural Research Series Report No. 3., Department of Civil Engineering, University of British Columbia, 1971.
3. Borg Madsen. Duration of Load Tests on Wet Lumber in Bending. Structural Research Series Report No. 4, Department of Civil Engineering, University of British Columbia, 1972.
4. Borg Madsen. Duration of Load Tests on Dry Lumber Subjected to Shear. Structural Research Series Report No. 6, Department of Civil Engineering, University of British Columbia, 1972.
5. Borg Madsen. Duration of Load Tests for Wood in Tension Perpendicular to Grain. Structural Research Series Report No. 7, Department of Civil Engineering, University of British Columbia, 1972.
6. O.C. Zienkiewicz. The Finite Element Method in Engineering Science. McGraw-Hill, London, 1971.
7. H.K. Ha and R. Sen. "HASENSXNDS". Computer program, University of British Columbia Civil Engineering Department Program Library, 1970.
8. S.P. Timoshenko and J.N. Goodier. Theory of Elasticity. pp. 90 - 97, 3rd Ed., McGraw-Hill, Toronto, 1970.

## Appendix A

### The Finite Element

#### A.1 The Potential Energy Theorem

The finite elements used in this paper were derived from strain energy considerations so that, as an introduction, the potential energy theorem should be examined.

Let  $\pi_e$  = potential energy of an element

$\pi$  = total potential energy

$U$  = total strain energy

$W$  = total potential energy of the  
load

$U_e$  = strain energy of an element

$W_e$  = potential energy of the load  
for one element

$\{P_e\}$  = matrix of loads acting on an  
element

$\{\delta\}$  = vector of displacements for an  
element

$[k_e]$  = elemental stiffness matrix

$\{X\}$  = vector of displacements for the  
entire problem

$[K]$  = master stiffness matrix

$[P]$  = master load vector

The potential energy theorem states that of all the displacement fields which satisfy compatibility and kinematic boundary conditions, the true displacement

field which satisfies equilibrium and stress boundary conditions provides a minimum for the potential energy. The total potential energy of an element is a function of both the strain energy and the potential energy of the load such that

$$\pi_e = U_e - W_e$$

$$U_e = \frac{1}{2} \{\delta\}^T [k_e] \{\delta\}$$

$$W_e = \{P_e\}^T \{\delta\}$$

It has been shown that given certain continuity between elements the elemental energies can be summed to produce the total potential energy of the problem.

$$\pi = \frac{1}{2} \{X\}^T [K] \{X\} - \{P\}^T \{X\} \quad (\text{A.1})$$

Applying the calculus of variations (A.1) to get a minimum potential energy gives

$$[K] \{X\} - \{P\} = 0 \quad (\text{A.2})$$

This is the standard form of the stiffness problem where  $\{P\}$  is the vector of external loads and  $[K]$  is a stiffness matrix which comes from the strain energy calculations.

## A.2 Derivation of the Six - Node Plane Linearly Varying Strain Orthotropic Triangle

Since it was necessary to be able to alter elastic modulae relative to the direction of the grain at every point, the element was derived in terms of its local coordinate axes. Fig. A.1 shows a typical element rotated at some angle to the global (X,Y) coordinate system.

- Let
- $u$  = displacement of a node in the global X direction
  - $v$  = displacement of a node in the global Y direction
  - $\xi$  = local coordinate axis parallel to the 1-2 side of the triangle
  - $\eta$  = local coordinate axis perpendicular to the  $\xi$  axis and passing through node 3
  - $\tilde{u}$  = displacement of a node in the local  $\xi$  direction.
  - $\tilde{v}$  = displacement of a node in the local  $\eta$  direction
- a,b,c = length of side

The provision of a linearly varying strain distribution in an element requires that the displacement field be quadratic in both directions.

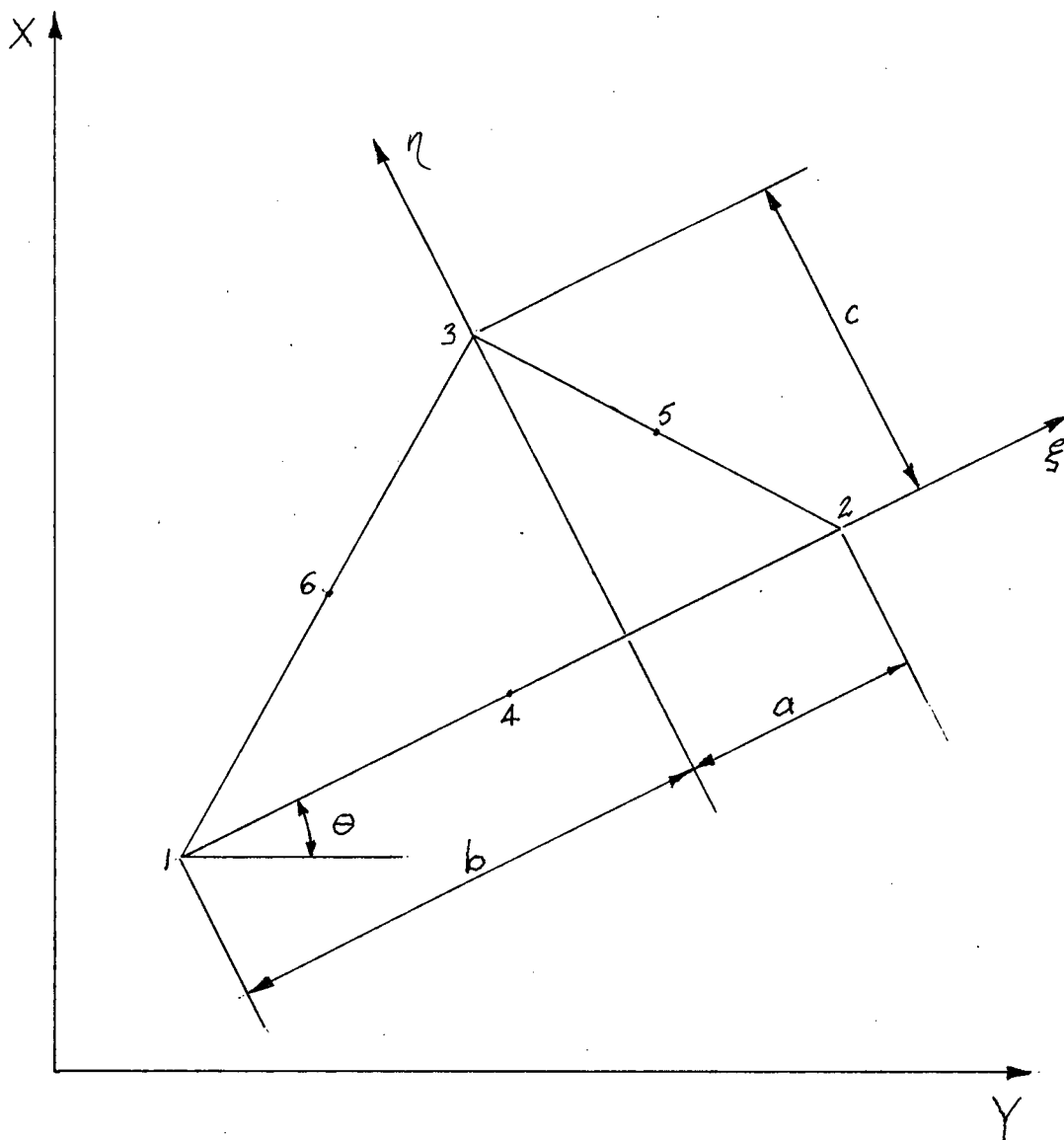


Fig. A-1

ELEMENT CONFIGURATION

$$\tilde{u} = a_1 + a_2 \xi + a_3 \eta + a_4 \xi \eta + a_5 \xi^2 + a_6 \eta^2 \quad (\text{A.3})$$

$$\tilde{v} = a_7 + a_8 \xi + a_9 \eta + a_{10} \xi \eta + a_{11} \xi^2 + a_{12} \eta^2$$

The twelve degrees of freedom necessary to be associated with the twelve constants of (A.3) were provided by  $\tilde{u}$  and  $\tilde{v}$  degrees of freedom at each of six nodes. Nodes 4, 5 and 6 were located at the midpoints of the sides of the triangle.

Given the global coordinates of the corner nodes, simple geometry was employed to calculate the length parameters  $a$ ,  $b$  and  $c$  and the angle  $\theta$ .

$$\cos \theta = \frac{x_2 - x_1}{r} \quad \sin \theta = \frac{y_2 - y_1}{r}$$

$$a = [(x_2 - x_3)(x_2 - x_1) - (y_3 - y_2)(y_2 - y_1)]/r$$

$$b = [(x_3 - x_1)(x_2 - x_1) + (y_3 - y_1)(y_2 - y_1)]/r \quad (\text{A.4})$$

$$c = [(y_3 - y_1)(x_2 - x_1) - (x_3 - x_1)(y_2 - y_1)]/r$$

$$r = \sqrt{(x_2 - x_1)^2 + (y_2 - y_1)^2}$$

The polynomial coefficients  $a_i$  of equations (A.3) were expressed as functions of the nodal displacements through the creation of a transformation matrix.

$$\tilde{u}_1 = \tilde{u}(-b, 0) = a_1 - a_2 b + a_5 b^2$$

(A.5)

$$\tilde{v}_1 = \tilde{v}(-b, 0) = a_7 - a_8 b + a_{11} b^2$$

and similarly for other displacements so that the form

$$\{\tilde{\delta}\} = [T] \{A\} \quad \text{was obtained}$$

$$\text{where } \{\tilde{\delta}\}^T = (\tilde{u}_1, \tilde{v}_1, \tilde{u}_2, \tilde{v}_2, \dots, \tilde{u}_6, \tilde{v}_6) \quad (\text{A.6})$$

$$\{A\}^T = (a_1, a_2, a_3, \dots, a_{11}, a_{12})$$

$$[T] = \begin{array}{c} \begin{array}{|c|c|c|c|c|c|c|c|c|c|c|c|} \hline 1 & -b & 0 & 0 & b^2 & 0 & 0 & 0 & 0 & 0 & 0 & 0 \\ \hline 0 & 0 & 0 & 0 & 0 & 0 & 1 & -b & 0 & 0 & b^2 & 0 \\ \hline 1 & a & 0 & 0 & a^2 & 0 & 0 & 0 & 0 & 0 & 0 & 0 \\ \hline 0 & 0 & 0 & 0 & 0 & 0 & 1 & a & 0 & 0 & a^2 & 0 \\ \hline 1 & 0 & c & 0 & 0 & c^2 & 0 & 0 & 0 & 0 & 0 & 0 \\ \hline 0 & 0 & 0 & 0 & 0 & 0 & 1 & 0 & c & 0 & 0 & c^2 \\ \hline 1 & \frac{a-b}{2} & 0 & 0 & \left(\frac{a-b}{2}\right)^2 & 0 & 0 & 0 & 0 & 0 & 0 & 0 \\ \hline 0 & 0 & 0 & 0 & 0 & 0 & 1 & \frac{a-b}{2} & 0 & 0 & \left(\frac{a-b}{2}\right)^2 & 0 \\ \hline 1 & \frac{a}{2} & \frac{c}{2} & \frac{ac}{4} & \frac{a^2}{4} & \frac{c^2}{4} & 0 & 0 & 0 & 0 & 0 & 0 \\ \hline 0 & 0 & 0 & 0 & 0 & 0 & 1 & \frac{a}{2} & \frac{c}{2} & \frac{ac}{4} & \frac{a^2}{4} & \frac{c^2}{4} \\ \hline 1 & -\frac{b}{2} & \frac{c}{2} & -\frac{bc}{4} & \frac{b^2}{4} & \frac{c^2}{4} & 0 & 0 & 0 & 0 & 0 & 0 \\ \hline 0 & 0 & 0 & 0 & 0 & 0 & 1 & -\frac{b}{2} & \frac{c}{2} & -\frac{bc}{4} & \frac{b^2}{4} & \frac{c^2}{4} \\ \hline \end{array} \\ (\text{A.7}) \end{array}$$

The transformation matrix was inverted to give

$$\{A\} = [T^{-1}] \{\tilde{\delta}\} \quad (\text{A.8})$$

The strain energy equation for plane stress is

$$U = \frac{1}{2} \iiint_V (\sigma_x \epsilon_x + \sigma_y \epsilon_y + \tau \gamma) dV \quad (\text{A.9})$$

where

$$\sigma_x = \frac{E_x}{1 - \nu_{xy}\nu_{yx}} (\epsilon_x + \nu_{xy} \epsilon_y)$$

$$\sigma_y = \frac{E_y}{1 - \nu_{xy}\nu_{yx}} (\epsilon_y + \nu_{yx} \epsilon_x) \quad (\text{A.10})$$

$$\tau = G \gamma$$

and for this problem,

$\sigma_x$  = normal stress in the local  
 $\xi$  direction

$\sigma_y$  = normal stress in the local  
 $\eta$  direction

$\tau$  = shear stress

$\epsilon_x$  = normal strain in the local  
 $\xi$  direction

$\epsilon_y$  = normal strain in the local  
 $\eta$  direction

$\gamma$  = shear strain

$E_x$  = Young's modulus in the local  
 $\xi$  direction

$E_y$  = Young's modulus in the local  
 $\eta$  direction

$G$  = shear modulus

$\nu_{xy}$  = Poisson's ratio defining  
the strain in the  $\xi$  direction  
resulting from stress in the

$\eta$  direction

$\nu_{yx}$  = Poisson's ratio defining the strain in the  $\eta$  direction resulting from stress in the  $\xi$  direction

Substituting (A.10) into (A.9) and assuming constant thickness of the element yielded

$$U = \frac{t}{2} \iint_A \left[ \frac{E_x}{1 - \nu_{xy}\nu_{yx}} (\epsilon_x^2 + \nu_{xy} \epsilon_x \epsilon_y) + \frac{E_y}{1 - \nu_{xy}\nu_{yx}} (\epsilon_y^2 + \nu_{yx} \epsilon_x \epsilon_y) + G \gamma^2 \right] dA \quad (\text{A.11})$$

The strains required in (A.11) were obtained in terms of the polynomial coefficients  $a_i$ ; from the assumed displacement fields (A.3)

$$\begin{aligned} \epsilon_x &= \frac{J\tilde{u}}{J\xi} = a_2 + a_4\eta + 2a_5\xi \\ \epsilon_y &= \frac{J\tilde{v}}{J\eta} = a_9 + a_{10}\xi + 2a_{12}\eta \\ \gamma &= \frac{J\tilde{u}}{J\eta} + \frac{J\tilde{v}}{J\xi} = a_3 + a_8 + (a_4 + 2a_{11})\xi + (2a_6 + a_{10})\eta \end{aligned} \quad (\text{A.12})$$

Substituting (A.12) into (A.10) gave

$$\begin{aligned}
U = & \frac{t}{2} \iint_A [\beta_x (a_2^2 + \nu_{xy} a_2 a_9) + \beta_y (a_9^2 + \nu_{yx} a_2 a_9) \\
& + (a_3^2 + a_8^2 + 2a_3 a_8) G] dA \\
& + \frac{t}{2} \iint_A \eta [2\beta_x a_2 a_4 + 4\beta_y a_9 a_{12} + (\beta_x \nu_{xy} + \beta_y \nu_{yx}) a_4 a_9 \\
& + (2\nu_{xy} \beta_x + 2\nu_{yx} \beta_y) a_2 a_{12} + 2G(2a_6 a_3 + 2a_6 a_8 + a_3 a_{10} + a_8 a_{10})] dA \\
& + \frac{t}{2} \iint_A \xi [4\beta_x a_2 a_5 + (\beta_x \nu_{xy} + \beta_y \nu_{yx}) a_2 a_{10} + 2(\beta_x \nu_{xy} + \beta_y \nu_{yx}) a_5 a_9 \\
& + 2\beta_y a_9 a_{10} + 2G(a_3 a_4 + 2a_3 a_{11} + a_4 a_8 + 2a_8 a_{11})] dA \\
& + \frac{t}{2} \iint_A \zeta \eta [4\beta_x a_4 a_5 + (\beta_x \nu_{xy} + \beta_y \nu_{yx}) a_4 a_{10} + 4(\beta_x \nu_{xy} + \beta_y \nu_{yx}) a_5 a_{12} \\
& + 4\beta_y a_{10} a_{12} + 2G(2a_4 a_6 + a_4 a_{10} + 4a_6 a_{11} + 2a_{10} a_{11})] dA \\
& + \frac{t}{2} \iint_A \xi^2 [4\beta_x a_5^2 + 2(\beta_x \nu_{xy} + \beta_y \nu_{yx}) a_5 a_{10} + \beta_y a_{10}^2 \\
& + G(a_4^2 + 4a_{11}^2 + 4a_4 a_{11})] dA \tag{A.14} \\
& + \frac{t}{2} \iint_A \eta^2 [\beta_x a_4^2 + 2(\beta_x \nu_{xy} + \beta_y \nu_{yx}) a_4 a_{12} \\
& + G(4a_6^2 + a_{10}^2 + 4a_6 a_{10})] dA
\end{aligned}$$

where  $\beta_x = \frac{E_x}{1 - \nu_{xy} \nu_{yx}}$   $\beta_y = \frac{E_y}{1 - \nu_{xy} \nu_{yx}}$

Equation (A.14) was integrated noting that

$$\iint_A f(\xi, \eta) dA = \int_0^c \int_{\frac{a}{2}\eta - a}^{-\frac{b}{2}\eta + b} f(\xi, \eta) d\xi d\eta \quad (\text{A.15})$$

to produce an elemental stiffness matrix  $[k1]$  in terms of the polynomial coefficients  $a_1 \dots a_{12}$

$$[k1] = \frac{t}{2} \begin{bmatrix} [k_{11}] & [k_{12}] \\ [k_{21}] & [k_{22}] \end{bmatrix} \quad (\text{A.16})$$

$[k_{ii}] =$ 

|   |                           |                      |                               |                                   |                             |
|---|---------------------------|----------------------|-------------------------------|-----------------------------------|-----------------------------|
| 0 | 0                         | 0                    | 0                             | 0                                 | 0                           |
|   | $\beta_x \frac{a+b}{2} c$ | 0                    | $\beta_x \frac{(a+b)c^2}{6}$  | $\beta_x \frac{(a^2-b^2)c}{3}$    | 0                           |
|   |                           | $G \frac{(a+b)c}{2}$ | $G \frac{(a^2-b^2)c}{6}$      | 0                                 | $G \frac{(a+b)c^2}{3}$      |
|   |                           |                      | $\beta_x \frac{(a+b)c^3}{12}$ | $\beta_x \frac{(a^2-b^2)c^2}{12}$ | $G \frac{(a^2-b^2)c^2}{12}$ |
|   |                           |                      |                               | $\beta_x \frac{(a^3-b^3)c}{3}$    | 0                           |
|   |                           |                      |                               |                                   | $G \frac{(a+b)c^3}{3}$      |

SYMMETRIC

(A.17)

$[k_{12}] =$

|   |                          |  |   |                            |  |
|---|--------------------------|--|---|----------------------------|--|
| 0 | 0                        | 0  | 0   | 0                          | 0  |
| 0 | 0                        | $\beta_x \psi_{xy} \frac{(a+b)c}{4}$<br>$\beta_y \psi_{yx} \frac{(a+b)c}{4}$         | $\beta_x \psi_{xy} \frac{(a^2-b^2)c}{12}$<br>$\beta_y \psi_{yx} \frac{(a^2-b^2)c}{12}$                                    | 0                          | $\beta_x \psi_{xy} \frac{(a+b)c^2}{6}$<br>$\beta_y \psi_{yx} \frac{(a+b)c^2}{6}$           |
| 0 | $G \frac{(a+b)c}{2}$     | 0  | $G \frac{(a+b)c^2}{6}$  | $G \frac{(a^2-b^2)c}{3}$   | 0  |
| 0 | $G \frac{(a^2-b^2)c}{6}$ | $\beta_x \psi_{xy} \frac{(a+b)c^2}{12}$<br>$\beta_y \psi_{yx} \frac{(a+b)c^2}{12}$   | $\beta_x \psi_{xy} \frac{(a^2-b^2)c^2}{48}$<br>$\beta_y \psi_{yx} \frac{(a^2-b^2)c^2}{48}$<br>$G \frac{(a^2-b^2)c^2}{24}$ | $G \frac{(a^3+b^3)c}{6}$   | $\beta_x \psi_{xy} \frac{(a+b)c^3}{12}$<br>$\beta_y \psi_{yx} \frac{(a+b)c^3}{12}$         |
| 0 | 0                        | $\beta_x \psi_{xy} \frac{(a^2-b^2)c}{6}$<br>$\beta_y \psi_{yx} \frac{(a^2-b^2)c}{6}$ | $\beta_x \psi_{xy} \frac{(a^3+b^3)c}{12}$<br>$\beta_y \psi_{yx} \frac{(a^3+b^3)c}{12}$                                    | 0                          | $\beta_x \psi_{xy} \frac{(a^2-b^2)c^2}{12}$<br>$\beta_y \psi_{yx} \frac{(a^2-b^2)c^2}{12}$ |
| 0 | $G \frac{(a+b)c^2}{3}$   | 0  | $G \frac{(a+b)c^3}{6}$  | $G \frac{(a^2-b^2)c^2}{6}$ | 0  |

(A.18)

$$[k_{21}] = [k_{12}]^T$$

(A.19)

$[k_{22}] =$ 

|   |                      |                            |                                 |                             |                                   |
|---|----------------------|----------------------------|---------------------------------|-----------------------------|-----------------------------------|
| 0 | 0                    | 0                          | 0                               | 0                           | 0                                 |
|   | $G \frac{(a+b)c}{2}$ | 0                          | $G \frac{(a+b)c^2}{6}$          | $G \frac{(a^2-b^2)c}{3}$    | 0                                 |
|   |                      | $\beta_y \frac{(a+b)c}{2}$ | $\beta_y \frac{(a^2-b^2)c}{6}$  | 0                           | $\beta_y \frac{(a+b)c^2}{3}$      |
|   |                      |                            | $G \frac{(a+b)c^3}{12}$         | $G \frac{(a^2-b^2)c^2}{12}$ | $\beta_y \frac{(a^2-b^2)c^2}{12}$ |
|   |                      |                            | $\beta_y \frac{(a^3+b^3)c}{12}$ |                             |                                   |
|   |                      |                            |                                 | $G \frac{(a^3+b^3)c}{3}$    | 0                                 |
|   |                      |                            |                                 |                             | $\beta_y \frac{(a+b)c^3}{3}$      |

SYMMETRIC

(A.20)

The transformation matrix was employed to produce an elemental stiffness matrix in terms of the generalized displacements in the local system.

$$\begin{aligned}
 U &= \frac{1}{2} \{A\}^T [k_1] \{A\} \\
 &= \frac{1}{2} [ [T^{-1}] \{\tilde{\delta}\} ]^T [k_1] [T^{-1}] \{\tilde{\delta}\} \\
 &= \frac{1}{2} \{\tilde{\delta}\}^T [k_2] \{\tilde{\delta}\}
 \end{aligned} \tag{A.21}$$

where  $[k_2] = [T^{-1}]^T [k_1] [T^{-1}]$

In order to assemble the elements by matching displacements at the nodes it was then necessary to bring each elemental matrix into the global system.

$$\{\tilde{\delta}\} = [R] \{\delta\} \tag{A.22}$$

Then  $U = \{\delta\}^T [k_e] \{\delta\}$

where  $[k_e] = [R]^T [T^{-1}]^T [k_2] [T^{-1}] [R]$  (A.23)

$\{\delta\}$  = vector of elemental displacements in the global system

$$[R] = \begin{array}{|c|c|c|c|c|c|} \hline [R,] & 0 & 0 & 0 & 0 & 0 \\ \hline 0 & [R,] & 0 & 0 & 0 & 0 \\ \hline 0 & 0 & [R,] & 0 & 0 & 0 \\ \hline 0 & 0 & 0 & [R,] & 0 & 0 \\ \hline 0 & 0 & 0 & 0 & [R,] & 0 \\ \hline 0 & 0 & 0 & 0 & 0 & [R,] \\ \hline \end{array} \quad (A.24)$$

iv

and

$$[R,] = \begin{array}{|c|c|} \hline \cos \theta & \sin \theta \\ \hline -\sin \theta & \cos \theta \\ \hline \end{array} \quad (A.25)$$

and  $\theta$  was defined in (A.4)

The matrix  $[k_e]$  is the elemental stiffness matrix used in the solution of the stiffness problem.

### A.3 Derivation of Strains and Stresses

Strains at any point  $(\xi, \eta)$  in an element can be calculated from equations (A.12) once the polynomial coefficients  $\{A\}$  have been calculated. In this program, strains were evaluated at the nodes so that they could be averaged between elements. To solve for  $\{A\}$ , the deformations in the global system for a given element were retrieved and rotated back into the local coordinate system.

$$\{A\} = [T^{-1}][R]\{\delta\} \quad (\text{A.26})$$

Using the strains, stresses were calculated using the orthotropic elasticity matrix for plane stress.

$$\{\sigma\} = [D]\{\varepsilon\}$$

where  $\{\sigma\}^T = (\sigma_x, \sigma_y, \tau) \quad (\text{A.27})$

$$\{\varepsilon\} = (\varepsilon_x, \varepsilon_y, \gamma)$$

$$[D] = \begin{array}{|c|c|c|} \hline \frac{E_x}{1-\nu_{xy}\nu_{yx}} & \frac{\nu_{xy} E_x}{1-\nu_{xy}\nu_{yx}} & 0 \\ \hline \frac{\nu_{yx} E_y}{1-\nu_{xy}\nu_{yx}} & \frac{E_y}{1-\nu_{xy}\nu_{yx}} & 0 \\ \hline 0 & 0 & G \\ \hline \end{array} \quad (\text{A.28})$$

A Mohr's circle approach was used to rotate these stresses into the global system for averaging at the nodes to produce a more accurate result. The averaged strains and stresses were then subjected to Mohr's circle in order to yield the directions and magnitudes of principal stresses and strains at the nodes.

## Appendix B

### Behaviour and Testing of the Element

#### B.1 Convergence

In order to converge onto a solution, the finite element displacement field assumed must provide strain-free rigid body motion, as well as constant strain modes. Further, plane stress finite elements require that the displacements in both the  $\xi$  and  $\eta$  directions be continuous along element edges. The first two criteria were clearly satisfied by the formulations of equations (A.3). To check the last criterion, the displacement along each edge of the triangle was found to be quadratic both parallel and perpendicular to the edge. Three constants were therefore required to define the displacement along the edge, and these were provided by the displacement in the appropriate direction along that edge at each of the three nodes. By forcing the displacements at each node along the edge of an element to match those of adjacent elements the criterion was automatically satisfied.

The rate of convergence was easily determined. Since the element displacement field was quadratic, the error from a Taylor's series truncation was of the order of some length parameter  $l$  cubed. Differentiating once gave an error in strain of the order of  $l^2$ . Strain is

raised to the second power in the strain energy expression so that an error of the order of  $\ell$  to the fourth power results. If this length parameter is taken as the reciprocal of the number of elements along an edge, the strain energy should converge as the order of  $1/N^4$ .

## B.2 Testing

The elements were tested in three cases. The first was the load case illustrated in Fig. B.1 where a uniformly distributed load was applied to the top edge of a membrane. This problem gave uniform vertical displacements, strains and stresses as required, of exactly the correct magnitudes. The second case was the thirty-two element cantilever shown in Fig. B.2. Here the results did not agree exactly with theory but were within reasonable bounds. The stress in the X direction was accurate to within a maximum of 6 per cent and the shear stress was accurate to within a maximum of 17 per cent error. This problem was run in order to compare the element with an isotropic finite element which had been programmed previously by a different method.<sup>7</sup> The results agreed exactly. A few other tests were run in which the modulae were reversed in some elements, and the results were as predicted by theory.

A third test of the program was made by modelling a circular hole in the centre of a plate that could be considered as infinitely long in the direction of loading,

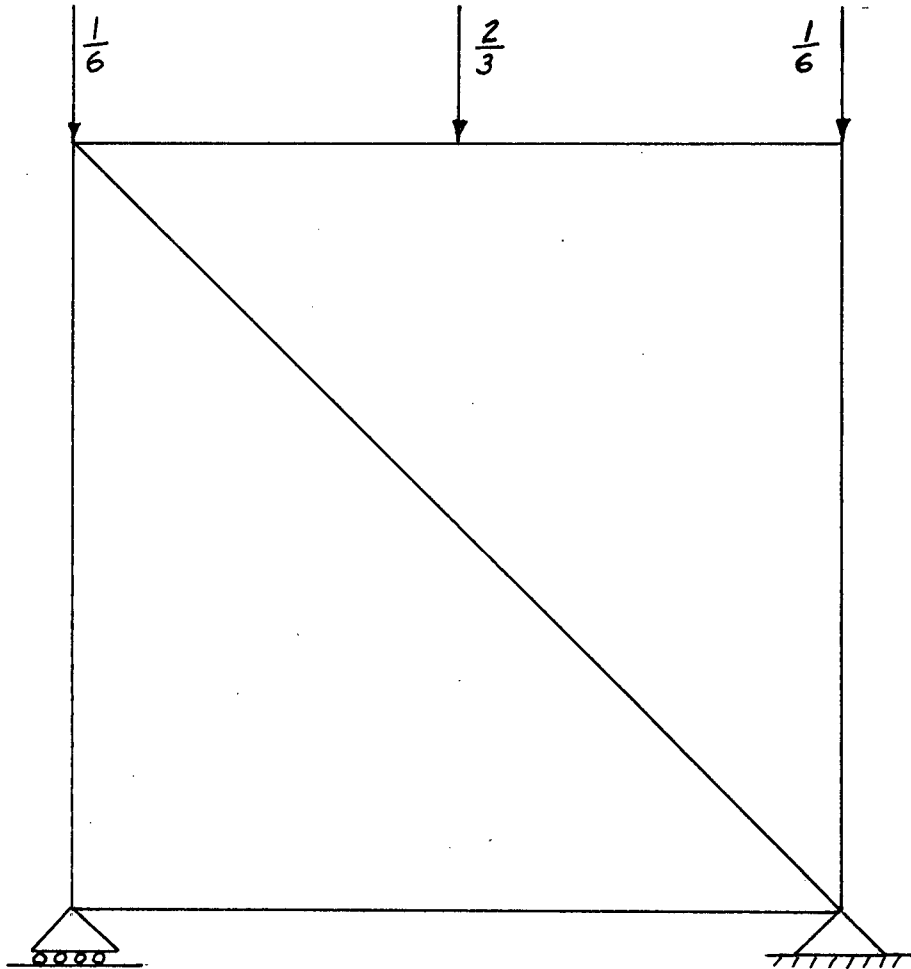


Fig. B-1 UNIFORMLY LOADED MEMBRANE

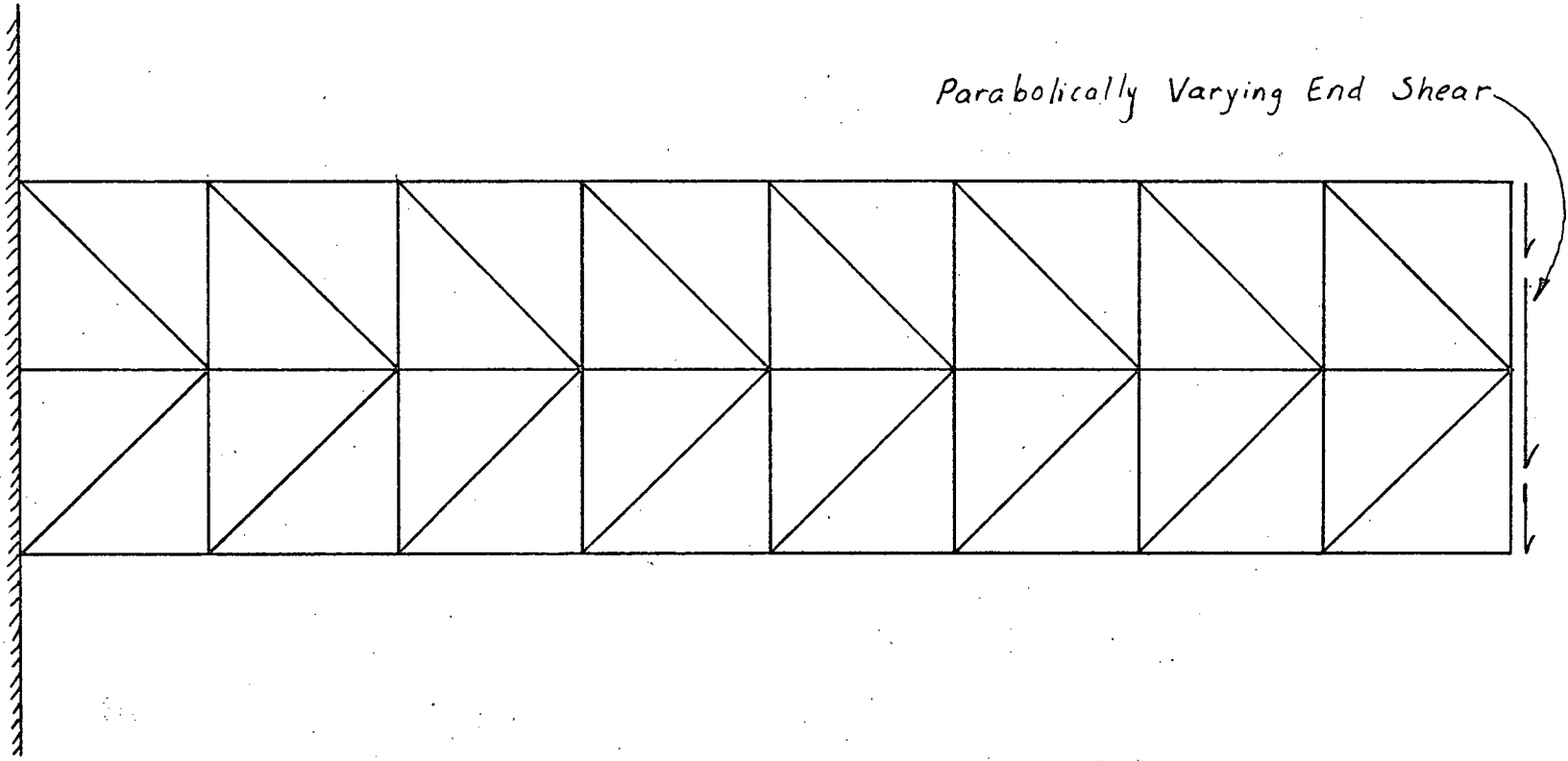


Fig. B-2 32 ELEMENT CANTILEVER

and of finite length in the transverse direction. The grid used was that created for the analyses of chapter 4 and is illustrated in Fig. 4.1. Fig. B.3 and Fig. B.4 show stress comparisons of the finite element solution (for the finite plate) with the analytic solutions for a plate infinite in both directions.<sup>8</sup> This comparison was made for a uniform tensile loading along the left hand side of the model, the upper left hand corner of which is shown in Figs. B.3 and B.4. The results were very similar in pattern and magnitude for stresses in the X direction where the finite element model might be considered infinite. In the Y direction, the stresses showed the same type of variation as for an infinite plate, but were of different magnitudes because of the equilibrium requirement that the stresses in the Y direction be zero at the free boundaries.

In the program as written, all elements have the same elastic modulae relative to their local coordinate axes, although the direction of orthotropy can be rotated through ninety degrees when required for ease of assembling the elements. The system of equations was solved using a Choleski decomposition type library routine.

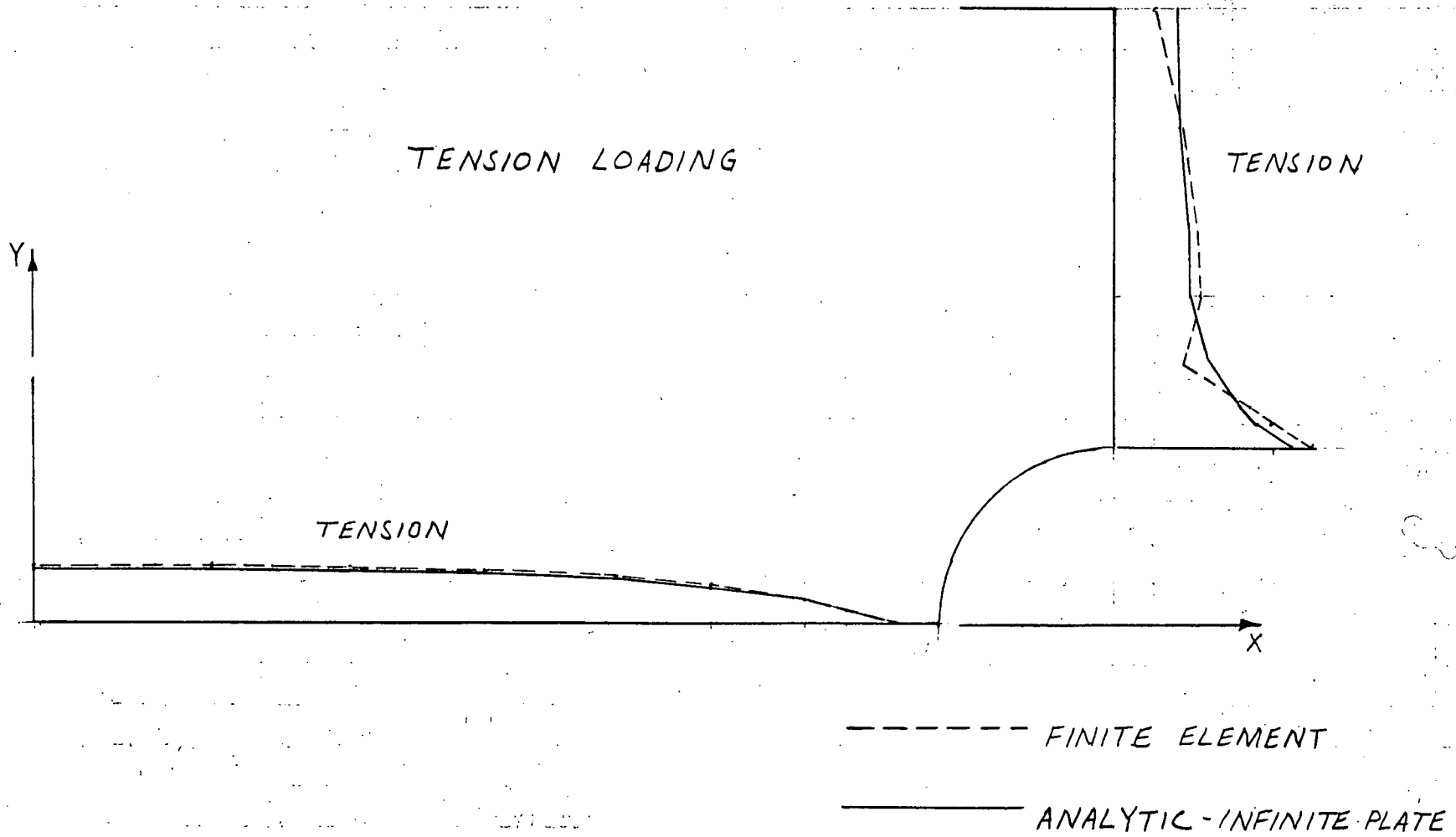


Fig. B-3 EDGE STRESSES X DIRECTION ISOTROPIC

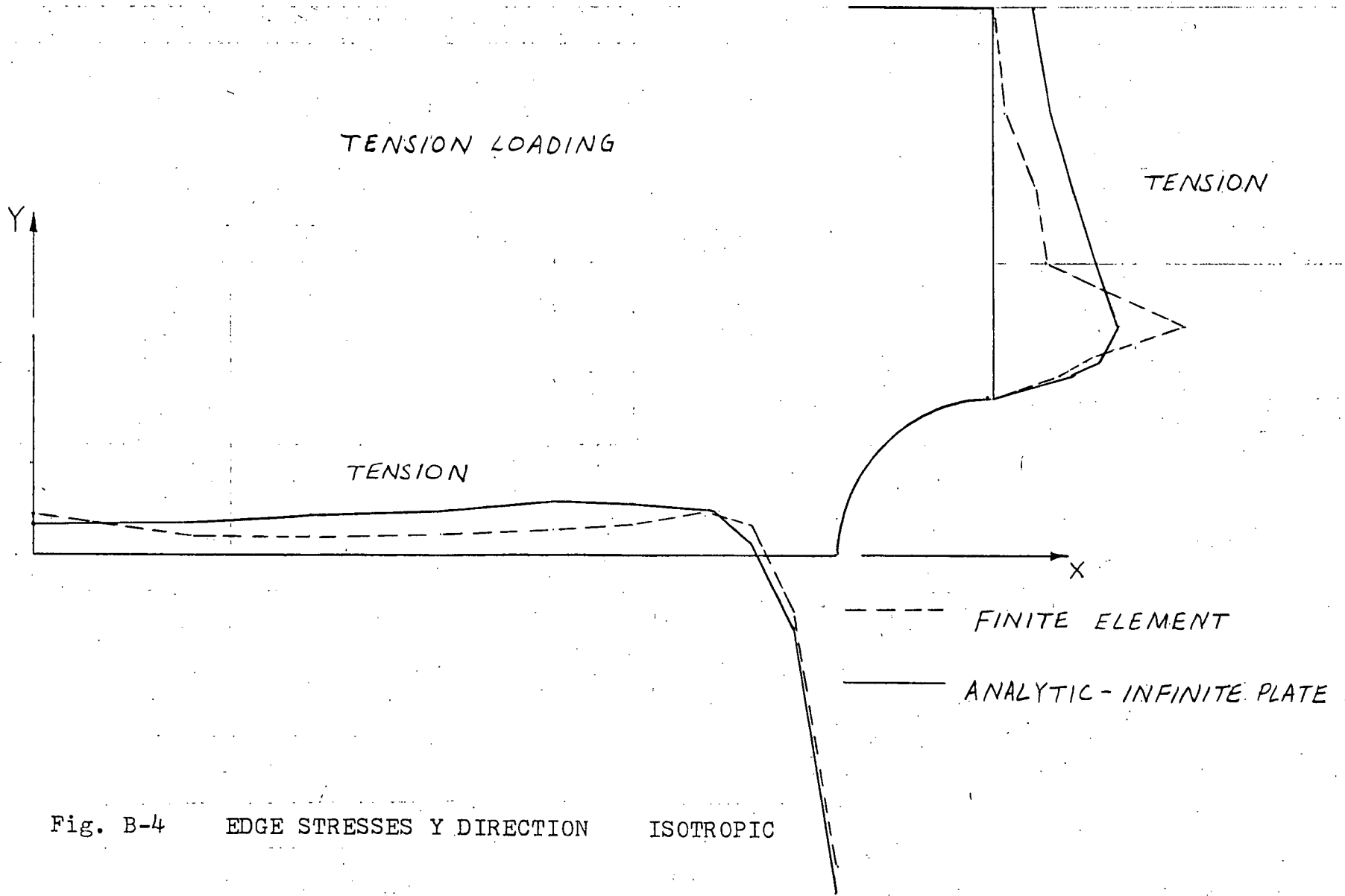


Fig. B-4 EDGE STRESSES Y DIRECTION ISOTROPIC

Appendix CThe Computer Program

|       |     |   |
|-------|-----|---|
| 2     |     | IMPLICIT REAL*8(A-F, G-Z)   |
| 3     |     | DIMENSION X(430), Y(430), ICC(430,6), IX(860), JX(860)                    |
| 4     |     | DIMENSION S(12,12), SS(12,12), T(12,12), P(12,12)                         |
| 5     |     | DIMENSION A(50000), LJ(12)  |
| 6     |     | DIMENSION DEL(12), AP(12)   |
| 7     |     | DIMENSION PM(860)   |
| 8     |     | DIMENSION SIGX(6), SIGY(6), TAU(6), EPSX(6), EPSY(6), C/M(6)              |
| 8.5   |     | DIMENSION EXX(430), EYY(430), EXY(430)                                    |
| 9     |     | DIMENSION SYX(430), SY(430), SXY(430), M/COUNT(430)                       |
| 10    |     | DIMENSION MTR(200), GDCS(12), EVERS(12)                                   |
| 11    |     | DIMENSION AGRESS(860)   |
| 12    |     | DIMENSION SIGLX(6), SIGLY(6), TAUCL(6)                                    |
| 13    | C   | DIMENSION X AND Y .GT. NUMBER OF NODES                                    |
| 14    |     | EPS=0.00  |
| 15    | C   | DIMENSION ICC .GE. NUMBER OF DEGREES OF FREEDOM                           |
| 16    | C   | DIMENSION IX AND JX .GE. NUMBER OF DEGREES OF FREEDOM                     |
| 17    | C   | DIMENSION A .GE. LG*LEAND BUT BE CONSISTENT THROUGH SUBROUTINES           |
| 18    | C   | DIMENSION PM .GE. NUMBER OF DEGREES OF FREEDOM                            |
| 19    | C   | ICC IS THE 6 NODE NUMBERS FOR EACH ELEMENT                                |
| 20    | C   | LJ IS THE LIST OF DEGREES OF FREEDOM FOR AN ELEMENT                       |
| 21    | C   | DEL IS A MATRIX OF GLOBAL DEGREES OF FREEDOM FOR AN ELEMENT               |
| 22    | C   | AP IS A STORAGE MATRIX USED IN THE STRESS SUBROUTINE WHICH MUST           |
| 23    | C   | MUST BE DIMENSIONED SAME AS NUMBER OF DEGREES OF FREEDOM                  |
| 24    | C   | PER ELEMENT   |
| 25    | C   | NSIZ MUST HAVE THE SAME MAGNITUDE AS THE FIRST DIMENSION OF ICC IN M/PROG |
| 26    |     | REWIND 1  |
| 27    |     | REWIND 2  |
| 28    |     | NSIZ=430  |
| 28.25 |     | IDPLUG=0  |
| 29    |     | REWIND 2  |
| 30    |     | DO 230 I=1,50000  |
| 31    |     | A(I)=0.00   |
| 32    | 200 | CONTINUE  |
| 33    |     | DO 235 I=1,430  |
| 35    |     | SXX(I)=0.00   |
| 36    |     | SYY(I)=0.00   |
| 37    |     | SXY(I)=0.00   |
| 37.2  |     | EXX(I)=0.00   |
| 37.4  |     | EYY(I)=0.00   |
| 37.6  |     | EXY(I)=0.00   |
| 38    |     | M/COUNT(I)=0.00   |
| 39    | 235 | CONTINUE  |
| 40    |     | DO 236 I=1,860  |
| 41    |     | PM(I)=0.00  |
| 41.25 | 236 | CONTINUE  |
| 42    |     | PM(1)=-1.00   |
| 43    |     | PM(2)=-4.00   |
| 44    |     | PM(4)=-2.00   |
| 45    |     | PM(6)=-4.00   |
| 46    |     | PM(8)=-2.00   |
| 47    |     | PM(10)=-4.00  |
| 48    |     | PM(12)=-2.500   |
| 48.25 |     | PM(14)=-6.00  |
| 48.5  |     | PM(16)=-3.00  |
| 48.6  |     | PM(18)=-6.00  |
| 48.7  |     | PM(20)=-3.00  |
| 48.8  |     | PM(22)=-6.00  |
| 48.81 |     | PM(24)=-3.00  |
| 48.82 |     | PM(26)=-6.00  |
| 48.83 |     | PM(28)=-1.500   |

```

49      WRITE(6,323)
50      323  FORMAT('0', 'MASTER LOAD VECTOR')
51      WRITE(6,323) (FM(L),L=1,200)
52      322  FORMAT(/,10(13.6))
53      CALL LAYOUT(X,Y,NSIZ,ICC,IX,JX,NE,AN,NVAR,NMAT,NDEC,NELR)
54      CALL FLAS(TL,G,EX,EY,LXY,UYX)
55      CALL BANDWF(ICC,JX,NE,NVAR,NV3,NSIZ,LPAND,NNOD)
56      DO 470 IN=1,NE
57      DO 471 L=1,NNOD
58      JT=ICC(IN,L)
59      NCCUNT(JT)=NCCUNT(JT)+1
60      471  CONTINUE
61      470  CONTINUE
62      DO 206 LL=1,NE
62.25   IF (IDEBUG.EC.0) GO TO 211
63      WRITE(9,212) LL
64      212  FORMAT('1', 'ELEMENT NO.',15)
64.25  211  CONTINUE
65      C1=ICC(LL,1)
66      C2=ICC(LL,2)
67      C3=ICC(LL,3)
68      X1=X(C1)
69      X2=X(C2)
70      X3=X(C3)
71      Y1=Y(C1)
72      Y2=Y(C2)
73      Y3=Y(C3)
73.25  IF (IDEBUG.EC.0) GO TO 250
74      WRITE(9,209) LL
75      209  FORMAT('0', 'ELEMENT STIFFNESS MATRIX FOR ELEMENT',15)
75.25  250  CONTINUE
76      CALL LST(X1,X2,X3,Y1,Y2,Y3,EX,EY,LXY,LX,R,G,TL,LL,NELR,IDEBUG)
76.25  IF (IDEBUG.EC.0) GO TO 251
77      WRITE(9,200)
78      220  FORMAT('1', 'ELEMENTAL STIFFNESS MATRIX')
79      WRITE(9,208) ((R(L,M),M=1,12),L=1,12)
80      208  FORMAT('1',12(13.2))
80.25  251  CONTINUE
81      DO 55 N=1,NVAR
82      DO 55 J=1,NNOD
83      LJ=(J-1)*NVAR
84      LJ(N+J1)=JX(NVAR*ICC(LL,J)-NVAR*N)
85      55   CONTINUE
85.25  IF (IDEBUG.EC.0) GO TO 252
86      WRITE(9,200) (LJ(KL),KL=1,12)
87      300  FORMAT('0', 'LJ IS',1215)
87.25  252  CONTINUE
88      CALL SETUP(A,NV3,LJ,3,LBAND,NSIZ)
89      206  CONTINUE
89.25  IF (IDEBUG.EC.0) GO TO 253
90      WRITE(9,200)
91      320  FORMAT('1', 'MASTER STIFFNESS MATRIX')
92      CALL DPMAT(A,168,168,168,168,1,1,65,3)
93.25  253  CONTINUE
94      RATIO=1.E-16
95      C    NOTE THAT DFBAND IS MORE EFFICIENT THAN DBAND ONLY WHEN WATERFIV
96      C    IS NOT USED
97      CALL DFBAND(A,FM,NDEC,LPAND,1,RATIO,DET,JEXP,0)
98      C    THE THIRD ENTRY IN CALL DBAND IS THE ORDER OF THE MASTER STIFFNESS
99      C    MATRIX--MUST BE EXACTLY THE SAME AS THE NUMBER OF NON-ZERO

```

```

100 C DEGREES OF FREEDOM IN THE PROBLEM
101 C PM NOW CONTAINS THE SOLUTION DISPLACEMENTS
101.25 WRITE(6,250) DET
101.5 150 FORMAT(' ', 'DETERMINANT OF MASTER STIFFNESS MATRIX IS', D20.8)
102 CALL EXPAND(LGROSS, NMAT, NVAR, PM, IX)
102.25 IF(1/(PUC.EC.)) GO TO 254
103 WRITE(9,101) NMAT
104 101 FORMAT(' ', 'NMAT=', I4)
105 WRITE(9,102) (JX(I), I=1, NMAT)
106 102 FCFMAT('O', 2015)
106.25 254 CONTINUE
107 WRITE(6,103) NVAR, NDEG
108 103 FORMAT('O', 'NVAR=', I5, 'NDEG=', I5)
109 WRITE(6,201) LPAND
110 201 FCFMAT('C', 'THE HALF BAND WIDTH IS', I4, /)
111 WRITE(6,202) NV3
112 202 FORMAT('O', 'THERE ARE', I3, IX, 'VARIABLES PER ELEMENT')
113 WRITE(6,779) RATIC
114 779 FCFMAT('C', 'RATIC=', D20.10)
115 WRITE(6,798)
116 798 FCFMAT('I', 'STRESSES RELATIVE TO ELEMENT AXES')
117 REWIND 1
118 REWIND 2
119 REWIND 3
120 WRITE(6,232)
121 232 FCFMAT('O', 'ELEMENT', 6X, 'NODE NUMBER', 6X, 'SIGX', 12X, 'SIGY', 12X, 'TA
122 *U', 12X, 'EPSX', 12X, 'EPSY', 12X, 'GAMMA', /)
123 DO 170 NA=1, NN
124 WRITE(6,233) NA
125 233 FCFMAT('-', 15)
126 CALL LSTRES(NM, PM, EX, EY, UXY, UYX, G, SXX, SYY, SXY, NF, ICC, NCLP, EXX, FYY,
126.25 =FXY, IDEBUG)
127 170 CONTINUE
128 DO 475 I=1, NN
129 SXX(I)=SXX(I)/NCCOUNT(I)
130 SYY(I)=SYY(I)/NCCOUNT(I)
131 SXY(I)=SXY(I)/NCCOUNT(I)
131.2 EXX(I)=EXX(I)/NCCOUNT(I)
131.4 FYY(I)=FYY(I)/NCCOUNT(I)
131.6 EXY(I)=EXY(I)/NCCOUNT(I)
132 475 CONTINUE
133 WRITE(6,505)
134 505 FORMAT('I', 10X, 'PRINCIPAL STRESSES AND DIRECTION RELATIVE TO THE
135 * GLOBAL SYSTEM')
136 WRITE(6,520)
137 C NOW CALCULATE THE PRINCIPAL STRESSES
138 DO 500 I=1, NN
139 520 FORMAT('C', ' NODE', 16X, 'PSIGX', 15X, 'PSIGY', 14X, 'ANGLE-DEG-CLCC')
140 SF=(SXX(I)-SYY(I))**2+4.00*SXY(I)**2
141 RA=.500*DSCRT(SF)
142 C=(SXX(I)+SYY(I))/2.00
143 C PSIGX & PSIGY ARE THE PRINCIPAL STRESSES
144 C ANGLE=ROTATION CLOCKWISE OF PRINCIPAL STRESSES FROM THE GLOBAL
145 C SYSTEM
146 PSIGX=C+FA
147 PSIGY=C-FA
148 TF=2.00*SXY(I)/(SXX(I)-SYY(I))
149 ANGLE=ATAN(TF)/2.00/3.14159*180.00
149.1 IF(SXX(I).LT.SYY(I)) ANGLE=90.00+ANGLE
150 WRITE(6,510) I, PSIGX, PSIGY, ANGLE

```

```

151      510  F(PPMAT(' ',14,F24.3,F20.3,F21.3)
151.25    WRITE(4,600) X(I),Y(I),ANGLE
151.5     600  F(PPMAT(2F10.4,F11.5)
152      560  CONTINUE
152.25   C   CALCULATE THE PRINCIPAL STRAINS
152.5     WRITE(6,550)
152.6     550  FORMAT('1',10X,'PRINCIPAL STRAINS AND DIRECTION RELATIVE TO THE
152.7     *GLOBAL SYSTEM')
152.8     WRITE(6,560)
152.81    560  FORMAT('0',1 NODE',16X,'PEPSX',15X,'PEPSY',14X,'ANGLE-DEG-CLOCK')
152.82    DO 570 I=1,NN
152.83    EF=(EXX(I)-FYY(I))*2+4.0D0*EXY(I)**2
152.84    FAF=.50D0*DSQRT(EF)
152.85    CF=(EXX(I)+FYY(I))/2.0D0
152.86   C   PEPSX & PEPSY ARE THE PRINCIPAL STRAINS
152.87   C   ANGLE=ROTATION CLOCKWISE OF PRINCIPAL STRAINS FROM THE GLOBAL AXES
152.88    PEPSX=CF+FAF
152.89    PEPSY=CF-FAF
152.9     TFC=2.0D0*EXY(I)/(EXX(I)-FYY(I))
152.91    ANGLE=ATAN(TFC)/2.0D0/2.14159*180.0D0
152.911   IF(EXX(I).LT.FYY(I)) ANGLE=90.0D0+ANGLE
152.92    WRITE(6,580) I,PEPSX,PEPSY,ANGLE
152.93    580  FORMAT(' ',14,F23.5,F19.5,F22.2)
152.931   WRITE(7,600) X(I),Y(I),ANGLE
152.94    570  CONTINUE
153      WRITE(6,476)
154      476  FORMAT('1',15X,'AVERAGE STRESSES AT THE NODES')
155      WRITE(6,477)
156      477  FORMAT('1',15X,'SIGX',15X,'SIGY',15X,'TAU')
157      DO 479 I=1,NN
158      WRITE(6,478) I,SXX(I),SYY(I),SXY(I)
159      478  FORMAT(' ',14,F22.6,2F19.6)
160      479  CONTINUE
160.1     WRITE(6,480)
160.2     480  FORMAT('1',15X,'AVERAGE STRAINS AT THE NODES')
160.3     WRITE(6,481)
160.4     481  FORMAT('1',15X,'EPSX',15X,'EPSY',15X,'GAMMA')
160.5     DO 482 I=1,NN
160.6     WRITE(6,482) I,EXX(I),EYY(I),EXY(I)
160.7     482  FORMAT(' ',14,F20.6,F19.6,F18.6)
160.8     482  CONTINUE
161      STOP
162      END
163      SUBROUTINE LAYOUT(X,Y,NSIZ,ICO,IX,JX,NF,NN,NVAR,NMAT,NDEG,NELF)
164      IMPLICIT REAL*8(A-H,O-Z)
165   C   X=X-COORDINATE OF EACH NODE
166   C   Y=Y-COORDINATE OF EACH NODE
167   C   ICO=LIST OF NODE NUMBERS FOR EACH ELEMENT
168   C   IX=0 IF NODAL DEGREE OF FREEDOM IS RESTRAINED
169   C   =1 IF NOT RESTRAINED
170   C   JX=ORDERED LIST OF THE DEGREES OF FREEDOM
171   C   NF=TOTAL NUMBER OF ELEMENTS
172   C   NN=TOTAL NUMBER OF NODES
173   C   NVAR=NUMBER OF VARIABLES PER NODE
174   C   NMAT=TOTAL NUMBER OF UNKNOWN
175   C   NDEG=COUNTER USED IN DETERMINING JX ENTRIES
176   C   NSIZ=GREATER THAN NUMBER OF ELEMENTS
177   C   JELREV=ELEMENT TO HAVE ELASTIC MODULAE REVERSED
178   C   NELREV IS THE TOTAL NUMBER OF THESE ELEMENTS
179   C   THIS SUBROUTINE READS ELEMENT AND NODE DATA

```

```

180 DIMENSION X(1),Y(1),ICC(NSIZ,6),IX(1),JX(1)
181 DIMENSION NPLR(200)
182 READ(5,40) NE,NN,NVAR,NLREV
183 40 FORMAT(4I5)
184 WRITE(6,41) NE,NN,NVAR,NLREV
185 41 FORMAT(/, ' TOTAL NO. OF ELEMENTS ',I5,5X, 'NO. OF NODES',I5,5X,
186 * 'VARIABLES PER NODE',I5,5X, 'NO. OF ELEMENTS REVERSED',I5,/)
187 WRITE(6,42)
188 42 FORMAT(/, ' NODE',7X, ' X-CCRD',6X, 'Y-CCRD',6X, ' CX', 6X, ' CY')
189 C CX AND CY INDICATE CONSTRAINT OF THE FIRST AND SECOND DEGREES OF FREEDOM
190 C AT THE NODE
191 C DO A NUMERICAL PROCEDURE TO READ IN IX AS A SINGLE ROW VECTOR
192 C READ IN NODE INFORMATION
193 C FOR SIDE NODES SET X AND Y ZERO AS THEY ARE NEVER USED---JUST
194 C READ IX BOUNDARY CONDITIONS
195 C DO 10 I=1,NN
196 I2=NVAR+1
197 I1=I2-NVAR+1
198 C KK IS THE NODE NUMBER--READ IN TO KEEP CARDS DECIPHERABLE
199 READ(5,43) K,X(I),Y(I),(IX(J),J=I1,I2)
200 43 FORMAT(I5,2F10.0,2I5)
201 C IX FOR EACH NODE HAS THE SAME NUMBER OF ENTRIES AS NVAR
202 WRITE(6,44) I,X(I),Y(I),(IX(J),J=I1,I2)
203 44 FORMAT(1X,I5,5X,F10.4,2X,F10.4,5X,2I4)
204 10 CONTINUE
205 WRITE(6,47)
206 47 FORMAT(/,5X, 'ELEMENT',5X, 'NODE NUMBERS')
207 C INPUT ELEMENT DATA
208 C FOR OPTHOPTIC TRIANGLES THE ORDER OF THE NODES INPUT MAY BE IMPORTANT
209 C INPUT NODE NUMBERS ANTICLOCKWISE STARTING WITH THE TWO PARALLEL
210 C TO THE BASE
211 C KK IS THE ELEMENT NUMBER
212 C DO 11 I=1,NE
213 READ(5,45) KK,(ICC(I,J),J=1,6)
214 45 FORMAT(7I5)
215 WRITE(6,46) I,(ICC(I,J),J=1,6)
216 46 FORMAT(5X,I5,5X,6I5)
217 11 CONTINUE
218 C DO 55 J=1,NF
219 NPLR(J)=C
220 55 CONTINUE
221 C REVERSE MODULI WHERE NECESSARY
222 IF(NLREV.EQ.0) GO TO 620
223 WRITE(6,620)
224 620 FORMAT('0', ' THESE ELEMENTS HAVE REVERSED MODULI')
225 DO 60 J=1,NLREV
226 READ(5,65) JFLREV
227 WRITE(6,625) JFLREV
228 625 FORMAT(' ',I20)
229 65 FORMAT(I5)
230 NPLR(JFLREV)=1
231 60 CONTINUE
232 630 CONTINUE
233 NMAT=NVAR*NN
234 NDEC=0
235 C NOW NUMBER DEGREES OF FREEDOM
236 DO 12 I=1,NMAT
237 IF(IX(I)) 1,2,3
238 NDEG=NDEG+1
239 JX(I)=NDEG

```

```

240      GO TO 12
241      2      JX(I)=C
242      GO TO 12
243      1      WRITE(6,17) I
244      17     FORMAT(//,'INPUT IX FOR DEGREE OF FREEDOM',I4,I1,' IS NEGATIVE')
245      12     CONTINUE
246      C      NDEC IS THE SIZE OF THE PROBLEM
247      RETURN
248      END
249      SUBROUTINE ELAS(TL,G,EX,EY,UXY,UYX)
250      IMPLICIT REAL*8(A-H,O-Z)
251      REAL(8,6) TL,G,EX,EY,UXY,UYX
252      6      FORMAT(F10.5,3F10.5,2F10.5)
253      WRITE(6,7)
254      7      FORMAT(//,I1,' THICKNESS',5X,'G',10X,'EX',8X,'EY',5X,'UXY',8X,'UYX'
255      *)
256      WRITE(6,8)
257      8      FORMAT(' ',3X,' INCHES',5X,'PSI',8X,'PSI',7X)
258      WRITE(6,9) TL,G,EX,EY,UXY,UYX
259      9      FORMAT('0',F8.3,2D11.2,D10.2,2D11.2)
260      RETURN
261      END
262      SUBROUTINE BANDWH(ICO,JX,NE,NVAR,NV3,NSIZ,LBAND,MNCD)
263      IMPLICIT REAL*8(A-H,O-Z)
264      C      THIS ROUTINE FINDS THE HALF BAND WIDTH LBAND
265      C      JX ETC. ARE AS DEFINED IN LAYOUT
266      C      NV3=NO. OF VARIABLES PER ELEMENT
267      DIMENSION ICO(NSIZ,6),JX(1),LJ(12)
268      DIMENSION NSTIFF(12)
269      COMMON /ELT2/LJ
270      EQUIVALENCE (NSTIFF,LJ(1))
271      C      MNCD=NO. OF NODES PER ELEMENT
272      C      DIMENSION LJ FOR THE NUMBER OF DEGREES OF FREEDOM PER ELEMENT
273      MNCD=6
274      LBAND=0
275      NV2=2*NVAR
276      WRITE(6,203)
277      203     FORMAT('0', 'ELEMENT NO.',20X,' DEGREES OF FREEDOM')
278      DO 3 I=1,NE
279      C      DETERMINE LJ= NO. OF DEGREE OF FREEDOM IN AN ELEMENT
280      C      (J+K) IS THE NUMBER FROM 1 TO NV3 OF THAT DEGREE OF FREEDOM
281      DO 4 J=1,NVAR
282      DO 4 K=1,MNCD
283      K1=(K-1)*NVAR
284      LJ(J+K1)=JX(NVAR*ICO(I,K)-NVAR+J)
285      4      CONTINUE
286      NV2=NVAR*MNCD
287      WRITE(6,204) I,(LJ(L),L=1,NV3)
288      WRITE(2) (LJ(L),L=1,12)
289      204     FORMAT('0',I5,20X,12I5)
290      C      FIND DIFFERENCES BETWEEN DEGREE NUMBERS WITHIN THE ELEMENT
291      C      MIN IS SOME NUMBER GREATER THAN THE BANDWIDTH
292      MAX=0
293      MIN=1000
294      DO 8 J=1,NV3
295      C      IF NO FREEDOM AT SOME COORDINATE, THE BAND WIDTH DOES NOT CHANGE
296      IF(LJ(J).EQ.0) GO TO 8
297      IF(LJ(J)-MAX) 6,6,5
298      MAX=LJ(J)
299      6      IF(LJ(J)-MIN) 7,8,6

```

```

300      7      MIN=LJ(J)
301      8      CONTINUE
302      NP1=MAX-MIN
303      IF (NP1.GT.(LEAND)) LRAND=NB1
304      3      CONTINUE
305      LEAND=LRAND+1
306      RETLEN
307      FND
308      SUBROUTINE LST(X1,X2,X3,Y1,Y2,Y3,EX,FY,UXY,UYX,R,G,TL,LL,NELR,ICDP
308.25 *UG)
309      IMPLICIT REAL*8(A-F,G-Z)
310      DIMENSION R(12,12),S(12,12),T(12,12),P(12,12)
311      DIMENSION P(12),F(12),RT(12,12),IPERM(30)
312      DIMENSION NELR(200)
313      DIMENSION APC(4),GDDS(12),EVENS(12)
314      COMMON /ELT1/S
315      COMMON /FLT3/AL,BL,CL,THETA
316      EQUIVALENCE (APC,AL)
317      EQUIVALENCE (STF,S(1,1))
318      C      STIFFNESS MATRIX FOR THE ORTHOTROPIC TRIANGULAR PLANE STRESS
319      C      ELEMENT WITH LINEARLY VARYING STRESS
320      DO 211 I=1,12
321      P(I)=0.00
322      F(I)=0.00
323      211  CONTINUE
324      C      CALCULATE RELEVANT LENGTH PARAMETERS FOR THE ELEMENT
325      C      SL=LENGTH OF SIDE 1-2
326      SL=(X2-X1)**2+(Y2-Y1)**2
327      SL=DSQRT(SL)
328      AL=((X2-X3)*(X2-X1)+(Y2-Y3)*(Y2-Y1))/SL
329      BL=((X3-X1)*(X2-X1)+(Y3-Y1)*(Y2-Y1))/SL
330      CL=((X2-X1)*(Y3-Y1)-(X3-X1)*(Y2-Y1))/SL
331      CC=(X2-X1)/SL
332      SI=(Y2-Y1)/SL
333      THETA=DARCCOS(CC)
334      WRITE(3) ABC
335      AREA=(AL+BL)*CL/2.00
336.25  IF (ICDBUG.EQ.0) GO TO 255
336      WRITE(9,215) LL,AREA
337.25  215  FORMAT(' ',ELEMENT NO.,I4,5X,'AREA IS',F10.5)
337.25  255  CONTINUE
338      IF (AREA.LE.0.00) GO TO 220
339      GO TO 222
340      220  WRITE(6,221) LL
341      221  FORMAT(' ',*****AREA OF ELEMENT',I4,2X,' IS NEGATIVE*****')
341.25  IF (ICDBUG.EQ.0) GO TO 256
342      222  WRITE(9,210) AL,BL,CL,CC,SI
342      210  FORMAT('C',A=',F10.5,2X,'B=',F10.5,2X,'C=',F10.5,2X,'COS=',F8.5,2
344 *X,'SIN=',F8.5)
344.25  256  CONTINUE
345      C      INITIALIZE P,S,T AND R MATRICES TO ZERO
346      C      R=ROTATION MATRIX
347      C      T=TRANSFORMATION MATRIX
348      C      S=PRODUCT OF T INVERTED AND R
349      C      P=TRANSPOSE OF S
350      C      T=INVERSE OF TRANSFORMATION MATRIX AFTER INV. STATEMENT
351      DO 5 I=1,12
352      DO 5 J=1,12
353      R(I,J)=0.00
354      RT(I,J)=0.00

```

```

355 S(I,J)=0.00
356 T(I,J)=0.00
357 F(I,J)=0.00
358 5 CONTINUE
359 C ROTATE ELASTIC MODULAE WHEN NECESSARY
360 IF(KFIR(LL).EQ.1) GO TO 600
361 GO TO 605
362 600 SFX='X
363 TX=FY
364 EY=SFYX
365 SUXY=LXY
366 LXY=LYX
367 LYX=SLXY
368 605 CONTINUE
369 C BUILD THE TRANSFORMATION MATRIX
370 R2=RL**2
371 C2=CL**2
372 A2=A1**2
373 T(1,1)=1.00
374 T(1,2)=-R1
375 T(1,5)=R2
376 T(2,7)=1.00
377 T(2,8)=T(1,2)
378 T(2,11)=R2
379 T(3,1)=1.00
380 T(3,2)=A1
381 T(3,5)=A2
382 T(4,7)=1.00
383 T(4,8)=A1
384 T(4,11)=A2
385 T(5,1)=1.00
386 T(5,3)=C1
387 T(5,6)=C2
388 T(6,7)=1.00
389 T(6,9)=C1
390 T(6,12)=C2
391 T(7,1)=1.00
392 T(7,2)=(A1-F1)/2.00
393 T(7,5)=T(7,2)**2
394 T(8,7)=1.00
395 T(8,8)=T(7,2)
396 T(8,11)=T(7,5)
397 T(9,1)=1.00
398 T(9,2)=A1/2.00
399 T(9,3)=C1/2.00
400 T(9,4)=A1**CL/4.00
401 T(9,5)=A2/4.00
402 T(9,6)=C2/4.00
403 T(10,7)=1.00
404 T(10,8)=T(9,2)
405 T(10,9)=T(9,3)
406 T(10,10)=T(9,4)
407 T(10,11)=T(9,5)
408 T(10,12)=T(9,6)
409 T(11,1)=1.00
410 T(11,2)=T(1,2)/2.00
411 T(11,3)=T(9,3)
412 T(11,4)=-R1*CL/4.00
413 T(11,5)=R2/4.00
414 T(11,6)=T(9,6)

```

```

415      T(12,7)=1.0C
416      T(12,8)=T(11,2)
417      T(12,9)=T(11,3)
418      T(12,10)=T(11,4)
419      T(12,11)=T(11,5)
420      T(12,12)=T(5,6)
421      C      ALL OTHER ENTRIES ARE ZERO
421.25    IF(ICEPUG.EC.0) GO TO 257
422      WRITE(S,212)
423      212    FORMAT('D', 'TRANSFORMATION MATRIX')
424      WRITE(S,214) ((T(L,M),M=1,12),L=1,12)
425      214    FORMAT(' ',12F10.5)
425.25    257    CONTINUE
426      C      NOW CALCULATE THE INVERSE OF THE TRANSFORMATION MATRIX
427      CALL DINVRT(T,12,12,DDET,DCOND)
427.25    IF(ICEPUG.EC.0) GO TO 258
428      WRITE(S,200) DDET,DCOND
429      200    FORMAT('-', 'DDET=',D15.6, 'DCOND=',D15.6)
430      C      NOW CONTAINS THE INVERTED TRANSFORMATION MATRIX
431      WRITE(S,213)
432      213    FORMAT('D', 'INVERSED TRANSFORMATION MATRIX')
433      WRITE(S,214) ((T(L,M),M=1,12),L=1,12)
433.25    258    CONTINUE
434      C      NOW CALCULATE THE ROTATION MATRIX
435      P(1,1)=CC
436      P(1,2)=SI
437      P(2,1)=-SI
438      P(2,2)=CC
439      DO 7 I=1,2
440      DO 7 J=1,2
441      R(I+2,J+2)=P(I,J)
442      R(I+4,J+4)=P(I,J)
443      R(I+6,J+6)=P(I,J)
444      R(I+8,J+8)=P(I,J)
445      R(I+10,J+10)=P(I,J)
446      7      CONTINUE
447      WRITE(S,278)
447.25    IF(ICEPUG.EC.0) GO TO 259
448      278    FORMAT(' ', 'ROTATION MATRIX')
449      WRITE(S,206) ((P(L,M),M=1,12),L=1,12)
450      206    FORMAT(' ',12C1).3)
450.25    259    CONTINUE
451      C      MULTIPLY T BY P TO GET S
452      CALL DGMULT(T,P,S,12,12,12,12,12)
452.25    IF(ICEPUG.EC.0) GO TO 260
453      WRITE(S,226)
454      226    FORMAT(' ', 'T INVERSE*P=S')
455      WRITE(S,227) ((S(I,J),J=1,12),I=1,12)
456      227    FORMAT(' ',12C1).3)
456.25    260    CONTINUE
457      WRITE(I) ((S(I,J),I=1,12),J=1,12)
458      C      REINITIALIZE P
459      DO 12 I=1,12
460      DO 12 J=1,12
461      P(I,J)=0.00
462      12     CONTINUE
463      C      NOW PUT INTO P THE ELEMENT STIFFNESS MATRIX IN TERMS OF POLYNOMIAL
464      C      COEFFICIENTS
465      PX=EX/(1.00-LYX*UXY)
466      PY=EY/(1.00-UYX*UXY)

```

```

467      LFX=PX*UXY
468      LDY=PY*LYX
469      C      INTEGRATION FACTORS
470      C1=CL*(AL+BL)/2.D0
471      C2=CL**2*(AL+BL)/12.D0
472      C3=CL*(AL**3+BL**3)/12.D0
473      C4=C1**2*(AL**2-BL**2)/24.D0
474      C5=CL**2*(AL+BL)/6.D0
475      C6=CL*(AL**2-BL**2)/6.D0
476      F(2,2)=C1*Bx
477      F(2,4)=C5*Bx
478      F(2,5)=C6**2.D0*Bx
479      F(2,9)=C1/2.D0*(UEX+UPY)
480      F(2,10)=C6/2.D0*(LEX+LEY)
481      F(2,12)=C5*(Lrx+Lry)
482      R(3,3)=C1*G
483      F(3,4)=C6*G
484      F(3,6)=C5**2.D0*G
485      R(3,8)=P(3,3)
486      R(3,10)=C5*G
487      F(3,11)=C6**2.D0*G
488      F(4,4)=C2*Bx+C3*G
489      R(4,5)=C4**2.D0*Bx
490      R(4,6)=C4**2.D0*G
491      R(4,8)=P(3,4)
492      F(4,9)=R(2,10)/2.D0
493      F(4,10)=C4/2.D0*(LEX+LEY+2.D0*G)
494      R(4,11)=C3**2.D0*G
495      R(4,12)=C2*(UEX+LYY)
496      F(5,5)=C3**4.D0*Bx
497      R(5,9)=2.D0*F(2,10)
498      R(5,10)=C2*(LEX+UEY)
499      R(5,12)=C4**2.D0*(LEX+LEY)
500      P(6,6)=C2**4.D0*G
501      F(6,8)=2.D0*F(3,10)
502      R(6,10)=R(6,6)/2.D0
503      F(6,11)=2.D0*F(4,6)
504      R(8,8)=R(3,3)
505      R(8,10)=R(3,10)
506      F(8,11)=2.D0*F(3,4)
507      F(9,9)=C1*By
508      R(9,10)=C6*By
509      F(9,12)=C5**2.D0*By
510      P(10,10)=C2*G+C3*By
511      F(10,11)=R(4,6)
512      R(10,12)=C4**2.D0*By
513      P(11,11)=C3**4.D0*G
514      R(12,12)=C2**4.D0*By
515      DO 900 IA=1,12
516      DO 900 IB=1,12
517      R(1F,1I)=F(IA,IB)
518      900  CONTINUE
519      DO 901 IA=1,12
520      DO 901 IB=1,12
521      F(1B,1A)=TL*F(1B,1A)
522      901  CONTINUE
522.25  IF(ICEPUG.EQ.0) GO TO 261
523      WRITE(9,276)
524      276  FORMAT('  ', 'UNTRANSFORMED STIFFNESS MATRIX')
525      WRITE(9,278) ((R(I,J),J=1,12),I=1,12)

```

```

525.25 261 CONTINUE
526 C B WILL CONTAIN THE TRANSPOSE OF S
527 CALL DQTRAN(S,P,12,12,12,12)
528 C PRODUCE THE ELEMENT STIFFNESS MATRIX IN GLOBAL COORDINATES
529 C REINITIALIZE T FOR USE AS AN INTERMEDIATE STORAGE MATRIX
530 DO 20 I=1,12
531 DO 30 J=1,12
532 T(I,J)=0.00
533 CONTINUE
534 CALL DCMULT(R,P,T,12,12,12,12,12,12)
535 DO 21 I=1,12
536 DO 21 J=1,12
537 R(I,J)=0.00
538 21 CONTINUE
539 CALL DCMULT(T,S,R,12,12,12,12,12,12)
540 C R NOW CONTAINS THE ELEMENT STIFFNESS MATRIX IN GLOBAL COORDINATES
541 C NOW CHANGE MODULAE BACK TO ORIGINAL FOR THE NEXT ELEMENT
542 IF (N*IF(LL).EQ.1) GO TO 610
543 GO TO 615
544 610 SEX=FX
545 FX=FY
546 FY=SEX
547 SUXY=UXY
548 LX=UYX
549 LYX=SUXY
550 615 CONTINUE
550.25 C CHECK TO SEE WHETHER INDIVIDUAL COLUMNS OF THE ELEMENTAL STIFFNESS
550.5 C MATRIX ARE IN EQUILIBRIUM
550.51 IF (IDEBUG.EQ.0) GO TO 262
550.6 WRITE(S,540)
550.7 940 FCPMAT('1','DEGREE OF FREEDOM',10X,'ODDS',10X,'EVENS')
550.8 DO 580 M=1,12
550.81 ODDS(M)=0.00
550.82 EVENS(M)=0.00
550.83 980 CONTINUE
550.84 DO 910 J=1,12
550.85 DO 920 I=1,11,2
550.86 ODDS(J)=ODDS(J)+R(I,J)
550.87 920 CONTINUE
550.88 DO 930 I=2,12,2
550.89 EVENS(J)=EVENS(J)+R(I,J)
550.9 930 CONTINUE
550.91 CONTINUE
550.92 DO 960 J=1,12
550.93 WRITE(S,550) J,ODDS(J),EVENS(J),R(1,J)
550.94 950 FCPMAT(' ',19,D24.8,D15.8,D40.8)
550.95 960 CONTINUE
550.96 262 CONTINUE
551 RETURN
552 END
553 SUBROUTINE SETUP(A,NV3,LJ,R,LEANC,NS1Z)
554 IMPLICIT REAL*8(A-F,O-Z)
555 DIMENSION LJ(1),A(50000),R(12,12)
556 C A=MASTER STIFFNESS MATRIX
557 C NV3=NO. OF VARIABLES PER ELEMENT
558 C LJ=CODE NUMBERS FOR THE ELEMENT
559 C F=ELEMENT STIFFNESS MATRIX
560 NE1=LEANC-1
561 DO 12 I=1,NV3
562 I=COLUMN NUMBER IN THE ELEMENT MATRIX

```

```

563      LJC=LJ(I)
564      IF(IJC) 12,12,107
565      107   DO 11 J=1,NV2
566      C     J=ELK NUMBER IN THE ELEMENT MATRIX
567      C     J VARIES FROM 1 TO NV2 SINCE WE WANT ONLY THE LOWER HALF OF THE MASTER
568      C     MATRIX STORED
569      LJP=LJ(J)
570      IF(IJP) 11,11,108
571      108   IF(IJC-LJR) 113,113,114
572      C     THIS PART OF THE SUBROUTINE IS ADAPTED FROM HOOLEY'S PLANE FRAME NOTES
573      113   L=(IJC-1)*NP1+LJR
574      GO TO 115
575      114   L=(IJP-1)*NP1+LJC
576      115   A(L)=A(L)+P(J,I)
577      791   CONTINUE
578      11   CONTINUE
579      12   CONTINUE
580      RETURN
581      END
582      SUBROUTINE LSTRES(NA,PM,EX,EY,LXY,LYY,C,SXX,SYX,SYX,NE,ICO,NELP,EX
582.25     +X,EYY,EXY,ICFPUG)
583      IMPLICIT REAL*8(A-F,D-Z)
584      DIMENSION LJ(12),PM(860)
585      DIMENSION NELP(200)
586      DIMENSION DEL(12),AP(12)
587      DIMENSION STF(144),NSTFF(12)
588      DIMENSION APC(4)
589      DIMENSION SIGX(6),SIGY(6),TAU(6),EPSX(6),EPSY(6),GAM(6),ICC(4*6)
590      DIMENSION SXX(430),SYY(430),SXY(430)
591      DIMENSION SIGLX(6),SIGLY(6),TAUCL(6)
591.2     DIMENSION EPSLX(6),EPSLY(6),GAML(6),EYY(430),EYX(430),EXY(430)
592      COMMON /ELT1/S(12,12)
593      COMMON /ELT2/LJ
594      COMMON /ELT3/AL,BL,CL,THETA
595      EQUIVALENCE (STF,S(1,1))
596      EQUIVALENCE (NSTFF,LJ(1))
597      EQUIVALENCE (APC,AL)
598      C     THIS SUBROUTINE PRODUCES STRESSES AT THE NODES RELATIVE TO
599      C     ELEMENT-NOT GLOBAL-AXES
600      C     S= T INVERSE*P FOR ELEMENT NA
601      C     NA=ELEMENT WORKED ON
602      C     PM=DISPLACEMENT SOLUTION VECTOR
603      C     EX,ETC., ARE ELASTIC CONSTANTS
604      C     SIGX=STRESS PARALLEL TO THE LINE JOINING THE FIRST TWO NODES OF
605      C     THE TRIANGLE
606      C     SIGY=NORMAL STRESS PERPENDICULAR TO SIGX
607      C     TAU= SHEAR STRESS
608      C     EPSX=STRAIN PARALLEL TO SIGX
609      C     EPSY=STRAIN PARALLEL TO SIGY
610      C     GAM= SHEAR STRAIN
611      C     DEL=MATRIX OF GLOBAL DISPLACEMENTS FOR AN ELEMENT
612      C     AP=MATRIX OF POLYNOMIAL COEFFICIENTS FOR AN ELEMENT
613      C     NELP ARRAY KNOWS WHICH ELEMENTS HAVE REVERSED MODULI
614      C     INITIALIZE
615      DO 150 I=1,12
616      DEL(I)=0.00
617      AP(I)=0.00
618      150   CONTINUE
619      DO 402 I=1,6
620      EPSX(I)=0.00

```

```

621      EPSY(I)=C.C0
622      CAX(I)=0.C0
623      SIGX(I)=C.C0
624      SIGY(I)=C.C0
625      TAL(I)=C.C0
626      4P2 CONTINUE
627      C      REVERSE MODULI WHERE NECESSARY
628      IF (NMLP(MA).EQ.1) GO TO 600
629      GO TO 605
630      600 SEX=FX
631      EX=EY
632      EY=SEX
633      SUXY=UXY
634      LXY=LYX
635      LY)=SUXY
636      605 CONTINUE
637      C      RETRIEVE MATRICES FROM MAIN PROGRAM
638      READ(1) STF
639      READ(2) NSTIFF
640      READ(2) AEC
641      C      SOME DEBUGGING CHECKS
641.25    IF (IDEFUC.EQ.0) GO TO 263
642      WRITE(9,54) NA
643      54   FORMAT('0', 'S FOR ELEMENT', I4)
644      WRITE(9,70) ((S(I,J),J=1,12),I=1,12)
645      70   FORMAT('-', 12D10.3)
646      WRITE(9,80) NA
647      80   FORMAT('0', 'LJ FOR ELEMENT', I4)
648      WRITE(9,100) (LJ(I),I=1,12)
649      100  FORMAT('-', 12I10)
649.25   263 CONTINUE
650      C      RETRIEVE ELEMENTAL DISPLACEMENTS IN GLOBAL COORDINATES FROM PM
651      DO 110 I=1,12
652      JL=LJ(I)
653      IF (JL.EQ.0) GO TO 180
654      DEL(I)=PM(JL)
655      GO TO 190
656      180  DEL(I)=0.C0
657      190  CONTINUE
658      110  CONTINUE
659      C      CALCULATE MATRIX OF POLYNOMIAL COEFFICIENTS AP
660      AP=T INVERTED*F*DEL
661      CALL DGMULT(S,DEL,AP,12,12,1,12,12,12)
661.25    IF (IDEFUC.EQ.0) GO TO 264
662      WRITE(9,130) NA
663      130  FORMAT('0', 'POLYNOMIAL COEFFICIENTS FOR ELEMENT', I4)
664      WRITE(9,140) (AP(K),K=1,12)
665      140  FORMAT('-', 6F15.6)
665.25   264 CONTINUE
666      UN=1.C0-UXY*UYX
667      C      CALCULATION OF STRAINS AND STRESSES AT THE NODES
668      EPSX(1)=AP(2)-2.C0*AP(5)*BL
669      EPSX(2)=AP(2)+2.C0*AP(5)*AL
670      EPSX(3)=AP(2)+AP(4)*CL
671      EPSX(4)=AP(2)+AP(5)*(AL-BL)
672      EPSX(5)=AP(2)+AP(4)*CL/2.C0+AP(5)*AL
673      EPSX(6)=AP(2)+AP(4)*CL/2.C0-AP(5)*BL
674      EPSY(1)=AP(9)-AP(10)*BL
675      EPSY(2)=AP(9)+AP(10)*AL
676      EPSY(3)=AP(9)+2.C0*AP(12)*CL

```

```

677      EPSY(4)=AP(9)+AP(10)=(AL-BL)/2.DO
678      EPSY(5)=AP(9)+AP(10)*AL/2.DO+AP(12)*CL
679      EPSY(6)=AP(9)-AP(10)*BL/2.DO+AP(12)*CL
680      A1=AP(3)/P(E)
681      A2=AP(10)+2.DO*AP(4)
682      A3=AP(4)+2.DO*AP(11)
683      GAM(1)=A1-A2*BL
684      GAM(2)=A1+A3*AL
685      GAM(3)=A1+A2*CL
686      GAM(4)=A1+A3*(AL-BL)/2.DO
687      GAM(5)=A1+A3*AL/2.DO+A2*CL/2.DO
688      GAM(6)=A1-A2*BL/2.DO+A2*CL/2.DO
689      EXM=EX/UM
690      EYM=EY/UM
691      XYFY=UXY*EXM
692      YXEY=LYX*EYM
693      DC=230*J=1,6
694      SF=0.DO
695      TF=0.DO
696      PHI=0.DO
697      PSI=0.DO
698      F=0.DO
699      SIGX(J)=EXM*EPSX(J)+XYEX*EPSY(J)
700      SIGY(J)=YXFY*EPSX(J)+EYM*EPSY(J)
701      TAL(J)=G*GAM(J)
702      C      RA=RADIUS OF MOHR'S CIRCLE FOR THIS STRESS CASE
703      SF=(SIGX(J)-SIGY(J))*2+4.DO*TAU(J)*2
703.5      SFSN=(EPSX(J)-EPSY(J))*2+4.DO*GAM(J)*2
704      FA=.5DC*DSQRT(SF)
704.5      FASN=.5DC*DSQRT(SFSN)
705      C      PHI=ORIGINAL ANGLE FROM PRINCIPAL STRESS PLANE
705.1      C      PHIN=ORIGINAL ANGLE FROM PRINCIPAL STRAIN PLANE
705.2      TFN=2.DO*GAM(J)/(EPSX(J)-EPSY(J))
705.3      PHIN=DATAN(TFN)
705.4      C      PSIN=ANGLE FROM GLOBAL SYSTEM TO PRINCIPAL STRAIN PLANE
705.5      IF(EPSX(J).LT.EPSY(J)) PHIN=PHIN+3.14159
706      TF=2.DO*TAU(J)/(SIGX(J)-SIGY(J))
707      PHI=DATAN(TF)
708      C      PSI=ANGLE FROM GLOBAL SYSTEM TO PRINCIPAL STRESS PLANE
709      IF(SIGX(J).LT.SIGY(J)) PHI=PHI+3.14159
710      PSI=PHI-2.DO*THETA
710.5      FSN=(EPSX(J)+EPSY(J))/2.DO
711      F=(SIGX(J)+SIGY(J))/2.DO
711.5      PSIN=PHIN-2.DO*THETA
712      C      SIGLX=NORMAL STRESS IN THE GLOBAL X-DIRECTION
713      C      SIGLY=NORMAL STRESS IN THE GLOBAL Y-DIRECTION
714      C      TAUGL=Shear stress relative to global axes
715      SIGLX(J)=F+FA*DCOS(PSI)
716      SIGLY(J)=F-FA*DCOS(PSI)
717      TAUGL(J)=RA*DSIN(PSI)
717.1      EPSLX(J)=FSN+FASN*DCOS(PSIN)
717.2      EPSLY(J)=FSN-FASN*DCOS(PSIN)
717.3      GAML(J)=FASN*DSIN(PSIN)
718      WRITE(6,231) ICC(NA,J),SIGX(J),SIGY(J),TAU(J),EPSX(J),EPSY(J),GAM(
719      # J)
720      231      FORMAT(' ',12X,15,2F16.3,2F16.8)
721      230      CONTINUE
722      C      SUM THE STRESSES AND STRAINS AT THE NCCES FOR AVERAGING
723      J1=ICC(NA,1)
724      J2=ICC(NA,2)

```

```

725      J2=ICG(NA,3)
726      J4=ICG(NA,4)
727      J5=ICG(NA,5)
728      J6=ICG(NA,6)
729      SXX(J1)=SXX(J1)+SIGLX(1)
730      SXX(J2)=SXX(J2)+SIGLX(2)
731      SXX(J3)=SXX(J3)+SIGLX(3)
732      SYY(J1)=SYY(J1)+SIGLY(1)
733      SYY(J2)=SYY(J2)+SIGLY(2)
734      SYY(J3)=SYY(J3)+SIGLY(3)
735      SXY(J1)=SXY(J1)+TALGL(1)
736      SXY(J2)=SXY(J2)+TALGL(2)
737      SXY(J3)=SXY(J3)+TALGL(3)
738      SXX(J4)=SXX(J4)+SIGLX(4)
739      SXX(J5)=SXX(J5)+SIGLX(5)
740      SXX(J6)=SXX(J6)+SIGLX(6)
741      SYY(J4)=SYY(J4)+SIGLY(4)
742      SYY(J5)=SYY(J5)+SIGLY(5)
743      SYY(J6)=SYY(J6)+SIGLY(6)
744      SXY(J4)=SXY(J4)+TALGL(4)
745      SXY(J5)=SXY(J5)+TALGL(5)
746      SXY(J6)=SXY(J6)+TALGL(6)
746.C5    FXX(J1)=FXX(J1)+EPSLX(1)
746.1    FXX(J2)=FXX(J2)+EPSLX(2)
746.15    FXX(J3)=FXX(J3)+EPSLX(3)
746.2    FXX(J4)=FXX(J4)+EPSLX(4)
746.25    FXX(J5)=FXX(J5)+EPSLX(5)
746.3    FXX(J6)=FXX(J6)+EPSLX(6)
746.35    FYY(J1)=FYY(J1)+EPSLY(1)
746.4    FYY(J2)=FYY(J2)+EPSLY(2)
746.45    FYY(J3)=FYY(J3)+EPSLY(3)
746.5    FYY(J4)=FYY(J4)+EPSLY(4)
746.55    FYY(J5)=FYY(J5)+EPSLY(5)
746.6    FYY(J6)=FYY(J6)+EPSLY(6)
746.65    EXY(J1)=EXY(J1)+GAML(1)
746.7    EXY(J2)=EXY(J2)+GAML(2)
746.75    EXY(J3)=EXY(J3)+GAML(3)
746.8    EXY(J4)=EXY(J4)+GAML(4)
746.85    EXY(J5)=EXY(J5)+GAML(5)
746.9    EXY(J6)=EXY(J6)+GAML(6)
747      C    CHANGE MODULE BACK FOR THE NEXT ELEMENT
748      IF(NELP(NA),EQ,1) GO TO 610
749      GO TO 615
750      610    SFX=FX
751      FX=FY
752      FY=SEX
753      SLXY=LXY
754      LX=UYX
755      LY=SUXY
756      615    CONTINUE
757      PFTLRN
758      EIF
759      SUBROUTINE EXPAND(ACROSS,NMAT,NVAP,PM,IX)
760      THIS SUBROUTINE EXPANDS THE SOLUTION VECTOR OF SIZE NNET BACK TO
761      C      SIZE NMAT BY INSERTING ZEROS WHERE ZERO BOUNDARY CONDITIONS
762      C      WERE APPLIED AND PRINTS IT OUT
763      C      ACROSS=EXPANDED SOLUTION VECTOR OF SIZE NMAT (RETURNED)
764      C      NMAT=GROSS SIZE OF THE PROBLEM
765      C      NVAP=NUMBER OF VARIABLES PER NODE OF ELEMENT
766      C      FM=NET SOLUTION VECTOR OF SIZE NNET

```

```

767 C IX=BOUNDARY CONDITION CODE VECTOR
768 C THIS SUBROUTINE WORKS ONLY IF ALL DEGREES OF FREEDOM AT A NODE
769 C ARE EITHER RESTRAINED OR UNRESTRAINED---SEE NDS BELOW
770 IMPLICIT REAL*8(A-F,C-Z)
771 DIMENSION FM(1),AGFCSS(1),IX(1)
772 LL=0
773 DO 5 I=1,NMAT
774 LL=LL+IX(I)
775 AGFCSS(I)=0.0E8
776 IF (IX(I).EQ.0) GO TO 5
777 AGFCSS(I)=FM(LL)
778 5 CONTINUE
779 NDS=NMAT/NVAR
780 WRITE(6,40)
781 40 FORMAT(1,' ',1X,'NDS',15X,'C=IX',15X,'DPLY')
782 DO 10 I=1,NDS
783 I1=NVAR*(I-1)+1
784 I2=I1+NVAR-1
785 WRITE(6,41) I,(AGFCSS(J),J=I1,I2)
786 41 FORMAT(15,2F20.5)
787 10 CONTINUE
788 RETURN
789 END
END OF FILE

```